



ELUCIDATING DEACTIVATION AND REACTION PATHS OF PHOTSENSITIVE ORGANIC SYSTEMS THROUGH COMPUTATIONAL METHODS.

Josep Casellas Soler

ADVERTIMENT. L'accés als continguts d'aquesta tesi doctoral i la seva utilització ha de respectar els drets de la persona autora. Pot ser utilitzada per a consulta o estudi personal, així com en activitats o materials d'investigació i docència en els termes establerts a l'art. 32 del Text Refós de la Llei de Propietat Intel·lectual (RDL 1/1996). Per altres utilitzacions es requereix l'autorització prèvia i expressa de la persona autora. En qualsevol cas, en la utilització dels seus continguts caldrà indicar de forma clara el nom i cognoms de la persona autora i el títol de la tesi doctoral. No s'autoritza la seva reproducció o altres formes d'explotació efectuades amb finalitats de lucre ni la seva comunicació pública des d'un lloc aliè al servei TDX. Tampoc s'autoritza la presentació del seu contingut en una finestra o marc aliè a TDX (framing). Aquesta reserva de drets afecta tant als continguts de la tesi com als seus resums i índexs.

ADVERTENCIA. El acceso a los contenidos de esta tesis doctoral y su utilización debe respetar los derechos de la persona autora. Puede ser utilizada para consulta o estudio personal, así como en actividades o materiales de investigación y docencia en los términos establecidos en el art. 32 del Texto Refundido de la Ley de Propiedad Intelectual (RDL 1/1996). Para otros usos se requiere la autorización previa y expresa de la persona autora. En cualquier caso, en la utilización de sus contenidos se deberá indicar de forma clara el nombre y apellidos de la persona autora y el título de la tesis doctoral. No se autoriza su reproducción u otras formas de explotación efectuadas con fines lucrativos ni su comunicación pública desde un sitio ajeno al servicio TDR. Tampoco se autoriza la presentación de su contenido en una ventana o marco ajeno a TDR (framing). Esta reserva de derechos afecta tanto al contenido de la tesis como a sus resúmenes e índices.

WARNING. Access to the contents of this doctoral thesis and its use must respect the rights of the author. It can be used for reference or private study, as well as research and learning activities or materials in the terms established by the 32nd article of the Spanish Consolidated Copyright Act (RDL 1/1996). Express and previous authorization of the author is required for any other uses. In any case, when using its content, full name of the author and title of the thesis must be clearly indicated. Reproduction or other forms of for profit use or public communication from outside TDX service is not allowed. Presentation of its content in a window or frame external to TDX (framing) is not authorized either. These rights affect both the content of the thesis and its abstracts and indexes.

UNIVERSITAT ROVIRA I VIRGILI

ELUCIDATING DEACTIVATION AND REACTION PATHS OF PHOTSENSITIVE ORGANIC SYSTEMS THROUGH COMPUTATIONAL METHODS.

Josep Casellas Soler

UNIVERSITAT ROVIRA I VIRGILI

ELUCIDATING DEACTIVATION AND REACTION PATHS OF PHOTSENSITIVE ORGANIC SYSTEMS THROUGH COMPUTATIONAL METHODS.

Josep Casellas Soler

Josep Casellas Soler

**Elucidating deactivation and reaction paths of
photosensitive organic systems through
computational methods.**

PhD Thesis

Supervised by Dra. María del Mar Reguero de la Poza

Grup de Química Quàntica
Departament de Química Física i Inorgànica



UNIVERSITAT ROVIRA i VIRGILI

Tarragona, May 2016

UNIVERSITAT ROVIRA I VIRGILI

ELUCIDATING DEACTIVATION AND REACTION PATHS OF PHOTSENSITIVE ORGANIC SYSTEMS THROUGH COMPUTATIONAL METHODS.

Josep Casellas Soler



UNIVERSITAT
ROVIRA I VIRGILI

Departament de Química Física i Inorgànica

Maria del Mar Reguero de la Poza, professora titular de Química Física, del Departament de Química Física i Inorgànica de la Universitat Rovira i Virgili,

Faig constar que aquest treball, titulat

“Elucidating deactivation and reaction paths of photosensitive organic systems through computational methods.”

que presenta Josep Casellas Soler per a l'obtenció del títol de Doctor, ha estat realitzat sota la meva direcció al Departament de Química Física i Inorgànica d'aquesta universitat i que aconsegueix els requeriments per poder optar a la Menció Internacional.

Tarragona, 10 de Maig de 2016

Dra. María del Mar Reguero de la Poza

UNIVERSITAT ROVIRA I VIRGILI

ELUCIDATING DEACTIVATION AND REACTION PATHS OF PHOTSENSITIVE ORGANIC SYSTEMS THROUGH COMPUTATIONAL METHODS.

Josep Casellas Soler

ACKNOWLEDGEMENTS

Aquesta tesi no hagués estat possible sense tot el suport que rebut del meu entorn, tant a la universitat com a casa, i que m'ha ajudat a tirar endavant aquest anys d'investigació. Voldria agrair-los aquí en aquestes paraules a tots aquells que hi han estat presents.

En primer lloc, i com no podia ser d'altra manera, a la meva directora de tesi Mar Reguero. Vull agrair-li tots els seus esforços per convertir-me en millor científic, per las seves crítiques constructives i pel seu bon humor quan els resultats no anaven tant bé durant aquests quatre anys.

També vull agrair-los a resta de membres sèniors del grup (Prof. Josep Maria Poblet, Dra. Anna Clotet, Dr. Antonio Fortea, Dr. Jordi Carbó i Dr. Xavier Lopez) els seus comentaris sempre encertats i necessaris que han contribuït d'una o altra forma al contingut d'aquesta tesi. Entre aquests, la Prof. Rosa Caballol i Dr. Cornelis de Graaf es mereixen una menció especial pel seu inestimable coneixement i proximitat. Haig d'agrair també sense dubte la feina de l'equip informàtic, José Carlos Ortiz i Elisenda Mas, que han fet el impossible per mantenir les màquines enceses i resoldre els dubtes tècnics que m'han sorgit. També em cal mencionar en Moisès Álvarez i la seva impressionant fórmula per a que poguéssim visualitzar els nostres resultats.

No voldria pas oblidar-me tampoc dels que han estat els meus companys de fatigues teòriques, dins i fora de la Rovira i Virgili. Començant pels forans: Maria, Sandra, Santi, Javi i Ferran pels bons dinars que hem gaudit i d'altres que potser vindran! I acabant per la promoció més nombrosa de la URV: Gerard, Mariano, Sergi, Magda i Victor. Vam començar junts i, tot i que els camins de la recerca ens han anat portant per camins diferents, espero mantenir el contacte un cop aquesta aventura del doctorat s'acabi. Especialment parlo de vosaltres dos, Gerard (encara hem d'escriure dos articles, Geisont!) i Mariano (a qui li preguntaré els meus dubtes computacionals?). Segur que tot ens anirà bé, n'estic convençut!

També voldria recordar aquells que ja han començat a volar sols, fa més o menys temps, però que sempre portaré amb mi: Gian, Pablo A., Xavi, Núria, Pablo J., tot i

que especialment a la Mireia i el Pedro. Mireia, vam compartir poc temps però reconec que la teva vitalitat per viure la vida (i la fotoquímica en particular) se'm va encomanar d'una manera que no hauria cregut possible, gràcies! Pedro, has representat el meu punt de referència durant quasi tres anys, un germà gran computacional a qui li podria preguntar qualsevol cosa, gràcies! Als "jovenets", Diego, Laura, Albert, Juan Carlos, Zhongling i Jianfang, penseu que un cop marxem els vells, us haureu de quedar fent que aquest vaixell suri... sou els futurs veterans! Per aquells que sou de pas al 202, Gantulga i Khalid, que l'aventura continuï agafant força, que no us aturi res!

I would also like to thank Mike Bearpark and his group for their warm welcome in the Imperial College and for teaching me how to work with new tools and perspectives. Especially I would also like to acknowledge the contribution of Lee Thomson for his explanations of the ONIOM method and the exploration of conical intersections, David Medive per gaudir d'unes bones converses en català que tant trobava a faltar i pels seus consells per començar la meva estada amb bon peu. I do not want to forget Morgane Vacher, Valentina Santolini, Clyde Fare and William Vigor who made my stay as enjoyable as possible.

Però la vessant més professional no ho ocupa tot. La família i els amics també han estat indispensables per a que arribes a aquest punt i fos capaç de fer-li front. Començaré pels meus amics de la llicenciatura, amb aquells amb qui no he perdut mai el contacte des de que vam acabar. Tots vosaltres, (Puig, Sandra, Alex, Alba, Ana, Mireia, Jordi, Raquel, Monllau i Munti) em feu recordar cada moment que la distància no és ni serà impediment a la voluntat de tornar-nos a trobar, aquí o més enllà.

Sempre hem sabut que hi ha gent que entrarà i sortirà de les nostres vides, que hi seran de pas, i que un dia no tornaran. A poc a poc, però, veus com un nucli es forma, que la vida continua i no marxen ni a les bones ni a les dolentes. És llavors que t'adones que has trobat un grup de gent ben especial, un grup amb el que ho voldràs compartir tot. Sou vosaltres, els amics de sempre (Eli, Ti, Ralet, Laia, Eric i Paula). Vosaltres heu estat les energies de tantes coses i de tants moments! Però deixeu-me que reservi un lloc especial als meus dos puntals, aquells que ho han vist tot de mi. Gio i Vic, heu representat l'amistat més indestructible de la que pot tenir ningú, com també mil nits de solucionar el món al nostre banc de la plaça i totes

aquelles caminades fins al cine per no veure res. Sou el millor que un pot tenir, i desitjo que el que el temps no ha pogut separar, no ho separi mai res.

Ja queden poques persones a qui agrair-li el que han fet per mi durant tots aquests anys, però no per això menys importants! (ans al contrari). La meva família: per una banda els meus pares, Josep i Carme, que s'han desviscut per mi i que han procurat que mai em faltés res. Els que han fomentat tot allò que sóc ara, esperonejant-me a tirar endavant cap allà on em volgués dirigir i donant-me els consells de mil vides. Mai podré agrair-vos-ho prou, ni en una ni en dues ni en dotze tesis. Per l'altra banda, al Joan, no només germà gran sinó també mentor i algú amb qui emmirallar-me. M'has inculcat el desig per la cultura i m'has obert els ulls amb el teu exemple per esforçar-me en allò que de debò em fes feliç. Darrere de grans homes, però, sempre hi ha grans dones i aquí no és pas una excepció: L'Eli, sempre amb una rialla, disposada a llargues converses i uns sopars exquisits. Finalment, als meus avis, encara que no heu pogut veure com tot acabava espero que allà on sigueu n'estareu tan cofois i orgullosos com jo.

No voldria acabar això sense mencionar a una noia que ha revolucionat la meva vida. Una persona a qui m'estimo amb la bogeria més absoluta i que ha vist enllà del que jo era quan encara jo ho desconeixia. Destí o atzar, el fet és que has omplert la meva vida de felicitat, de petits i grans moments, d'històries inoblidables i de records inesborrables. No seria aquí sense tu, petita, sense la teva empenta i recolzament. Aquest trosset et pertany, Núria.

UNIVERSITAT ROVIRA I VIRGILI

ELUCIDATING DEACTIVATION AND REACTION PATHS OF PHOTSENSITIVE ORGANIC SYSTEMS THROUGH COMPUTATIONAL METHODS.

Josep Casellas Soler

CONTENTS

Chapter 1. Introduction	1
1.1. General introduction.....	1
1.2. Scope and structure.....	7
1.3. Objectives.....	11
1.4. Bibliography.....	12
Chapter 2. Molecular photochemistry	13
2.1 Approach to Schrödinger's theory.....	13
2.2 Born-Oppenheimer approximation	15
2.3 Potential Energy Surfaces (PES)	16
2.4 Matter-radiation interaction.....	18
2.5 Non-adiabatic interactions.....	21
2.6 Bibliography.....	25
Chapter 3. Theory and applied methods	27
3.1 The Hartree-Fock based methods.....	28
3.1.1 Multiconfigurational methods using Active Spaces: CASSCF and RASSCF.....	30
3.1.2 Second order perturbation approximation on Active Space: CASPT2 method	32
3.1.3 Variational approach to dynamical correlation: DDCI method.....	35
3.2 Density Functional Theory (DFT)	37
3.3 Modelling the solvent: Polarizable Continuum Model (PCM)	40
3.4 Molecular Mechanics	41
3.5 Bibliography.....	42

Chapter 4. Azobenzene and phenylazopyridine isomerization ...45

4.1	Introduction.....	45
4.2	Scope.....	53
4.3	Computational strategy.....	54
4.4	Azobenzene results	56
4.4.1	Franck-Condon Region	57
4.4.2	Minimum energy points on excited state surfaces.....	60
4.4.3	Reaction mechanisms	65
4.4.4	Global description of the proposed mechanism.....	75
4.5	Phenylazopyridine results.....	78
4.5.1	Franck-Condon Region.....	78
4.5.2	Minimum energy points on excited state surfaces.....	79
4.5.3	Reaction mechanisms	84
4.5.4	Global description of the proposed mechanism.....	87
4.5.5	Simulation of the absorption spectrum	89
4.6	Conclusions.....	94
4.7	Bibliography	98

Chapter 5. Phenylphenalenone photocyclisation 101

5.1	Introduction.....	101
5.2	Scope.....	106
5.3	Computational strategy.....	107
5.4	Results	111
5.4.1.	Ground state minima and vertical excitations.....	113
5.4.2.	Equilibrium geometries on excited state surfaces	115
5.4.3.	Reaction mechanisms	119
5.5	Conclusions.....	128
5.6	Bibliography	129

Chapter 6. Dehidrosqualene photophysics	131
6.1. Introduction	131
6.2. Scope	136
6.3. Computational strategy	138
6.4. Results.....	140
6.4.1. Franck-Condon Region and calibration of computational methodologies	141
6.4.2. Excited state surfaces and reaction paths under C_{2h} symmetry constraint.....	146
6.4.3. The effect of the flexibility on the absorption.....	150
6.5. Conclusions	155
6.6. Bibliography	156
Chapter 7. Final conclusions	159
7.1. Azobenzene and phenylazopyridine.....	159
7.2. Phenylphenalenone.....	160
7.3. Dehidrosqualene.....	161
List of contributions	163

UNIVERSITAT ROVIRA I VIRGILI

ELUCIDATING DEACTIVATION AND REACTION PATHS OF PHOTSENSITIVE ORGANIC SYSTEMS THROUGH COMPUTATIONAL METHODS.

Josep Casellas Soler

El que importa és no deixar de fer-se preguntes - Albert Einstein

UNIVERSITAT ROVIRA I VIRGILI

ELUCIDATING DEACTIVATION AND REACTION PATHS OF PHOTSENSITIVE ORGANIC SYSTEMS THROUGH COMPUTATIONAL METHODS.

Josep Casellas Soler

FIRST CHAPTER:

INTRODUCTION

1.1. GENERAL INTRODUCTION

Historically, humanity has tried to understand nature, learn its secrets and find ways to make use of its wisdom. This fact has never changed, but what has changed is the refinement of the tools and ideas to get it. One of the basic sources of knowledge is intuition, a tool that allows us to draw parallels between particular known situations and unknown experiences and implement and adapt the solution that had worked before. However, in the last century the functionality in science of this tool has been questioned.

Since the beginning of the twentieth century, the world has been immersed in the chemical discovery of the atomic world. Until then, the application of the classical laws to explain a very large part of the phenomena of the physical world worked properly although some fringes needed some polishing. The reason for these fringes was attributed primarily to issues of instrument precision and they seemed to indicate that the end of the era of great discoveries in physics was close. They were wrong. Since the first theoretical hypothesis developed by Planck in 1900 in order to address these issues, the microscopic and macroscopic world have been moving away. The forces that govern both worlds have been shown to be different

and irreconcilable, and physical principles that seemed obvious do not apply any longer.

This incompatible behaviour is a certainty still today so, in this landscape, intuition finds nothing to grab on to in the science of the microscopic. We must be aware, therefore, of certain prejudices and preconceived ideas we could transfer from the macroscopic to the microscopic world and be prepared to dismiss our intuition so that it does not become an obstacle for situations where it is not trained. This is the first and necessary step in the world of quantum theory.

The assumption that started the physical revolution was introduced by Planck as an apparently small modification to the classical theories by saying that the energy of the light could not have any value but only certain discrete values.^[1,2] To understand this idea, we can put the example of a ladder where you can put your foot on each of the steps but not between them. This idea was thought to be an artefact, a quick fix to solve the old fringe of the black-body radiation. In fact, many scientists including Planck himself doubted about the challenging implications derived from his anti-intuitive hypothesis and supported, at first, the established model of light being a continuous entity. However, his assumption went much further than expected, solving efficiently the issue of fitting the predicted emission curve of the black-body to the real curve known by the physicists of the time. This theoretically small modification, although it was not easily understandable, was the first piece of a radical change of enormous proportions, a general reformulation for the microscopic world.

As a result of this first piece, another classical problem could be tackled. We are talking about the photoelectric effect. This effect involves the generation of electric current by a beam of light shining on a certain metal. The collective experience said that the probability that this effect happens was not proportional to the intensity of light, as expected by Maxwell's classical wave theory of light, but to the frequency associated to this light. In short, if the frequency was not large enough, the effect did not occur regardless of the amplitude and temporal length of exposure to light. Increasing this frequency also meant an increase in voltage (electron energy), and this pointed to a direct relationship between energy and frequency.

After Einstein became aware of Planck's breakthrough, he proposed a hypothesis based on Planck's work for this effect where light had to be constituted by packets of light, which we now call photons.^[3] As a result of applying this hypothesis, the radiation-matter interaction is now quantified. Following the reasoning, if the light contains photons energetic enough (frequency high enough), the effect will be present and it will be amplified by the amount of photons (intensity). On the contrary, if the energy of the photons is not enough, logic tells us that the effect will not occur. Empirical evidence ended up agreeing with this hypothesis^[4] and, like in the case of Planck, this theory led Einstein to the Nobel Prize that he received years later.

The quantization of the light and its interaction with matter suggested that the last could also be quantized. This idea led to the Bohr atomic model, the simplest model to explain the issue at hand. To introduce this point it should be noted that the classical theories so far lead physicists to a dead end: matter as we know it, could not exist. The electromagnetic theory of James Clerk Maxwell, one of the most elegant and accurate theories of that time, predicted that any accelerated charge emits an electromagnetic wave. Applying Maxwell's theory, the electrons should emit radiation at all times and, accordingly, lose energy until they would fall to the core. Given that these events did not happen, Bohr reasoned that if the values of energy were quantized, electrons could not be gradually losing energy but only release certain amounts.^[5] His model considered that the electrons were orbiting the nuclei, like in a planetary model, in several stable orbits without emitting light being each of these orbits associated to a discrete value of energy. Electrons can go up and down on these orbits by absorbing or releasing exactly the energy of the gap between them. Although this model has currently been outdated, the success of these ideas was spectacular and their predictions were extremely accurate. This work gave him access, like to Einstein, to the Nobel Prize years later.

Although these issues were dealt with individually as patches, they made evident the need for a completely new theoretical framework that could accommodate the treated aspects. This background, which is the basis of all the research carried out nowadays in this field, was developed in parallel by Heisenberg and Schrödinger along with their mentors Bohr and Einstein respectively among others. The first mathematical context established by Heisenberg, called matrix mechanics, was based on the concept of quantization of matter and energy previously exposed.^[6]

This interpretation complicated enormously the mathematical translation of the physical observables and led many scientists of the time to continue looking for a less abstract paradigm. That was not the case of Erwin Schrödinger, which effort led him to propose a successful equation to describe microscopic systems, based on wave mechanics.^[7]

The idea that spurred this new theory was simple. According to the hypothesis of Louis de Broglie,^[8] in the same way that light exhibits properties of particles, matter can also be understood as particle waves. Therefore, both concepts of wave and particle have to coexist as an entity for quantum-scale objects. Using this concept, Schrödinger proposed a different formulation emphasizing the wave nature of matter and light after realizing that the mathematical description of electromagnetic waves is much simpler than the description of particles and was already well-known. However, as it turned out, the result was not evident because the wave function properly fulfilling the equations of classical mechanics had the distinction of being not real but complex. This complexity was a challenging attribute to understand (was the electron real?) but the mathematical simplification compared to Heisenberg approach was so obvious that the scientific community willingly inclined towards Schrödinger's theory.

Heisenberg and Schrödinger's approaches were proved afterwards to be equivalent by complementary works of Schrödinger and others.^[9] However, this new formulation did not resolve the inherent uncertainty in microscopic systems demonstrated by Heisenberg's matrix mechanics. This uncertainty points to a fundamental limit of precision for pairs of properties that can be known simultaneously, such as position and momentum. This phenomenon was called the Heisenberg's uncertainty principle and, although it was vastly discussed and criticized, uncertainty reappeared in a probabilistic manner in Schrödinger's theory by the hands of Born.^[10] Wave mechanics will be the mathematical framework in which we are going to rationalize all light-induced processes.

In the interest of theoretically describing a system and be able to compare it with empirical results, it is necessary to take into account a complete treatment of the atom (electrons and nuclei). How we approach this depends mostly on the complexity and size of the system in study, although only a few physical systems can be fully treated with analytical solutions of Schrödinger's theory. In order to be

capable of solving case studies, an important conjecture must be applied: the Born-Oppenheimer (BO) approximation. If there were not for the BO approximation, the original formulation of Schrödinger could only be solved for chemical systems like hydrogen-like atoms or molecules, the simplest systems since they lack electron repulsion. BO approximation assumes that the motion of atomic nuclei and electrons can be handled independently considering the differences of mass, and consequently of speed, between both elements.^[1] When this assumption is applied, the Schrödinger equation can be solved separately for nuclei and electrons although it is usual to only be interested in the electronic part treating the nuclei as in fixed positions.

As a result of solving the Schrödinger equation, the total energy for a given system of interest is computed. These energies are useful when we want to study chemical processes that occur thermally by calculating the relative energies of reactants, products and transition states. In other words, “thermally” implies that all the electrons are positioned in the most stable configuration for each distribution of the nuclei all the time, what is called the ground state (GS). However, there is a different kind of processes that proceed through more energetic electronic configurations that correspond to solutions of the Schrödinger equation with higher energy values. These are called excited states and given that the systems spontaneously tend to the less energetic state, excited states tend to return to the ground state. When the energy emitted or absorbed in a change of state is light energy, the process is framed in the field of photochemistry or photophysics, depending on whether or not it leads to a different chemical species. When in this way a system is promoted to an excited state, the surplus of energy supplied by the light can allow reactions otherwise inaccessible by thermal processes.

In this context, the focus of our research is going to be centred on these photochemical and photophysical processes and the detailed description of their reaction mechanisms to explain how they occur step by step. If a hypothesis fulfils the experimental evidences, we assume that this mechanism correctly describes the reaction pathway.

Throughout history, experimental chemists have put a great deal of effort in order to obtain information about the reactions of interest. However, experimental techniques are at a disadvantage given the usual high speed in-between the steps of

the mechanisms of photochemical reactions and the importance on non-equilibrium species. The new ultra-fast techniques that have begun to appear in recent years could alleviate these problems although it will continue being a difficult task. In this landscape, the conjunction of the development of computational quantum theory and computational power has brought up a new actor in the scene. Just in a few decades, computational chemistry has become not only a complement but a powerful tool to explain and even predict chemical phenomena.

This thesis aims to deepen the knowledge of the mechanism of some fascinating photochemical reactions applying the theoretical background of wave mechanics. It is focused on the computational study of photosensitive molecular organic systems, and our goal is to elucidate the reaction and deactivation mechanisms for these compounds when they are activated by light absorption. For doing so, it is necessary to characterize the low energy electronic states and determine their role in the spectroscopy and photochemistry of each of the systems studied. Given that a chemical reaction implies movements on the nuclei, it is necessary to know the change of energy of these electronic states as a function of the nuclear positions, because these functions constitute the potentials that determine the movement of the atoms. Consequently these potentials are going to give us the clues to correctly predict the behaviour of the system under study. The graphical representation of these potentials (energy vs nuclear positions) generates multidimensional surfaces (or hypersurfaces) called potential energy surfaces, PES. The localization of singular points on these surfaces (stationary and crossing points) and the comprehension of the interaction between states are essential to offer a complete understanding of the mechanisms explored.

Unfortunately, although the computational chemistry provides methods to calculate very accurately electronic energies, the study of excited state reactivity is very demanding in methodological and computational requirements. The methods used have to be flexible enough to account for several electronic states of different nature, and to be able to provide energies with the same level of accuracy for all of them. It is also necessary to explore large areas of the PES, and the software must provide computational methods to locate and optimize the geometry of singular points. Accounting for all these requirements has proven to be unattainable for most practical cases due to time and computational demands, so the most recent

methodologies depend on the knowledge of the researcher about the characteristics of the system to be studied in order to cut out, to some extent, the scope of the problem and apply approximations that will not decrease noticeably the accuracy of the results. But we should be aware that this advantageous starting point of having some previous knowledge about the system can be a handicap if our preconceived ideas become “wishful thinking” regarding the research we develop. We have to be aware of the whole set of possible reaction paths and do not let our judgment to be limited to the more evident answers. Photochemistry offers us an almost endless supply of paths and all of them must be explored without biases.

1.2. SCOPE AND STRUCTURE

The first topic treated in this thesis is the study of the photoinduced properties of the organic family of azoderivates. Azoderivates have been used extensively in molecular switches thanks to the reversible isomerization reaction induced when absorbing UV light. This photoisomerization is extremely rapid, occurring even in picosecond timescales.

The reaction studied here takes place while light is irradiating the most stable isomer, in our case the *trans*- isomer. The irradiation allows the system to reach a high-energy state from which the relaxation path to the ground state will produce the *cis* isomer. When the source of light is turned off, the *cis* isomer can return thermally to the *trans* isomer.^[12] The elucidation of the mechanism of this reaction has been focused historically in two members of this family, azomethane and azobenzene, but the one that has focused most of the attention recently has been azobenzene. Long scrutiny on this compound has revealed one of the most interesting and unusual features: the dependence of its quantum yield of photoisomerization on the excitation wavelength. It means that there must be two different excited states accessible upon UV excitation and that both could give place to photoisomerization, following different reaction mechanisms.

In spite of the great amount of experimental evidences accumulated up to now and the computational studies that have been devoted to this system during the last forty years, the complete mechanism for this transformation is still under debate. The reason is that none of the proposed mechanisms can explain all the recently observed features, brought to light by the improved experimental techniques

developed lately. In the interest of addressing these issues, two compounds of the azo family had been studied in parallel: azobenzene and phenylazopyridine, a pyridine derivate which is an almost unknown azoderivate, selected in the frame of a collaborative project with a fellow researcher. It is expected that the detailed knowledge of these mechanisms will allow the tuning of quantum yields and rates of thermal isomerization to adapt the properties of these systems to potential specific applications like storage of solar energy in the chemical bonds. In fact, azoderivates as a base of high-energy density solar thermal fuels are a clear alternative that should be investigated.^[13]

The second system studied is related with the phenomena of photosensitization. Photosensitization is a type of light-induced reaction that is mediated by a light-absorbing molecule or photosensitizer, which transfers the absorbed energy to the target reactant that is consequently excited. The photosensitizer usually returns to its original state, while the target reactant evolves from its excited state. In this work we are interested in photosensitizers of the family of phenalenone, which can transfer the energy to the triplet ground state of molecular oxygen to generate excited singlet oxygen. Phenalenone and its phenylderivates are involved in plant self-defence strategies regulating the production of excited singlet oxygen. This oxygen species has been recognized as an important oxidizing intermediate, capable of damaging organic tissue and it has proven ability to kill microbial cells including bacteria, fungi and viruses, and even cancer cells.^[14,15] However, this ability is a double-edge sword because it can also damage healthy tissue, so in all cases it is important to keep a careful balance in the use of different photosensitizers with different levels of effectiveness in oxygen sensitization to avoid unwished secondary effects.

For this reason, plants can generate different derivatives of phenalenone, which are not equally effective in producing singlet oxygen. In fact, the parent system, phenalenone, is a very effective oxygen photosensitizer while some of their derivatives are not. This is the case of 9-phenylphenalenone, the compound studied in this thesis. Our group have already elucidated the photochemistry of phenalenone to understand its capability as oxygen sensitizer.^[16] This time, our aim is to elucidate the processes that compete with photosensitization in 9-phenylphenalenone to determine the differentiating factors between this

compound and the parent system, which make them show such different properties.

Finally, the third topic of interest is focused on the family of carotenoids. Carotenoids are organic pigments present in plants and other photosynthetic organisms. They are responsible for harvesting light and preventing tissue damage caused by the self-produced singlet oxygen. This fundamental protective effect can be achieved by either removing the excess of light from chlorophyll molecules or quenching the excited oxygen directly. Due to its antioxidant properties, the protective effect of carotenoids has been matter of extensive research for the last decades.^[17]

The implication of dark excited states (states that do not absorb or emit light directly) on the photochemistry of carotenoids was a novelty forty years ago. Since then, several dark excited states have been located by means of experimental spectroscopy and, as the structure of the members of the carotenoid family gets more complex, the number of possible photochemical processes involving excited states is enlarged.^[18] However, the pathways of these processes have only been elucidated for few carotenoids.^[19] Theoretical approach to study phenomena where dark states are involved is clearly advantageous in front of experimental techniques due to the lack of interaction between light and this kind of states. Therefore, the collaboration of the two approaches, theoretical and experimental, becomes essential.

In order to investigate the photochemical properties that make carotenoids efficient antioxidants, a member of the carotene subfamily was chosen as an object of study, dehidrosqualene. Squalene is present in many plants and animals, including humans, as a biochemical intermediate of sterols like cholesterol, steroid hormones or vitamin D and as a chemoprotective substance from cancer.^[20] All carotenes share a basic structure based on unsaturated hydrocarbons of polyene type and do not contain heteroatoms. Due to the unsaturated structure, most carotenes are planar and its most stable configuration is all-*trans*. However, the selected carotene contains sp³ carbons prone to tetrahedral geometry, so the simplification of assuming all-*trans* planar geometry for this system could be invalid.

The computational methodology used has been mainly a combination of the complete active space self-consistent field (CASSCF) with a second order perturbative treatment of the CAS reference function (CASPT2). Other methods have also been used in particular cases, like the difference dedicated configuration interaction (DDCI) method, density functional methods and even molecular mechanics methods.

On top of the intrinsic interest of knowing the mechanisms of the phenomena explained, each one of the systems mentioned will be used to calibrate computational strategies that can be used in the study of other systems of similar characteristics.

- Using phenylazopyridine as target system, a computational protocol to reproduce experimental absorption spectra of flexible systems has been analysed.
- The study of the 9-PhPN has been a challenge for the computational methods used, due to the large size of the system. We have analysed the performance of different active spaces to calibrate the accuracy of the results they provide.
- In dehidrosqualene we have studied the influence of the conformation on the excited state energies. Given the large size and the flexibility of this compound, the number of low energy conformations is enormous, so it is important to question the validity of the approximation of using the most symmetric conformation to perform the study of the excited state chemistry of this compound.

This thesis is structured as follows: Chapter 2 lay out the key concepts to be considered in studies of molecular photochemistry. Chapter 3 describes the theoretical methodologies and tools related to the elaboration of this research. Chapter 4 is committed to the elucidation of the photoisomerization reaction mechanism for azoderivates. Chapter 5 is dedicated to the competitive photochemical processes present in phenylphenalenone derivates that make them more or less effective in oxygen photosensitization. Possible derived photoproducts were also studied. In chapter 6 the photochemistry of carotenoids as antioxidants is

explored. Also, structural flexibility is analysed and commented. Finally in chapter 7, the main conclusions extracted from previous chapters are collected.

1.3. OBJECTIVES

The final objectives of this thesis have two aspects: first to elucidate the processes that explain the photochemical properties of some organic compounds, and second, to calibrate computational strategies that could be used in systems which size or complexity do not allow the use of standard methodologies.

These objectives can be detailed as follows.

- To elucidate the mechanism of the *trans-cis* photoisomerization of azobenzene and phenylazopyridine. The mechanism proposed for azobenzene should explain the dependence of the isomerization quantum yields on the initial excitation and on the degree of constraint of the rotation of the system.
- To reproduce the experimental absorption spectrum of phenylazopyridine in methanol.
- To determine the photoprocess that competes with population of the triplet states in 9-phenylphenalenone and is responsible of the low quantum yield of singlet oxygen sensitization that this compound shows in comparison with its parent system, phenalenone.
- To calibrate different reductions of the active spaces in ab initio configurational methods to be applied to large systems, by means of the comparison of the results obtained when applied to the study of 9-phenylphenalenone.
- To determine the nature of the low energy excited states of dehidrosqualene, the interplay between them and the role they play in the photochemistry of this compound.
- To analyse the influence on the accuracy of the computed energies of excited states when, in flexible systems like dehidrosqualene where many conformations can coexist, only the most symmetric conformation is taken into account.

1.4. BIBLIOGRAPHY

1. Planck, M. *Ann. Phys.*, **1901**, 4, 553.
2. Planck, M. *Dtsch. Phys. Ges.*, **1900**, 2, 202.
3. Einstein, A. *Ann. Phys.*, **1905**, 17, 132.
4. Millikan, R. *Phys. Rev.*, **1914**, 4, 73.
5. Bohr, N. *Phyl. Mag.*, **1913**, 26, 1.
6. Heisenberg, W. *Z. Phys.*, **1925**, 33, 879.
7. Schrödinger, E. *Naturwissenschaften*, **1926**, 14, 664.
8. de Broglie, L. *Compt. Ren.*, **1923**, 177, 507.
9. Schrödinger, E. *Ann. Phys.*, **1926**, 79, 734.
10. Born, M. *Z. Phys.*, **1926**, 37, 863.
11. Born, M., Oppenheimer, R. *Ann. Phys.*, **1927**, 84, 457.
12. Griffiths, J. *J. Chem. Soc. Rev.*, **1972**, 1, 481.
13. Kolpak, A. M. *Nano Lett.*, **2011**, 11, 3156.
14. Grossweiner, L. I. *The science of phototherapy: An introduction* Netherlands, **2005**.
15. C. Flors, C., Fryer, M. J., Waring, J., Reeder, B., Bechtold, U., Mullineaux, P. M., Nonell, S., Wilson, M.T., Baker, N. R. *J. Exp. Bot.*, **2006**, 57, 1725.
16. Segado, M., Reguero, M. *Phys. Chem. Chem. Phys.*, **2011**, 13, 4138.
17. Edge, R., McGarvey, D. J., Truscott, T. G. *J. Photochem. Photobiol. B*, **1997**, 41, 189.
18. Polívka, T., Sundström, V. *Chem. Phys. Lett.*, **2009**, 477, 1.
19. Polívka, T., Sundström, V. *Chem. Rev.*, **2004**, 2021.
20. Nishino, H. *J. Cell. Biochem.*, **1997**, 67, 86.

SECOND CHAPTER:

MOLECULAR PHOTOCHEMISTRY

2.1. APPROACH TO SCHRÖDINGER'S THEORY

Molecular photochemistry is a branch of chemistry concerned with the chemical processes where light is involved in systems formed by a few molecules. Usually, the process is initiated by light absorption.^[1] The range of frequencies of light that most commonly induce transitions between the electronic levels of an organic molecule is UV–visible (200–700 nm). Eventually, the promoted electrons have to return to the ground state electronic configuration. These phenomena can be unfolded in two directions, either finding a path that ends up giving different products (in photoreactive systems) or returning to the original compound (in photostable ones). The extra energy obtained by light absorption allows the system surmounts barriers that would be otherwise inaccessible. Therefore, photochemical reactions proceed differently than thermal reactions because the first ones have open reactivity channels that are inaccessible for thermal processes.

In order to study theoretically these processes, the formalism of quantum mechanics is necessary since Newton's laws of motion do not apply to atomic and molecular systems. The equivalent equation in this realm is the time-dependent Schrödinger equation, equation named after Erwin Schrödinger who developed this

approach in 1926.^[2] His equation is a differential equation that describes how the quantum state of a physical system changes over time as

$$i\hbar \frac{\partial}{\partial t} \psi(\vec{q}, t) = \hat{H} \psi(\vec{q}, t)$$

This equation defines a (non-relativistic) particle of mass moving along the space. In his approach, the quantum state of a system is described by a complex wave function, which contains all the information about it, and that depends on both nuclear and electronic coordinates, represented by \vec{q} , and on the time (t). Although ψ is not real, by applying suitable mathematical operators, real values of observables can be obtained. In this case, \hat{H} represents the Hamiltonian operator that accounts for the sum of the kinetic plus potential energy of the particles that form the system, and is given by

$$\hat{H} = \left(\frac{-\hbar^2}{2m} \nabla^2 + V(\vec{q}, t) \right)$$

A particular solution of this equation has centred most of the efforts:

When ψ is an eigenfunction of the Hamiltonian operator, ψ corresponds to a stationary state and the eigenvalue E is the energy of the state ψ .

This statement means that in many problems the Schrödinger potential $V(\vec{q}, t)$ has not explicit time dependence and, in these cases, time coordinates of the wavefunction can be decoupled from the space coordinates. This separation leads the wavefunction to be a product of two functions, one spatial and one temporal

$$\psi(\vec{q}, t) = \psi(\vec{q})\phi(t)$$

Separating terms, the resulting equation

$$\hat{H}\psi(\vec{q}) = E\psi(\vec{q})$$

is known as the time-independent Schrödinger equation. This equation does not have a single solution. To solve it means to find all the eigenfunctions ψ that fulfil the equation, and their corresponding eigenvalues E . The set of all eigenvalues constitutes the spectrum of the Hamiltonian and contains a discrete part and also a continuous part.

2.2. BORN-OPPENHEIMER APPROXIMATION

Due to its complexity, solving the Schrödinger equation to acquire all the relevant information of a chemical system is only feasible for very simple cases. In the context of atomic and molecular systems, the Born-Oppenheimer approximation (BO) was devised to allow separating again the wavefunction into its electronic and nuclear terms. This approximation, which is ubiquitous in quantum chemistry, is based on the great difference between the nuclear and electronic masses. This difference makes the nuclei to be considered as stationary because the speed of their movement is much smaller than the speed of the electrons. First, the Hamiltonian operator can be separated accordingly in terms corresponding to these two kind of particles

$$\hat{H} = \hat{H}_e + \hat{H}_N$$

where

$$\hat{H} = \underbrace{-\sum_i \frac{1}{2} \nabla_i^2 - \sum_{i,A} \frac{Z_A}{r_{iA}} + \sum_{i>j} \frac{1}{r_{ij}}}_{\hat{H}_e = \hat{T}_e + \hat{V}_{ee} + \hat{V}_{Ne}} - \underbrace{\sum_A \frac{1}{2M_A} \nabla_A^2 + \sum_{A>B} \frac{Z_A Z_B}{R_{AB}}}_{\hat{H}_N = \hat{T}_N + \hat{V}_{NN}}$$

Applying the BO approximation (assuming stationary nuclei), nuclear kinetic energy of the nuclei \hat{T}_N is neglected and the repulsion \hat{V}_{NN} between nuclei is considered constant although the electrons can still “feel” the nuclei attraction as point charges. The remaining Hamiltonian is

$$\hat{H} = -\sum_i \frac{1}{2} \nabla_i^2 - \sum_{i,A} \frac{Z_A}{r_{iA}} + \sum_{i>j} \frac{1}{r_{ij}} + \overbrace{\sum_{A>B} \frac{Z_A Z_B}{R_{AB}}}^{\text{Constant}}$$

$$\hat{H} = \hat{H}_e + ct.$$

But any constant added to an operator only adds to the operator eigenvalues (energies) and has no effect on the operator eigenfunctions (wavefunction of the system). Therefore, using the electronic Hamiltonian in the Schrödinger equation, we will obtain the electronic wavefunction which describes the quantum motion of the electrons.

$$\widehat{H}_e \phi(\vec{r}; \vec{R}) = E_e \phi(\vec{r}; \vec{R})$$

where the energy obtained as the eigenvalue will only be the electronic energy. However, this approach does not subdivide the problem into two completely independent parts, because the resolution of this electronic equation depends explicitly on the electronic coordinates \vec{r} but also parametrically on the nuclear coordinates \vec{R} . This implicit dependence means that the electronic wavefunction depends on the arrangements of the nuclei. Finally, the total energy of the system is calculated for fixed nuclei adding the constant nuclear repulsion.

$$E_{tot} = E_{elec} + \sum_{A=1}^M \sum_{B>A}^M \frac{Z_A Z_B}{R_{AB}}$$

Although BO approximation is useful in many cases, this approximation cannot be applied if the speeds of the nuclei and electrons are of the same order or if a small change in the positions of the nuclei leads to a large change in the electronic wavefunction. In these cases the BO approximation breaks down, but even then it keeps its usefulness as a conceptual tool and will continue being used due to the simplification that it brings of the resolution of the Schrödinger equation.

2.3. POTENTIAL ENERGY SURFACES

A potential energy surface (PES) is a mathematical function that gives the energy of a molecule as a function of its geometry.^[3] This concept arises as a result of the separation of terms brought to the Schrödinger equation by the BO approximation, where the energy is calculated for each nuclear configuration. A set of calculated energy values resulting of infinitesimally changing the nuclear geometry configures these surfaces. For their graphical representation, energy is placed on the vertical axis and the nuclear coordinates on the horizontal axis. These nuclear coordinates can be defined as a function of one or more internal coordinates depending on the

Second chapter: Molecular photochemistry

changes of the molecular structure that are interesting for the particular problem studied. It can be simply a bond distance, or a complex combination of nuclear motions. We must bear in mind that a molecule of N atoms will have $3N$ coordinates, although three of them are translations and others three are rotations (two if the molecule is linear) that are not energetically relevant. The total energy of the system depends, then, on $3N-6(5)$ coordinates that are the variables. This function of the energy gives birth to a hypersurface, hardly comprehensible for our minds that work in a 3-dimensional space. This is the reason why it is usual to project these hypersurfaces into 2D or 3D representations, but it is essential to keep the possible maximum amount of relevant information to be able to understand the complexity of each and every system.

Due to their power to represent complex situations, PESs have become fundamental to elucidate detailed descriptions of reaction mechanisms. The processes that altogether form a reaction mechanism can be divided on thermal and photochemical depending on the kind of energy involved in them, thermal or luminesce. There is another feature that characterizes these phenomena, that is the number of PES involved in the process: while thermal reactions involve only the surface of the ground state, in photochemical reactions there are at least two PES that play a role in the electronic transitions (often the ground state and one excited state).

In all cases, the description of the topography of these surfaces is the first aim of the computational study because the topographical features of the PES govern the different possible outcomes that can unfold. In thermal reactions only the topography of the ground state surface needs to be studied. On the other hand, photochemical reactions are more complicated to be studied because usually not only the topography of the surfaces is important, but also the interaction between them. The crucial difference between these concepts is that while the topography of a surface can be described in general terms inside the BO approximation, the interaction cannot. This distinction gives birth to a classification of the processes in adiabatic (in the adiabatic approximation or BO) and non-adiabatic (where the BO approximation cannot be applied).

Following this description, once matter is excited, there are two possible kind of pathways in which a molecule can deexcite. The first pathway is through non-

adiabatic processes that take place when in a specific nuclear disposition two states are degenerate (they have the same energy) so a transfer between surfaces is probable. In this change of electronic state there is not any kind of emission, so this decay process is non-radiative. This phenomenon is mathematically characterized as a conical surface (double cone) and it acts like a funnel between surfaces for a change of electronic state of the same spin. If a reaction path can reach the ground state using only these channels, no emission will be present. The efficiency of these non-adiabatic points is crucial in many reaction mechanisms so conical intersections will be analysed in more detail. In contrast, adiabatic processes occur when there is not an implication of other excited states than the one which absorbed the irradiation. If after adiabatically reaching the minimum of the excited state surface the gap with the ground state is large, the emission of a photon can take place in order to radiatively decay back to the ground state. These phenomena are primary processes, and the real reaction mechanisms often combine both of them. As an example, it is conceivable, and also frequent, to find systems where the emitting excited state is different from the one that absorbed the energy as a result of a previous non-adiabatic crossing between excited state surfaces.

2.4. MATTER-RADIATION INTERACTION

All absorption and emission processes occur when an electromagnetic wave interacts with an atom or molecule. If the energy of the light is equivalent to the transition gap between two stationary electronic states, the coupling of both electric fields enables a transition. These electronic transitions occur in a time scale much smaller than the one of the movement of the nuclei, so it is assumed that there are not geometrical changes during the transition. This rule is called Franck-Condon principle and, on the potential energy surfaces where geometrical change is represented on the horizontal axis, absorptions and emissions are consequently visualized as vertical transitions.^[4]

However, the probability for a photon to be absorbed or emitted between a given couple of selected stationary states, not only depends on the irradiated energy but also on the states involved. During the irradiation, the molecule is polarized inducing a Transition Dipole Moment (TDM). This dipole moment can be represented as a vector that quantifies the phase factor between two states and it is

Second chapter: Molecular photochemistry

usually measured in Debye (D). The transition dipole moment is calculated applying the dipole moment operator on the wavefunctions

$$TDM_{n \rightarrow m} = \sum_{\alpha=x,y,z} \langle \phi_n | \hat{\mu}_\alpha | \phi_m \rangle$$

where ϕ_n and ϕ_m represent the wavefunction of the initial (n) and final (m) states of the transition and $\hat{\mu}$ the dipole moment operator of the radiation in each direction of space. The square of TDM is proportional to the intensity of the interaction, a magnitude called oscillator strength, which is a classical measurement of the absorption and emission probability. This value allows predicting which excited state of a particular system has the highest probability of light absorption and emission. The exact relation between TDM and the oscillator strength, f , is:

$$f = \frac{2}{3} |TDM_{n \rightarrow m}|^2 \Delta E_{nm}$$

However, we have to be aware that f is a measure of probability and it is usually calculated under several approximations. Therefore, possible absorption (or emission) by other states must not be discarded. Moreover, as explained in the previous section, several excited states can be populated indirectly so, when analysing the states that can be involved in a reaction mechanisms, all the low energy states should be investigated. This task is not trivial because usually several competing processes can take place. It is necessary, then, not only to identify the possible processes, but also to predict which one will be more probable and in which proportion.

Let us analyse the steps of a photochemical reaction. Starting immediately upon absorption, the first deactivation process is vibrational relaxation. This is a very fast process that occurs when part of the absorbed energy is diffused as kinetic energy between vibrational levels so during this step the electronic state is unchanged. However, in order to complete the deactivation from the excited state, the electronic level must change and therefore, different deactivation processes have to take control. If the excited state populated by the radiation is a high excited state, it is usual that the fastest process is the non-radiative decay by means of vibrational coupling because vibrational levels strongly overlap within the electronic levels.

This preference changes when the system reaches the lowest excited states, where the probability of these processes is substantially lower. In low-energy states, the fastest process is the relaxation (change of geometry) following the gradient of the surface, that is, following the coordinate that more quickly decreases the energy. Eventually, the system can reach a point of minimum energy of the surface, which represents a stable species. However, if along this minimum energy path or in its vicinity there is a crossing of surfaces, an additional radiationless process can be open. Through these points of degeneracy of electronic states a transition can happen. If the states involved in the transition are of the same multiplicity, the process is called Internal Conversion (IC), while if the states have different multiplicity we talk of an Intersystem Crossing (ISC). The probability of the transition greatly depends on the multiplicity of the states involved.

Deactivation can also proceed through radiative processes although they usually take place only from the lowest excited state as stated by Kasha's rules.^[5] Due to the light emission, these phenomena are also known as photoluminescence. There are two types of photoluminescence depending on the multiplicity of the emitting excited species. If the emitting state has the same multiplicity as the ground state, the transition is allowed and the process, called fluorescence, is very fast. The emitting species has consequently short lifetime.

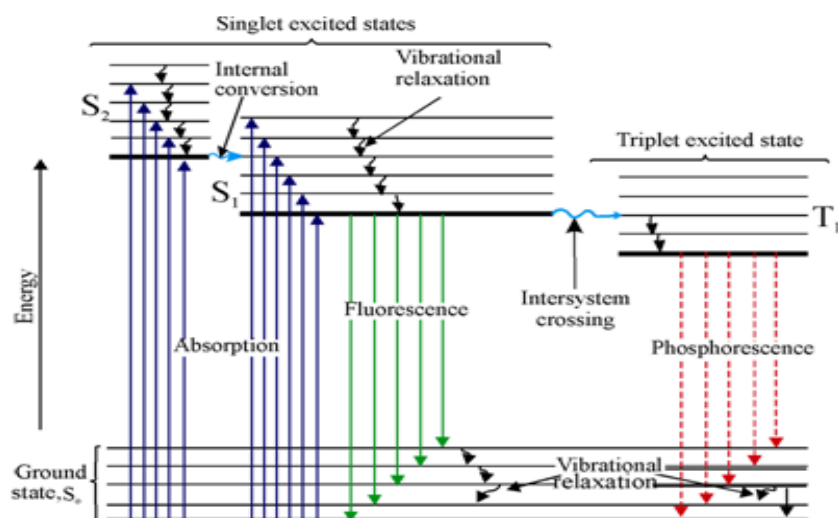


Figure 2.1 – Jablonski diagram.

On the other hand, if the multiplicity of the excited state is different from that of the ground state, this process is called phosphorescence and it corresponds to a slower emission, associated with forbidden transitions. Taking into account that the ground state is almost always a singlet, phosphorescence can take place only if a higher multiplicity is populated through a non-radiative interaction. In order to study all the possible processes, a diagram is used to illustrate the electronic states of a molecule and the transitions between them. This diagram is called Jablonski diagram (Figure 2.1) and both radiative and non-radiative mechanisms are represented in it.

2.5. NON-ADIABATIC INTERACTIONS

In the previous two sections, a general overview of the possible reaction paths in photochemistry has been outlined. One of the most important aspects treated in this overview is that the Born-Oppenheimer approximation, even though is very useful in most cases, fails in the proximity of crossings between surfaces. The reason for this failure is that BO approximation considers the coupling between electronic distribution and nuclear movement to be zero. Given that in the vicinity of these interaction points a small change in the position of the nuclei leads to a large change in the electronic configurations, this approximation is not valid in these circumstances. To understand the function of these surface crossings is very useful to draw parallels with the concept of transition states in thermal reactions. A transition state symbolizes the decisive step between two chemical species located on the same surface, while a conical intersection embody the same concept but between electronic states.^[6] Therefore, the location of these surface crossings or conical intersections, as they are called, is crucial in the study of photochemical reactions.

Being aware of the important significance of the crossings, Hund proposed in 1927 a qualitative argument stating that if two potential curves cross, the electronic states must be degenerate at the point of crossing.^[7] Two years later, von Neumann and Wigner mathematically demonstrated that the potential energy surfaces of electronic states in diatomic molecules cannot cross if the involved states have the same symmetry.^[8] The essence of their proof, also pointed out by Teller,^[9] was as follows: We consider two intersecting adiabatic electronic states ψ_1 and ψ_2 , which are expanded in terms of two non-adiabatic states ϕ_1 and ϕ_2 ,

$$\psi_1 = c_{11}\phi_1 + c_{21}\phi_2$$

$$\psi_2 = c_{12}\phi_1 + c_{22}\phi_2$$

ϕ_1 and ϕ_2 are orthogonal to all the remaining electronic states and to each other. The adiabatic electronic energies are the eigenvalues of the Hamiltonian matrix

$$H = \begin{pmatrix} H_{11} & H_{12} \\ H_{21} & H_{22} \end{pmatrix}$$

where $H_{ij} = \langle \phi_i | H | \phi_j \rangle$. The eigenvalues of H are given by

$$E_{1,2} = \frac{(H_{11} + H_{22})}{2} \pm \sqrt{(H_{11} - H_{22})^2/4 + H_{12}^2}$$

At the point of intersection between excited state surfaces, the energy of both states must be equal so in order to obtain those solutions, two conditions must be enforced.

$$H_{11} = H_{22} \quad \text{and} \quad H_{12} = H_{21} = 0$$

Fulfilling the first condition will ensure the energetic degeneration between states while the second condition indicates that the interaction between states have to be zero in a real crossing. In terms of crossing, the first condition constitutes the crossing although without the additional non-interaction condition this crossing could be avoided. In this case, there is an energy separation between the involved states due to H_{12} despite the equivalent values of H_{11} and H_{22} .

To fulfil these two conditions, two independent nuclear coordinates must have some determined values. Taking into account that a diatomic molecule only has one independent coordinate ($3N-5=1$, the nucleus-nucleus distance), it is clear why it is not possible to fulfil the two conditions for the crossing in diatomic systems. Therefore, H_{12} cannot be different from zero between states of the same symmetry and the non-crossing rule will apply. However, in the cases where the two electronic terms considered are of different symmetry (spatial or spin), the matrix element H_{12} vanishes identically and only one equation remains, which can be satisfied.^[10] In the case of polyatomic molecules, the situation is more complex since the number of coordinates is more than enough to archive degeneracy even

Second chapter: Molecular photochemistry

between states of the same symmetry. In these polyatomic systems, two dimensions can be distinguished from the rest in a conical intersection, which are the first derivatives against the nuclear coordinates of the conditions of the conical intersection:

$$X_1 = \frac{\partial(H_{ii} - H_{jj})}{\partial q} \quad X_2 = \frac{\partial H_{ij}}{\partial q}$$

These coordinates develop a subspace called branching space that contains all the combinations of nuclear movements which lifts the degeneracy. These two vectors are called Gradient Difference (X_1) and Derivative Coupling (X_2) and form the orthogonal plane that cut the double cone region characteristic of a conical intersection (Figure 2.2). This nomenclature is the most widespread although funnel or bi-funnel have also been historically used.^[11,12] The remaining space, after the reduction to the $3N-6(5)-2$ degrees of freedom, is called the intersection space, where the two states remain degenerated. This space consists in a hyperline of infinite points where the energies of both states can change but the degeneracy continues. Most usually the lowest energy point of degeneracy (the minimum in the intersection space) is the most chemically interesting.

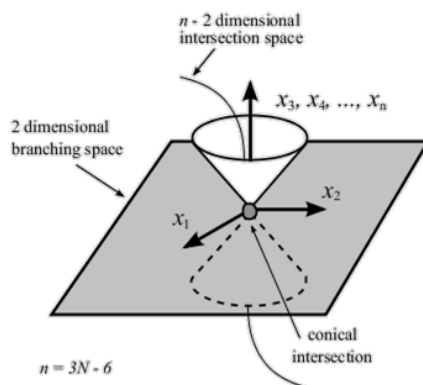


Figure 2.2 – Representation of a conical intersection.

Conical intersections can also be classified by the topology of the surfaces involved near the crossing. The nomenclature for this was established for Ruedenberg and it defines the evolution of an excited reactant when it reaches a crossing (Figure 2.3). The first case is the peaked intersection where the vertex of the crossing is the

highest energy point of the lower surface and the lowest point for the upper surface. This topography is usually a very efficient path to allow the radiationless decay to a lower excited state or to the ground state. In most cases, since the gradients of the two surfaces have opposite sign, there are two accessible minima one of each electronic state at the lower surface. The second type is the sloped intersection which is characterized by a crossing point that is not the lowest point for the upper surface. This trait means that there is an energetic barrier between the minimum and the crossing point that could partially hinder the decay. Moreover, this type of intersection has gradients with the same sign on both surfaces and they are useful in photophysics because both minima (of lower and upper states) are energetically lower than the intersection. A third type of conical intersection called intermediate is usually mentioned to cover the possibility of gradient zero around the critical point.^[13]

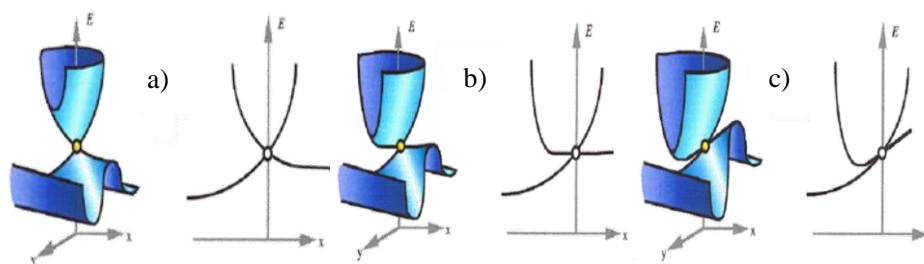


Figure 2.3 – Types of conical intersections. a) peaked; b) intermediate; c) sloped.

However, the topology near the conical intersection is not the only key aspect in play. There are two additional important features: the position of the funnel along the reaction coordinates and the topology on the interacting states before and after reaching the crossing. In the first case, there could be conical intersections close to the reactants that lead the relaxation paths back to the original compound or close to photoproducts so that not-adiabatic processes take place once all the geometrical changes have occurred. In the second case, the presence of energy barriers or local minima on the upper state before reaching the conical intersection could be obstacles that affect the reactivity.

As stated before, the existence of a conical intersection is bounded to two conditions. However, the failure to comply the non-interacting condition could energetically separate the states as happens in the vicinity of this critical point.

Even when H_{11} and H_{22} values are equal, if H_{12} is not zero, the energies of the states involved are given by:

$$E_1 = H_{11} - H_{12}$$
$$E_2 = H_{11} + H_{12}$$

Depending on how large is the value of the exchange term H_{12} , the depth of the avoided crossing will vary significantly. If the difference is small, a small change of geometry will involve a substantial modification of the wavefunction while, if the difference is large, the modification will be slower. At the crossing point, the calculated energies now represent a minimum for the upper surface and a transition state for the lower one.

At the end of the 1980s, improved computational methodologies became available which were suitable for computing ground and excited states in a balanced way. This computational support gave rise to a new conception for conical intersections, which were considered before as extremely rare or inaccessible, and that now are known to be frequent if not ubiquitous in organic systems.

2.6. BIBLIOGRAPHY

1. Klessinger, M., Michl, J. *Excited states and photochemistry of organic molecules*; VCH Publishers: New York, **1994**.
2. Schrödinger, E. *Naturwissenschaften*, **1926**, *14*, 664.
3. Truhlar, D. G. *Potential Energy Surfaces* New York, **2001**; Vol. 13.
4. Condon, E. *Phys. Rev.*, **1926**, *25*, 1182.
5. Kasha, M. *Farad. Discuss.*, **1950**, *9*, 14.
6. Bernardi, F., Olivucci, M., Robb, M. A. *Chem. Soc. Rev.*, **1996**, 321.
7. Hund, F. *Z. Physik*, **1927**, *40*, 742.
8. Von Neumann, J., Wigner, E. P. *Z. Physik*, **1929**, *30*, 467.
9. Teller, E. *J. Phys. Chem.*, **1937**, *41*, 109.
10. Landau, L. D., Lifshitz, E. M. *Quantum chemistry (Non-relativistic theory)* Moscow, **1963**.
11. Zimmerman, H. E. *J. Am. Chem. Soc.*, **1966**, *88*, 1566.
12. Michl, J. *J. Mol. Photochem.*, **1972**, *4*, 243.

-
13. Domcke, W., Yarkony, D., Köppel, H. *Conical intersections: Electronic structure, dynamics & spectroscopy*; World Scientific Publishing: Singapore, **2004**.

THIRD CHAPTER:

THEORY AND APPLIED METHODS

In the previous chapter, we have introduced the basic concepts and approximations essential for the description of the reactivity of any photochemical system. However, this objective can only be achieved if we are able to solve the Schrödinger equation for the system of interest, and to describe the topography of the potential energy surfaces that represent the electronic states involved in the reactivity. But in the case of polyelectronic systems, it is not possible to solve exactly the Schrödinger equation, so the application of approximations is required and the use of computational methods a real need. But even in this case, the complexity grows rapidly with the number of electrons and the extremely high computational cost points to the necessity of devising computationally efficient approximations to solve the mathematical problem. It is for this reason that new methods have been being continuously developed since last century to face this goal.

This chapter is going to provide general information about the computational methods used throughout the studies presented in this thesis and other related necessary aspects. Focusing on the field of theoretical photochemistry, the aim is the description of the photochemical process of absorption, relaxation, deexcitation and emission in which several excited states could be involved. However, in order to study in a balanced way both ground state and excited states, it is essential to

include more than a single electronic configuration in the wavefunction, which is the usual choice for thermal ground state processes.

In this section, therefore, we will mostly present an overview of multiconfigurational methods, which are implemented in several computational packages. Specifically, the list of employed ab initio methods includes: Complete Active Space Self Consistent Field (CASSCF),^[1] second order perturbation theory on top of CASSCF (CASPT2),^[2] the restricted version of both (RASSCF and RASPT2)^[3] and the variational DDCI method.^[4] In cases where only the ground state had to be explored, the theoretical framework of DFT has been used, since it offers the possibility of having accurate energies at relatively low cost. We have also used molecular dynamics and the classical approach of molecular mechanics for a conformational study. In some cases we also have included solvent effects by means of the polarizable continuum model (PCM). These methodologies are going to be summarized here to give a frame for the works presented in the next chapters, without the intention of a detailed description of the methodology used, which is beyond the scope of this PhD dissertation.

The standard computational package used in this thesis has been MOLCAS 7.6.^[5] Gaussian 09 (Revision C.01) code^[6] has been used to localize conical intersections (procedure not fully implemented in MOLCAS), when solvent effects had to be included and for DFT and molecular mechanics calculations with the UFF force field.^[7] For molecular dynamics we have used the package Gromacs 4.5.4^[8] with AMBER99 force field.^[9] In the case of DDCI calculations, the suite of programs CASDI has been used.^[10]

3.1. THE HARTREE-FOCK BASED METHODS

Hartree-Fock is one of the simplest methodologies of approximation to the wavefunction and the energy of a quantum many-body system and its origins date back to the late 1920s, shortly after the discovery of the Schrödinger equation in 1926. The basis for this method was devised by D. R. Hartree and it is based in a simple principle: The approximate wavefunction is given by a linear combination of antisymmetrized products of one electron functions called spin-orbitals, in turn composed of a spatial function (orbital) and a spin function. This antisymmetric combination, proposed by V. A. Fock in 1930, was necessary in order to satisfy the Pauli principle and is usually represented as a determinant called Slater

Third chapter: Theory and applied methods

determinant. Starting from a set of orbitals as guess and applying the variational principle, the HF non-linear equations^[11,12] are capable of generating the lowest-energy determinant by means of iteratively varying the spin orbitals in a process that is called Self-Consistent Field (SCF). In fact, this is equivalent to find the molecular orbitals that best describe the system of interest, which are defined as linear combination of the atomic orbitals.

However, this approach also lies on several simplifications that, if not corrected, can lead to large deviations from experimental results. One of the most important and to which more efforts have been devoted is the inclusion of the electron correlation that is completely neglected in HF through the mean field approximation. Within this approximation, the electron-electron interaction is replaced by an interaction between each electron and an average field formed by the remaining electrons simplifying the issue from an n-body system to a 1-body problem. This change clears up the resolution of many-body interactions that usually are very difficult to solve but also omits the instant effect of the other electrons on the motion of each electron. This effect is what is called electron correlation and it must be included if the goal is to improve the description of any system.

This electron correlation is sometimes divided into two qualitatively different kinds of correlation: dynamic and non-dynamic. Dynamic correlation refers to the instantaneous electron-electron repulsion due to their relative movement. On the other hand, the non-dynamic correlation term was created to account for the nearly degenerate electronic configurations responsible for the difference between the total electron correlation energy and the dynamic correlation. This situation can be illustrated with the H₂ case where the electronic configuration that defines the ground state in a minimal basis set corresponds to both electrons occupying the σ molecular orbital: $|\phi_{\sigma}\bar{\phi}_{\sigma}\rangle$. If we write this determinant in the basis of atomic spin orbitals, the result looks like a sum of four determinants

$$|\phi_{\sigma}\bar{\phi}_{\sigma}\rangle = |\phi_A\bar{\phi}_A\rangle + |\phi_A\bar{\phi}_B\rangle + |\phi_B\bar{\phi}_A\rangle + |\phi_B\bar{\phi}_B\rangle$$

It is important to realize that the first and last terms are ionic structures where both electrons are placed on the same hydrogen atom. Following the example, if we stretch H₂ molecule, the contribution of these ionic structures becomes required in

the description of HF, which only assumes that one electron configurations is dominant. However, these structures should not contribute to the wavefunction and, in fact, due to these terms the interaction energy is overestimated. In order to cancel the ionic terms, let us consider an excited state where both electrons are in the antibonding σ orbital and combine both wavefunctions linearly (both contains a mixture of covalent and ionic terms). From this configuration interaction, the correct asymptotic wavefunction is obtained, where the ionic terms are cancelled exactly but at the expense of needing more than one determinant to describe the electronic structure of the states. Similar cases are very common in excited states of organic molecules, so they have to be dealt correctly within the photochemical problems studied in this work.

Despite these definitions, there is not a clear physical separation between both (dynamic and non-dynamic) terms, although both correlations are better accounted for when increasing the flexibility in the description of the electronic structure. This can be accomplished by expanding the number of determinants in the quantum calculations, what is usually strictly limited by the computational cost. For this reason, several approaches have been devised in order to truncate the expansion keeping the most part of the correlation, although some have proved to be more effective than others in doing so. Several of them have been applied in this work, and these are going to be described in the following sections.

3.1.1. Multiconfigurational methods using Active Spaces: CASSCF and RASSCF

The first method treated here is CASSCF, which is nowadays the most widely one used for describing excited states. In this methodology an active space is defined, formed by those molecular orbitals that show an occupation significantly far from 2 or 0 in any of the states or geometries of interest. A finite set of determinants is generated by all possible combinations of occupation numbers of these “active” orbitals with their electrons. These determinants are used then in the configuration interaction that expands the wavefunction that describes the state of the system. Those linear combinations are referred to as Configuration State Functions or CSF's and, unlike in other methods, they are optimized varying both orbital and wavefunction coefficients to obtain the description of the electronic distribution with the lowest possible energy. On the other hand, this differential treatment for a set of orbitals leaves behind the not active orbitals, which are going to be treated as in HF. Among these ones, there is a first set of orbitals, referred to as inactive, that

Third chapter: Theory and applied methods

remain double occupied in all cases. The number of inactive electrons is easily deductible because they are twice the number of inactive orbitals. The rest of the orbitals, which are referred to as virtual, are not going to be populated in any case. The size of this set depends on the basis set chosen for the calculations.

From this description of the method it is easy to derive that choosing correctly the active space will largely determine the success of any study carried out using this methodology. Given that the CASCF energy depends on the active space used, to be sure that the energies obtained at different points of the potential energy surfaces for different states are comparable, the active space used in all calculations should be the same. Unfortunately, this is not always possible. In these cases care should be taken when calculating relative energies since they can provide good qualitative results, but quantitative accuracy is doubtful. It is useful to know that this methodology also ensures that any rotation inside the active subset do not affect the value of the energy.

However, even with the use of an active space, the complete expansion of the CAS wavefunction could still be too large, to the extent that we can be forced to leave out orbitals that could have some weight in the description of the reaction studied. In these cases, a more flexible formulation of CASSCF can help by dividing the active space in several subspaces using chemical intuition and also careful evaluation, so that we can reduce the computational cost. This methodology is called RASSCF (for Restricted Active Space), and divide the active space in the consecutive subspaces, RAS1, RAS2 and RAS3, where different levels of restrictions are imposed.

- RAS1 subspace consists of the set of orbitals with occupation close to 2, from which a limited number of excitations are allowed. This number has been set to two in the cases that RASSCF method has been used in this work.
- RAS2 subspace is the equivalent to the active space in CAS so it is formed by the relevant orbitals that are expected to have partial occupations (significantly different from zero and two).
- RAS3 subspace will include the orbitals with occupations close to zero, where a limited number of excitations are allowed (two in the use of the RASSCF method in this work).

Two techniques that modify the implementation of the computation of the active space methods have been used systematically in this thesis. The first one is the level shift technique that helps to avoid oscillating convergence of the SCF by increasing the energy of the virtual orbitals in cases of degeneration of the wavefunction or mixing of states.^[13] In second place, the state average formalism has been employed, in which one single set of molecular orbitals is used to compute all the states of a given spatial and spin symmetry. This approach is very useful when high energy excited states must be obtained because it is difficult to converge these calculations due to root flipping or other numerical problems derived from the near degeneracy of the states.

Given that wavefunctions describe states of the systems, they can be used to obtain other properties apart from energy. Especially significant in this work is the calculation of transition dipole moments, which are proportional to the transition probabilities between states. This information has been obtained using a CAS State Interaction methodology (CASSI) implemented in the MOLCAS package, which provides transition density matrices to quantify the interaction between several wavefunctions.^[14]

3.1.2. Second order perturbation approximation on Active Space: CASPT2 method

Although CASSCF is one of the most appropriate methods to describe the potential energy surfaces for ground and excited states, it suffers from a drawback which is the lack of inclusion of the dynamic correlation. As said before, the static correlation is accounted by the multiconfigurational character of the wavefunction and it is fully included in the formalism. However, only the part of the dynamic correlation due to the active electrons is included causing that, unfortunately, CASSCF is not able to provide quantitatively accurate energies in some cases especially when working with excited states.

In order to take into account as much as possible of the full electron correlation derived from electron-electron interaction, therefore, this method is usually applied in combination with second order perturbation theory (CASPT2) because it has shown not only to be precise but also efficient. Although CASPT2 is going to be discussed, the same relationship can be extended to the restricted version RASPT2. The perturbative approach was inspired by the division of the Hamiltonian operator already proposed for Møller and Plesset in 1934^[15] that involve the

Third chapter: Theory and applied methods

separation of the total Hamiltonian in two parts. The first part consists in an unperturbed reference Hamiltonian (H_0), coupled with a second term (V) that represents a weak perturbation to the system:

$$\hat{H} = \hat{H}_0 + \hat{V}$$

Assuming that the exact solutions of the equation

$$\hat{H}_0\psi^{(0)} = E^{(0)}\psi^{(0)}$$

are already known, the eigenfunctions and eigenvalues of the total Hamiltonian are found solving

$$\hat{H}\psi = (\hat{H}_0 + \hat{V})\psi = E\psi$$

In the CASPT2 method the reference Hamiltonian is the CASSCF one, and the perturbation includes the electron correlation. If the disturbance is not too large, this can be expressed and calculated as a correction using approximate methods. The resulting wavefunctions and absolute energies are expected to be only slightly different, in the sense that the correlation recovery is not large, but it is incredibly important. To improve systematically the procedure and be able to converge to the final solution, the eigenfunctions are expanded as an infinite series depending on a certain parameter λ . As the name of the method suggests, the series is truncated to the second power of λ , which means that the second order correction for the energy will be computed and, subsequently, also the first order correction of the wavefunction must be calculated. Thanks to the inclusion of the best part of the dynamic correlation, CASPT2 has become a very used method to quantitatively calculate the energies of ground and excited states. Nevertheless, it is not exempt from problems. Let's comment on four of them:

- The initial definition of the zeroth order Hamiltonian used in the version of the method implemented in MOLCAS package, led to certain overestimation of the correlation energy for open shell systems. This error was posteriorly corrected introducing a shift on the active orbital energies called IEPA that adjusted the energies to the electron affinity or ionization

energy depending on the case. In this thesis the IPEA correction was set to the default value, with a fixed parameter of 0.25.^[16]

- Another problem is the inclusion of intruder states that indicates an incorrect partition of the Hamiltonian operator. These states appear in the first order correction of the wavefunction and usually arise from excitations to Rydberg orbitals that are not included in the active space. In order to correct this problem, the orbitals involved in the excitations that give place to the intruder states could be included in the active space and, therefore, expand the reference wavefunction. However, this solution is often not applicable due to the cost associated with the larger active space. The second option, much more creative and used, is to apply an energy shift to the first order configurations not spanned by CASSCF and correcting afterwards the error of the energy introduced by the use of this shift. The shift can be real or imaginary, but the latter offers some advantage for weak intruder states, so the imaginary shift technique has been the one used in this work. The specific value has to be adapted in each system studied by comparing the weight of the reference CASSCF wavefunction since it should be roughly the same in all calculations.
- The third problem emerges when a single wavefunction is not an adequate reference for the perturbative treatment. This situation occurs when two electronic states are very close in energy after introducing the effect of the dynamic correlation so that the interaction among them is not negligible. For these cases, instead of using the single state (SS) version of the CASPT2, an extension called multi-state CASPT2 might be used. In it, an effective Hamiltonian matrix is constructed for a number of CASSCF wavefunctions obtained in the SS calculation. In this matrix, the diagonal elements are the CASPT2 energies and the extradiagonal elements are the couplings between states up to second order. The eigenvectors of this matrix provide the mixing of the CASCSF functions that give the perturbed modifies CAS configuration interaction (PM-CAS-CI) functions, and the eigenvalues give the corresponding MS-CASPT2 energies.^[17,18]
- Finally, the last problem that will be commented here is the computational cost of the geometry optimization procedure. At this level, the gradients can only be calculated numerically in many software suites as is the case of

MOLCAS, so the search of critical points at CASPT2 level will not be used for routine calculations but only in some particular cases where CASSCF method does not provide a good description of the state.

3.1.3. Variational approach to dynamic correlation: DDCI method

The Difference Dedicated Configuration Interaction (DDCI) method is a variational multireference method specifically designed to calculate energy differences, and it has been widely used for magnetic coupling constants, ionization potentials and electron affinities among others. In this method, the configuration space is formed adding single and double excited configurations to a reduced active space used as reference. The first step in the scheme, therefore, is the definition of a minimal reference CAS capable of describing the electronic states of interest and partitioning the set of orbitals into three spaces, in the same way than in a conventional CASSCF procedure, where the occupied and virtual orbitals are considered inactive.

In the expanded configuration space, several types of determinants can be distinguished depending on the involvement of the inactive orbitals. From all the possible types of determinants, the most numerous ones are those that include a double excitation from the doubly occupied to virtual orbitals. According to the theoretical framework of second order perturbation theory, these determinants do not contribute to the extra diagonal elements of the effective Hamiltonian and they just add a constant shift to the diagonal elements. It is logical to conclude that these determinants do not contribute to energy differences between electronic states. Given that the aim of the DDCI method is to get accurate relative energies, double excitations between inactive orbitals are not included in the DDCI formalism. The remaining determinants, the ones interacting with orbitals of the CAS space, are going to be included in the configuration space in order to variationally consider the effect of the dynamic electron correlation.

Since it is a variational method, DDCI has the advantage that is not contracted indicating that the coefficients of the determinants on the configuration space in the wavefunction are optimized, instead of remaining fixed like in the perturbative approach. This variation is due to the interaction between the active space determinants with the ones included as a result of the expansion. The same feature could be included in CASPT2 only by enlarging the CAS space, which is ineffective.

In comparison with CAS*SDCI calculations, DDCI not only reduces the number of determinants, but also scales more favourably. On the other hand, DDCI method has some limitations: 1) It cannot give good absolute energies. 2) The energy depends on the definition of the set of the active spin-orbitals. 3) It suffers from size-consistency related errors that can be sizable, depending on the type of system treated.

However, these issues can be addressed independently:

- 1) If the method is used to obtain relative energies in vertical excitations, DDCI results are very accurate. In reactivity studies, if the potential energy surface of any state is taken as reference, DDCI method is useful to determine the topography of the PES of the other states involved in the reactivity.
- 2) The orbital set used for DDCI can greatly affect the energies because they are computed in the context of CASSCF using optimized orbitals specific to each state. When states of the same multiplicity are calculated, this problem can be tackled using the state average technique so that the orbitals of each state are averaged and the energies are computed using a unique set. It should be noted that this approach is not possible for states of different multiplicity although there are some alternatives. In order to treat these cases, we can make use of the iterative DDCI version in which the average density matrix is calculated (from the density matrices of each state) and diagonalized to obtain a natural orbital set.^[19] The integrals are recalculated on the basis of these new orbitals and the density matrices of each state are averaged again, consecutively until the energy has converged to a self-imposed criterion.
- 3) Finally, although the size-consistent error is much smaller than in other methods, it may become significant when a large number of active electrons are correlated. In this case, the most straightforward way to correct this error is to apply the Davidson correction (DC) in a basic development given by the following expression where C_0^2 is the weight of the CASSCF wavefunction in the DDCI expansion.^[20]

$$E^{DDCI+DC} = E^{CASCI} + (2 - C_0^2)(E^{DDCI} - E^{CASCI})$$

3.2. DENSITY FUNCTIONAL THEORY

The Density Functional Theory represents an alternative formulation to the conventional ab initio methods of introducing the effects of electron correlation into the solution to the electronic Schrödinger equation. The basis of this method was rigorously established by Hohenberg and Kohn in 1964 by proving that ground state electronic energy of a many-electron system is determined completely by the electron density $\rho(\vec{r})$.^[21] Comparing with the wavefunction-based methods, the significance of this approach was clearly unveiled. While a wavefunction rely upon four coordinates for each electron (three spatial and one spin), the electronic density only depends on the spatial coordinates independently from the number of electrons.

For some decades prior their contribution, some attempts established how several components of the energy depend on the electron density, although these efforts were not very successful in chemical applications. However, Hohenberg-Kohn first theorem goes further to demonstrate that for any system of interacting particles in an external potential, the density is uniquely determined. In other words, any observable can be written as a functional of the electron density of the ground state. Given that $\rho(\vec{r})$ determines the total number of electrons and also establishes the external potential, it is concluded that $\rho(\vec{r})$ determines the Hamiltonian and the wavefunction of the ground state. If one attempts to proceed in this direction, computing the energies after determining the Hamiltonian and the wavefunction, it does not mean any simplification over the Molecular Orbital theory since we are not avoiding explicitly solving the Schrödinger equation. The determination of the energy without recourse to the wavefunction was devised later and it will be discussed below. Hohenberg and Kohn also demonstrated in a second theorem that the density also obeys the variational principle, so any trial density results in a greater or equal energy to the exact energy of the ground state.

In this context, the electronic Hamiltonian operator is defined as

$$\hat{H}_e = \hat{T} + \hat{V}_{ee} + \hat{V}_{ext}$$

These terms are similar to the ones explicitly stated in the second chapter although several issues should be noted. First, an external potential operator is introduced

for the attraction between electrons and nuclei. Second, defining the electron-electron self-repulsion in a continuous charge distribution is straightforward starting with the coulombic repulsion. However, in contrast to the classical case, the quantum mechanical electron-electron repulsion must take into account that electrons are fermions (particles with half-integer spin), which cannot occupy the same spatial position. Third, the kinetic energy is poorly described in this scheme.

In order to correct this, Kohn and Sham suggested in 1965 to use a much simpler non-interacting model system of electrons with small correction terms.^[22] For this approach it is crucial to define an effective potential in which the ideal system has the same overall ground state density as the real system. The effect of this approach is the splitting of the kinetic energy in two parts at a cost of reintroducing the orbitals and increasing the complexity to $3N$ variables. The first term of this partition accounts for the kinetic energy of a system of non-interacting particles with an expression identical to that used in Hartree-Fock. The second term introduces the correction derived from the difference with the real interacting system.

The electron-electron repulsion is also divided in two terms, the first containing the classical expression for the repulsion, and the second adding a correction for the energetic errors introduced by assuming classical behaviour. This term also contains all the effects of self-interaction. Adding kinetic and potential correction terms together, a new energy term is created called exchange-correlation energy. All these expressions are contained in the Kohn-Sham (KS) one-electron operator that is defined as

$$h_i^{KS} = -\frac{1}{2}\nabla_i^2 + \int \frac{\rho(\vec{r}')}{|\vec{r}_i - \vec{r}'|} d\vec{r}' - \sum_k^{nuclei} \frac{Z_k}{|\vec{r}_i - \vec{r}_k|} + V_{xc}[p(\vec{r})]$$

This operator contains, in order of appearance, kinetic energy, Coulomb repulsion, nuclei-electron attraction and exchange-correlation potential. As it can be noted, the expression for the exchange-correlation term is unknown and, therefore, the operator is approximated. However, it is important to highlight that this model is potentially exact since the ground-state density can be calculated exactly, unlike other methods with exact operators but approximate wavefunctions.

Summarizing, the application of the Kohn-Sham approach proceeds from a set of trivial molecular orbitals χ_i in which $\rho(\vec{r}) = \sum |\chi(\vec{r})|^2$. It has been discussed that the Kohn-Sham orbitals does not have physical significance, although several authors have indicated its higher interpretative power in comparison to HF orbitals in MO schemes.^[23] In order to optimize these orbitals, we can make use of the second theorem of Hohenberg and Kohn although instead of determining the density that minimizes the energy, the orbitals are varied. This process is carried out using a Slater determinant and the rigorous decomposition of the electron density into contributions from one-electron orbitals to iteratively solve the pseudoeigenvalue equation

$$h_i^{KS} \chi_i = \varepsilon \chi_i$$

However, the variational principle only holds for the exact functional and not for an approximate one used here (due to the exchange-correlation unknown expression). Therefore, it can well happen that the energies obtained from approximate density functional theory are lower than the exact ones. It should be also noted that the exact wavefunction of non-interacting fermions can be represented easily as Slater determinants but one must not identify the Slater determinant generated from the KS orbitals with the true many-electron wavefunction. This is not either in the reach nor the objective of density functional theory.

From this point, the difficulty comes when trying to develop an exchange-correlation functional that fits in the best possible way the system described by the study. This point has been intensively studied for a long time and has developed a multitude of functionals despite of the lack of a systematic method for improvement. The usual way to test the suitability of a functional is comparing its results for a set of simple compounds with results from another more accurate methodology and estimating errors and deviations.

Several attempts of approximating the exchange-correlation energy have been made during the development of DFT. The simplest but at the same time a tremendously useful approximation is the Local Density Approximation (LDA). In this approach, the exchange-correlation energy can be computed exclusively from the local value of the electron density. This approximation works well in cases where electron density is spatially uniform. An improvement was introduced when this is not the case through the dependence not only on the local value of the

density but also on the gradient of the density. This is the Generalized Gradient Approximation or GGA. The B97D functional used in this thesis is of this type. An advance was made with meta-GGA functionals containing also the kinetic energy density. Going up in complexity along the so-called Jacob's ladder of DFT, we find hybrid functionals that include a known percentage of exact exchange from a HF calculation. Some of the last group functionals, like B3LYP and PBE0, have been very broadly successful describing ground-state processes and have become reference methods even for many non-theoretical chemists. Although DFT has been proven to be more robust than other single determinant methods, multideterminantal states are not correctly described by DFT, so its application to excited states, where this character is more common, must be done with caution.

3.3. MODELLING THE SOLVENT: PCM

Despite the titanic effort that has been made in order to have a set of theoretical tools based on quantum mechanics to describe correctly and effectively all kinds of systems, the truth is that these methods have been focused mainly in treating isolated molecules that reproduce accurately only the gas phase. However, it has been known for a long time in experimental chemistry that the solute-solvent interactions can decisively affect the reactivity by altering structures and reaction mechanisms. In this direction, the development of computational strategies able to include the role of solvents in *ab initio* methods have been in vogue recently although we will focus only in a particular model of solvation used in conjunction with CASSCF and CASPT2 methods.

The model used in this work is a continuum model where the solvent is described by a continuous field without intern structure that is polarized by the solute causing an electrostatic response, which is the agent that affects the molecular properties of the solute. Therefore, this model is called Polarizable Continuum Model or PCM.^[24] This method was initially devised by Tomasi and co-workers in 1981. It creates a solute cavity via a set of overlapping spheres centred on the solute atoms that keeps the shape of the molecule. This building method of the solute's cavity is based on Karplus and York conductor screening model,^[25] which uses a continuous surface charge to improve the robustness of the reaction field.

In order to quantify the interaction between the solvent field and the solute, the surface of the cavity is calculated by partitioning the spheres in small elements called tesserae. This approach allows the surface integrals to be computed as finite sums while allowing certain flexibility on the precision-cost rate. Continuous models have, though, some limitations such as its inability to describe specific chemical interactions, like hydrogen bonding. If these interactions are necessary for the study of a given system, the PCM method alone is not the most appropriate and it will be necessary to add discrete solvent molecules to interact with the solute.

3.4. MOLECULAR MECHANICS

Molecular mechanics (MM) is the classical approach to describe molecular systems by calculating the energies by decomposition in bonding and non-bonding terms. This is fundamentally different from quantum chemical calculations where no reference is made whatsoever to chemical bonding. In the MM framework, balls are used as a model for atoms because it does not contemplate the existence of electrons or objects of similar dimension and with speeds comparable to that of light, since in those cases quantum mechanics must be introduced. In addition, the bonds between atoms are modelled as springs with larger or smaller force constants. Using this method, the total Molecular Mechanics energies can be separated in several contributions arising from distortions from “ideal” bond distances (stretching), bond angles (bending) and torsion angles together with non-bonded interactions.

$$E_{MM} = E_{STRET.} + E_{BEND.} + E_{TOR.} + E_{ELEC.} + E_{VDW} + E_{CROS.}$$

The stretch term represents the energy between covalently bonded atoms and it is the simplest, given in terms of Hooke’s Law quadratic form. This formulation is derived from a spring model, where equilibrium distances are determined from experimental data or accurate quantum chemical calculations. This situation means that any “real” MM equilibrium values are ideal parameters without being balanced with neighbouring interactions. However, this approach is only a good approximation in regions near the equilibrium (when the bond distance tends to infinity the model predicts infinitely positive energy), which indicates the need for devising further corrections to the quadratic model. In this direction two adjustments can be raised: 1) including more terms in the Taylor expansion of the

stretch term or 2) using the Morse function. In the force fields used in this thesis, AMBER 99 and UFF, the first one just includes the quadratic term while the second corrects it using the Morse model. This latter model is a more accurate description since it implicitly includes anharmonic terms near the equilibrium and leads to a finite energy for breaking bonds at the expense of computational efficiency. The same situation is observed for the bending term, where it can also be approximated using a harmonic form, as in the AMBER case, but also as a small cosine Fourier expansion, as in the UFF case, what provides a better description of large amplitude motions. The reason for this different description is the range of applicability of each force field because while UFF is universal (contains parameters for every atom), AMBER is specific for biomolecules and therefore limited to a particular combination of atoms.

The third term represents the torsion contribution to the total energy caused by the twisting of all molecular bonds, which requires a form that reflects its inherent periodicity. In this case, a periodic Fourier series expansion is used as model for this contribution in the force fields used in this thesis, although the formalism in each case is slightly different. The division of the energy is completed by the inclusion of non-bonded interactions, which can be decomposed into electrostatic and van der Waals. The first term accounts for the interaction between point charges while the second refers to the residual attractive or repulsive forces that do not arise from the other interactions. Finally, a crossing term is added to try to account for couplings between the different energy terms. These terms are defined similarly in the force fields employed in this work.

3.5. BIBLIOGRAPHY

1. Roos, B. O., Taylor, P. R., Siegbahn, P. *Chem. Phys.*, **1980**, *48*, 157.
2. Andersson, K., Malmqvist, P. A., Roos, B. O., Sadlej, A. J., Wolinski, K. *J. Phys. Chem.*, **1990**, *94*, 5483.
3. Malmqvist, P. A., Rendell, A., Roos, B. O. *J. Phys. Chem.*, **1990**, *94*, 5477.
4. Miralles, J., Castell, O., Caballol, R., Malrieu, J. P. *Chem. Phys.*, **1993**, *172*, 33.

Third chapter: Theory and applied methods

5. Aquilante, F., Vico, L., Ferré, N., Ghigo, G., Malmqvist, P. A., Neogrády, P., Pedersen, T. B., Pitonak, M., Reiher, M., Ross, B. O., Serrano-Andrés, L., Urban, M., Veryazov, V., Lindh, R. *J. Comput. Chem.*, **2010**, *31*, 224.
6. Frisch, M. J., Trucks, G. W., Schlegel, H. B., Scuseria, G. E., Robb, M. A., Cheeseman, J. R., Scalmani, G., Barone, V., Mennucci, B., Petersson, G. A., Nakatsuji, H., Caricato, M., Li, X., Hratchian, H. P., Izmaylov, A. F., Bloino, J., Zheng, G., Sonnenberg, J. L., Hada, M., Ehara, M., Toyota, K., Fukuda, R., Hasegawa, J., Ishida, M., Nakajima, T., Honda, Y., Kitao, O., Nakai, H., Vreven, T., Montgomery Jr., J. A., Peralta, J. E., Ogliaro, F., Bearpark, M. J., Heyd, J., Brothers, E. N., Kudin, K. N., Staroverov, V. N., Kobayashi, R., Normand, J., Raghavachari, K., Rendell, A. P., Burant, J. C., Iyengar, S. S., Tomasi, J., Cossi, M., Rega, N., Millam, N. J., Klene, M., Knox, J. E., Cross, J. B., Bakken, V., Adamo, C., Jaramillo, J., Gomperts, R., Stratmann, R. E., Yazyev, O., Austin, A. J., Cammi, R., Pomelli, C., Ochterski, J. W., Martin, R. L., Morokuma, K., Zakrzewski, V. G., Voth, G. A., Salvador, P., Dannenberg, J. J., Dapprich, S., Daniels, A. D., Farkas, Ö., Foresman, J. B., Ortiz, J. V., Cioslowski, J., Fox, D. J.; Gaussian, Inc.: Wallingford, CT, USA, **2009**.
7. Rappe, A. K., Casewit, C. J., Colwell, K. S., Goddard, W. A., Skiff, W. M. *J. Am. Chem. Soc.* **1992**, *114*, 10024.
8. Hess, B., Kutzner, C., Van der Spoel, D., Lindahl, E. *J. Chem. Theory Comput.*, **2008**, *4*, 435.
9. Cornell, W. D., Cieplak, P., Bayly, C. I., Gould, I. R., Merz, K. M., Ferguson, D. M., Spellmeyer, D. C., Fox, T., Caldwell, J. W., Kollman, P. A. *J. Am. Chem. Soc.*, **1995**, *117*, 5179.
10. Ben Amor, N., Maynau, D. *Chem. Phys. Lett.*, **1998**, *286*, 211.
11. Hall, G. G. *Proc. R. Soc. Lond. A*, **1951**, *205*, 541.
12. Roothaan, C. C. J. *Rev. Mod. Phys.*, **1951**, *23*, 69.
13. Roos, B. O., Andersson, K., Fülscher, M. P., Serrano-Andrés, L., Pierloot, K., Merchán, M., Molina, V. *J. Mol. Struct.*, **1996**, *388*, 257.

-
14. Malmqvist, P. Å. *Int. J. Quantum Chem.*, **1986**, 30, 479.
 15. Møller, C., Plesset, M. S. *Phys. Rev.*, **1934**, 46, 618.
 16. Ghigo, G., Roos, B. O. Malmqvist, P. A. *Chem. Phys. Lett.*, **2004**, 396, 142.
 17. Roos, B. O. *A Perturbation-Variation Treatment of the Multi-State Problem in CASPT2.*, **1996**.
 18. Finley, J., Malmqvist, P. A., Roos, B. O., Serrano-Andrés, L. *Chem. Phys. Lett.*, **1998**, 288, 299.
 19. García, V. M., Castell, O., Caballol, R., Malrieu, J. P. *Chem. Phys. Lett.*, **1995**, 238, 222.
 20. Cabrero, J., Caballol, R., Malrieu, J. P. *Mol. Phys.*, **2002**, 100, 919.
 21. Hohenberg, P., Kohn, W. *Phys. Rev.*, **1964**, 136, B864.
 22. Kohn, W., Sham, L. J. *Phys. Rev.*, **1965**, 140, A1133.
 23. Cohen, M. H., Frydel, D., Burke, K., Engel, E. *J. Chem. Phys.*, **2000**, 113, 2990.
 24. Tomasi, J., Mennucci, B., Cammi, R. *Chem. Rev.*, **2005**, 105, 2999.
 25. York, D. M., Karplus, M. *J. Phys. Chem. A.*, **1999**, 103, 11060.

FOURTH CHAPTER:

AZOBENZENE AND PHENYLAZOPYRIDINE PHOTOISOMERIZATION

4.1. INTRODUCTION

Azobenzene is an organic compound that has a singular behaviour due to the possibility of switching between isomers using particular wavelengths of light. During this process called isomerization reaction, we can identify two isomers, *trans* and *cis*, which involve different degrees of stability although *trans* is usually the most stable one. This isomerization process was observed first by Hartley in 1937^[1] although the discovery of this family of compounds dates back to the mid-1800s. Hartley's first experimental evidences indicated that azobenzene changed its colour when it was irradiated with sunlight, a change that could be reversed if the product was kept in a dark room for a certain time (Figure 4.1). This investigation finally uncovered the *cis* isomer previously unknown.

The high rates of these forward and backward reactions, the fatigue resistance of the system, the stability of both *trans* and *cis* isomers and the possibility of tuning the properties of azo-derivatives by substitution give to azo compounds a wide range of potential applications. To avoid a large list of references, we just cite reference [2] for a recent review on the subject. Their applications are enlarged thanks to the readiness of these molecules to be incorporated in polymers and other kinds of materials like liquid crystals, self-assembled monolayer, micelles,

biomaterials etc., and to the possibility to tune their properties by means of ring substitution.

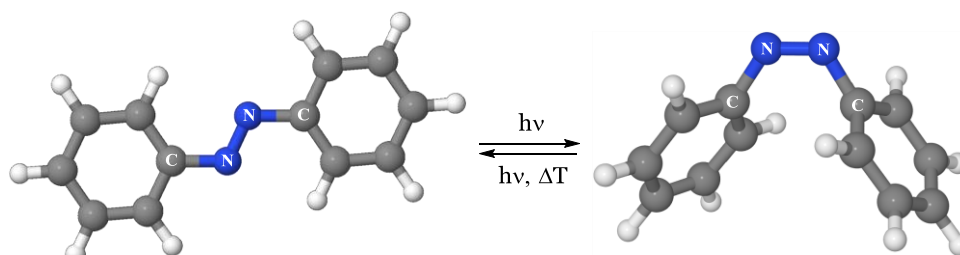


Figure 4.1 - Azobenzene photoisomerization.

A first series of applications are derived from the substantial change of shape of the molecule undergone in the isomerization. For example, the photo-mechanical properties of azobenzenes can be applied in micropumps or valves (to mimic the beat of a heart), molecular motors, wipers or articulations in robotics. Their strong electronic absorption also makes them interesting candidates for light energy harvesting and storage applications. Given that the photochromic properties can be tuned by ring substitution, azobenzene derivatives can be tailored to work in much of the solar spectrum, as solar fuels and as pigments or dyes. It is also possible to modulate the back isomerization rate with appropriate ring substituents. If this back reaction is slow, azobenzenes can be used in information storage materials; if fast, in information-transmitting systems. If the substituents have adequate electron-donor acceptor properties, azobenzenes acquire nonlinear optical properties.

All this range of potential applications has attracted much interest in the study of their photoisomerization reaction. In spite of this and the early attempts to study systematically this system, from the experimental as well as from the theoretical point of view, the mechanism of this reaction is not completely clarified, and is still the subject of intense debate.

The first systematic spectroscopic study of azobenzene and its derivatives was carried out by Birnbaum in 1953.^[3] In these spectra, two major absorption bands are found in the UV-visible region corresponding to the $S_0 \rightarrow S_1$ (weak band at 430nm; S_1 of $n\pi^*$ character) and $S_0 \rightarrow S_2$ transitions (strong band at $\nu=320$ nm; S_2 of $\pi\pi^*$

Fourth chapter: Azobenzene and Phenylazopyridine

character). It should be noted that the first attempts to reproduce the electronic spectra theoretically are attributed to Beveridge in 1966.^[4]

After these initial studies, one of the first aspects that were widely discussed was the role of triplet states during the deactivation mechanism. In this direction, Jones and Hammond^[5] calculated the decay factor of the reaction produced by direct irradiation of azobenzene and compared it with the result of the indirect reaction produced by sensitization. The decay factors were sufficiently different to justify the non-intervention of triplet states. In addition, the sum of the quantum yields of forward and backwards isomerization was high, what could not be explained by a mechanism occurring through those triplet states. This statement was also partially sustained by Dyck in 1962.^[6] Despite these evidences, first Fischer^[7] and then Ronayette^[8] repeated the previous experiments and found no significantly enough differences of decay factors for the backwards isomerization and, therefore, the role of triplet states in the *cis* to *trans* isomerization could not be ruled out. All these insights were also collected by Griffiths several years later.^[9] In 1979, Bortolus^[10] re-examined the issue of the involvement of the triplet states in the photoisomerization of azobenzene derivatives and established that the quantum yield of the lowest triplet state was very low and, therefore, did not participate in the photochemical process of the *trans* to *cis* isomerization.

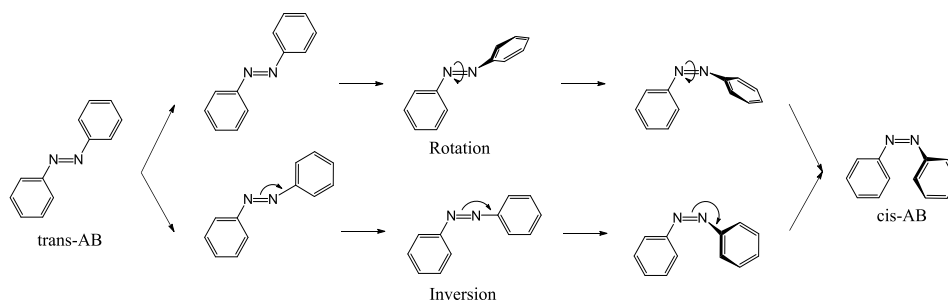


Figure 4.2 – Classical mechanisms proposed for the isomerization of azobenzene.

A particular characteristic of azobenzene photoisomerism is the dependence of the quantum yield on the excitation wavelength.^[9,11] It means that the reaction mechanism is different when the initial excitation populates the first or the second of the singlet excited states. In response to that, two traditional mechanisms were proposed following two specific reaction coordinates: in-plane inversion at one of the two nitrogen atoms (for excitation to the first excited $n\pi^*$ state) and twisting

around the N=N double bond (for excitation to the second excited state $\pi\pi^*$), represented in Figure 4.2. Nowadays, more complex reaction coordinates, represented in Figure 4.3, are also proposed. In order to explore these pathways, many studies have been performed either experimentally as well as theoretically, and a summary of the most important advances is needed to grasp the complete picture.

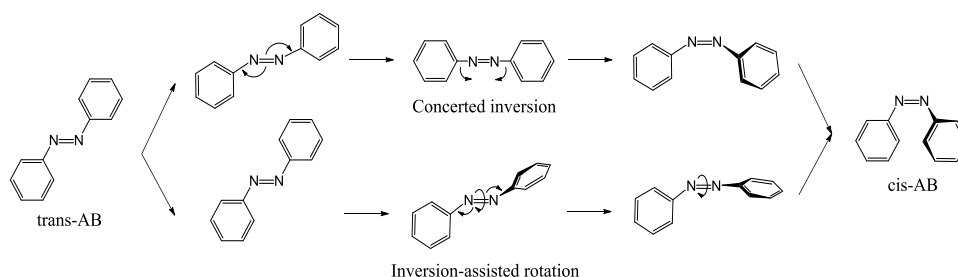


Figure 4.3 - Novel mechanisms proposed for the photoisomerization of azobenzene.

One of the first experimentalists who studied the mechanism of photoisomerization was Nerbonne,^[12] which conducted several experiments where the isomerization was carried out inside a rigid matrix of liquid crystals. He concluded that the large changes of enthalpy and entropy observed were caused by the preferred rotation mechanism. But in 1982 Rau proved that photoisomerization was also possible following an inversion coordinate,^[11,13] after blocking the rotation mechanism using bidentate ligands. In those experiments, Rau did not prove that inversion was the only active mechanism, but comparing the band shape for the excitation to the first excited state in free and rotation-blocked systems and seeing that they were similar, he concluded that inversion should be the preferred mechanism for the first excited state and rotation for the second. Regarding the issue of quantum yields, Rau discovered that in rotation-blocked azobenzenes the quantum yield became almost wavelength independent (same results when exciting separately to $S_1(n\pi^*)$ or to $S_2(\pi\pi^*)$, azobenzene-2-phane results in Table 4.1).

Table 4.1 - Quantum yields of isomerization from *trans* to *cis* of azobenzene and rotation-blocked systems, azobenzene-2-phane and β -CDx-azobenzene.

	Azobenzene	Azobenzene-2-phane ^[11]	β -CDx - Azobenzene ^[14]
$\Phi (n\pi^*)$	0.23	0.24	0.13
$\Phi (\pi\pi^*)$	0.10	0.21	0.13

Fourth chapter: Azobenzene and Phenylazopyridine

Several years later, Bortolus developed an analogous study in a system where an ether crown was used as a method of blocking the rotation (β -CDx-Azobenzene). His results also showed the same quantum yields for isomerization through S_1 and S_2 although with smaller values (Table 4.1). These facts indicate that in non-constrained systems the mechanism that operates when the isomerization takes place along S_1 or S_2 are different, although a connexion between reaction paths must exist when the rotation is blocked.

The results of a computational study published by Monti soon afterwards,^[15] supported the same hypothesis and established what can be considered the traditional theory of the mechanism of the photoisomerization of azobenzene, that was not questioned along the next decade. Monti's results showed that the initial relaxation along the S_2 ($\pi\pi^*$) state corresponded to a rotation. But soon along this downhill path, a bifurcation offers two possible deactivation channels. The first one correspond to a radiationless decay to the *trans* ground state, and the second to an internal conversion to the S_1 ($n\pi^*$) state. On that surface, the rotation shows a large energy barrier, so the inversion is the only possibility to lead the system to the *cis* product. The bifurcation along the $\pi\pi^*$ path would explain, for the first time, the different quantum yield measured for isomerization when the system was excited to the $n\pi^*$ or $\pi\pi^*$ excited states. This study also supported the lack of involvement of triplet states in the mechanism of *trans*-to-*cis* photoisomerization.

In the following years, a large number of experimental studies supported the hypothesis proposed in Monti's computational work. A study by Biswas,^[16] based on a comparison of resonance Raman excitation profiles, indicated that the coordinate of inversion seemed to be the most favourable for the isomerization. Nägele^[17] also backed this proposal after measuring the femtosecond transient absorption during the photoisomerization along the $n\pi^*$ state. His measurements indicated that the reaction proceeded following a steep and barrierless inversion pathway for both, *trans*-to-*cis* and *cis*-to-*trans*, although the first one showed a weaker gradient. In the same line, Lednev^[18,19] measured the ultrafast time-resolved electronic absorption of rotation-blocked and rotation-free azobenzene derivatives and found that the results were consistent with the inversion mechanism for $n\pi^*$ when rotation was blocked. However, when this constraint was not applied, a bottleneck in the rotation mechanism on the $\pi\pi^*$ surface caused a fast internal conversion to $n\pi^*$.

On the basis of Raman band analysis, Fujino^[20,21] showed that the frequencies for N=N stretching were equal for the ground state and the $n\pi^*$ state and therefore the N=N bond order could not change on that excited state. Taking into account that rotation needs longer N-N distances to take place, Fujino concluded that inversion was the most favourable mechanism for isomerization on the $n\pi^*$ state. He also suggested that when the system is excited to the S_2 ($\pi\pi^*$) state, an internal conversion to a vibrationally excited S_1 ($n\pi^*$) takes place with a quantum yield close to one. From there, azobenzene tends to go back to the ground state *trans* isomer, lowering the yield of the isomerization when excited to the S_2 state.

But some doubts about the traditional mechanism started to appear with theoretical studies. First, the potential energy surfaces obtained by Cattaneo^[22] in 1999 indicated that, for both $n\pi^*$ and $\pi\pi^*$ excited states paths, rotation and inversion were possible although from the $\pi\pi^*$ state a crossing with a double-excited $n^2\pi^{*2}$ state was also possible. This alternative path could explain the different lifetimes and the lower quantum yield of isomerization along this state. The same study elaborated for the *cis* isomer did not show the presence of this crossing, indicating that a steep slope along the torsion coordinate is the prime direction for the backwards isomerization on the $\pi\pi^*$ state. The computational work of Ishikawa^[23] supported the same hypothesis on the basis of a S_1/S_0 rotated conical intersection found at a geometry with a 90° value for the dihedral CNNC angle. A crossing between $\pi\pi^*$ and $n^2\pi^{*2}$ is again proposed as the justification for the low quantum yield for isomerization from the $\pi\pi^*$ state, in competition with an efficient conversion from the $n\pi^*$ state to the *cis* ground state.

One of the few experimental supports of the mechanism of rotation on the $n\pi^*$ surface comes from the femtosecond fluorescence anisotropy measurements of Chang^[24] where the variation of the orientation of the induced dipole moment in non-viscous solvents points to this direction. But similar measurements on viscous solvents resulted on the support of the concerted inversion mechanism. Also, experimental evidences presented by Satzger^[25] indicate that the decay from $n\pi^*$ occurs in a bi-phasic fashion, in contradiction to the results of Fujino.

Trying to clarify arguments in the debate, Schultz^[26] stated in a simple way the facts that a proposed mechanisms for photoisomerization of azobenzene should

Fourth chapter: Azobenzene and Phenylazopyridine

explain in order to be taken into account: first, the wavelength dependence on the quantum yields; second, the changes when the rotation is blocked (although there were doubts about the real blockage of rotation of the constrained azobenzene derivatives used in some studies^[24]); finally, it should be borne in mind that the quantum yield of internal conversion from $\pi\pi^*$ to $n\pi^*$ is equal to one and that the crossing point between these states had to be planar. The involvement of higher energy states could be crucial for the mechanism and, therefore, it should not be ruled out.

Since then, much more theoretical work has been done to investigate the photochemistry of azobenzene, from the stationary point of view, studying the potential energy surfaces of the low-energy states^[25-29] or running dynamic calculations.^[30-36] Based on these works, alternative mechanisms different from pure rotation or inversion, have been proposed. Calculating minimum energy paths (MEP) on the $n\pi^*$ surface, Cembran^[27] suggested that the dominant mechanism follows a path that mixes rotation and inversion. Diau^[37] located the $n\pi^*/S_0$ conical intersection and proposed a new and more affordable mechanism known as concerted inversion, where both NNC angles invert at the same time (see Figure 4.3). The larger quantum yield of photoisomerization along the $n\pi^*$ state can be explain due to the existence of the direct channel of deexcitation from this excited state to the ground state through the CI located between these states.^[28] This mechanism was proposed to be an alternative reason for the observed *trans-to-cis* photoisomerization quantum yields on $\pi\pi^*$ excitation being much lower than the $n\pi^*$ excitation. Gagliardi^[38] found a crossing point between the $\pi\pi^*$ and $n^2\pi^{*2}$ states near the FC geometry, what could explain the low quantum yields observed for photoisomerization along the $\pi\pi^*$ surface and supports the speculation that after excitation to the $\pi\pi^*$ state, the isomerization process does not occur on its surface. This result was experimentally supported by time-resolved photoelectron spectroscopy spectra that provided the first observation of the double excited state.^[29] In the same study, the lower photoisomerization quantum yields from the $\pi\pi^*$ state were explained as the consequence of near planar conical intersections with large NNC angles, not accessible if the molecular motion is restricted.

One of the first dynamic studies on this reaction was carried out by Grannucci^[30], who pointed to a dominant rotational mechanism for $n\pi^*$ mixed with the opening of the CNN angles. In fact, mixed mechanisms are often found in dynamic

simulations like in the works of Yuan,^[31] Tiberio,^[32] Bandara,^[33] Maurer^[34] or Böckmann.^[35] Especially interesting in the first article mentioned is the assertion that Yuan considers the crossing between $\pi\pi^*$ and $n^2\pi^{*2}$ as the crucial point to explain the small quantum yield of the isomerization along the $\pi\pi^*$ state. On the other hand, Maurer suggests that the $\pi\pi^* \rightarrow n\pi^*$ decay takes place at planar geometries close to the *trans* isomer. Meanwhile Böckmann proposes the deformation to pedal-like structures, not contemplated before, as a favoured relaxation coordinate in the dynamics of the system along the $n\pi^*$ PES. This coordinate is also taken into account in the work of Weingart.^[36]

The most recent computational^[39-41] and experimental^[41] works are focused on the dynamics along the $n\pi^*$ state. In general, all of them agree in suggesting that the rotation is the main coordinate of decay to S_0 and isomerization, although some authors indicate a certain involvement of secondary coordinates^[33,42,43] (rotation of phenyl groups, displacement of the N-N moiety, inversion). In general, though, the evolution of the system when excited to the $\pi\pi^*$ state is not studied. In this landscape, the mechanism of the photoisomerization of azobenzene remains an open question. The study we have developed in this thesis wants to be a step forward towards the objective of solving the rotation-inversion dichotomy that has characterized the research of azobenzene for more than 50 years. We want to offer a full route for the isomerization of this compound exploring the topography of the potential energy surfaces of the low-energy states of azobenzene, using an ab initio methodology that includes the dynamic electron correlation to accurately locate stationary points and calculate relative energies.

This project did not finish with azobenzene, but the acquired knowledge has also been applied to an azobenzene derivative. Given its role as a molecular switch, azo compounds have also been used in coordination complexes as a trigger of photoresponsive properties. However, in contrast to the extensive studies on azobenzene, there are only a few concerning the isomerization of azo derivatives. Our interest is focused specifically on phenylazopyridine (PAPy), an azobenzene where one of the benzene rings is replaced by a pyridine ring. PAPys have been extensively studied for decades in synthesis and characterization of metallic complexes, and a vast literature can be found. These compounds are often used as ligands in transition metal complexes, but the study of photoisomerizable ligands and the light-induced processes that they give place to has only recently started in

Fourth chapter: Azobenzene and Phenylazopyridine

the works of Venkataramani,^[44] Bannwarth^[45] and Hirose.^[46] The light induced *trans*-to-*cis* isomerization of phenylazopyridine plays a fundamental role in the room-temperature switchable spin crossover of Ni-porphyrine derivatives. One of these complexes, where the photoreactive ligand is the 3-PAPy, has already been investigated in our group^[47]. In this photochemical process, the lone pair on the nitrogen of the pyridine can be coordinated or not with the metal, changing the coordination number of the latter and, consequently, its multiplicity leading to the spin crossover. The study presented here wants to provide more detailed information in the mechanism of photoisomerization of this ligand, to tackle the study of the complex from different perspectives.

The study of the isomerization of pyridine analogues of azobenzene dates from more than 40 years ago with the article of E. Brown^[48] where the first measurements were carried out to determine the thermodynamic parameters for the reaction. However, the first mechanistic study of the photoisomerization of this compound did not appear until 2009, when Wang^[49] characterized in detail the potential energy surfaces of the ground and first excited states for 2-PAPy and 4-PAPy. Their results indicated that photochemistry of 4-PAPy was very similar to that of azobenzene, but subtle differences were predicted for 2-PAPy in the path of rotation on the $n\pi^*$ state where a faster decay was observed.

In the Ni-porphyrin complex studied in our group, the PAPy isomer of interest is the 3-PAPy, for which no mechanistic studies have been published, to our knowledge, up to date. This isomerization reaction seems similar to the one already studied for azobenzene so therefore, we will focus in answering two interrelated questions: 1) Does the extra N with its lone pair change at all the photochemistry of 3-PAPy relative to that of azobenzene? 2) Are there significant differences between the photoisomerization mechanisms of both molecules?

4.2. SCOPE

In this work, we will first determine the mechanism of isomerization of *trans*-azobenzene that must involve a fast deactivation process after UV-visible irradiation. We must take into account that the efficiency of this process is not very high (low quantum yields) and, therefore, there must exist some paths leading back to the original reactant. The thermal mechanism to return from the *cis* to the *trans*

isomer will also be investigated. One of the key aspects that this mechanism must be able to explain is the wavelength dependence of the quantum yield of photoisomerization experimentally detected. This effect is profusely described in the bibliography but the reasons used to explain it are also diverse. The final aim is to provide mechanistic information useful for the design of switchable systems, by tuning the quantum yield of isomerization and the rate of the thermal back-reaction.

A parallel study will also be carried out on phenylazopyridine with the same objectives, making use of the experience acquired in azobenzene. This last system has also been sampled in order to reproduce theoretically the absorption spectra. This is an objective of computational interest, in order to validate the protocol used by comparison of the computational results with the scarce experimental information available.

These extensive ab initio studies were conducted using the CASSCF/MS-CASPT2 methodology. The potential energy surfaces of the ground state and the lower singlet excited states were explored, i.e., $n\pi^*$, $n_{py}\pi^*$ (for PAPy), $\pi\pi^*$ and $n^2\pi^{*2}$. On these surfaces, the minima, transition states and conical intersections were localized and optimized. Relative energies and oscillator strengths were determined for each of these geometries. The reaction pathways were also examined to follow the structural changes and the successive events that occur after the initial absorption of light. Both, optimized geometries of stationary points and paths give rise to a complete view that will lead to the proposal of a mechanism to explain all the characteristics observed experimentally of the reactions studied.

4.3. COMPUTATIONAL STRATEGY

The study of the mechanistic profiles of azobenzene and phenylazopyridine were conducted following the CASSCF/MS-CASPT2 protocol. CASSCF method was used for optimizations in the states that did not need the effect of the dynamical electron correlation in order to be correctly described. This is the case for the ground state, the double-excited $n^2\pi^{*2}$ state and the $n_{py}\pi^*$ state of phenylazopyridine. On the stationary points located on these surfaces, the energetics was refined with the MS-CASPT2 method. In the case of $n\pi^*$ and $\pi\pi^*$ states, MS-CASPT2 was used for both geometry optimizations and relative energy calculations.

Fourth chapter: Azobenzene and Phenylazopyridine

To include in the active space the whole π system of azobenzene it would be necessary to take into account 18 electrons in 16 orbitals. Unfortunately, to use this size of active space in standard calculations is unaffordable, so the active space was cut back extracting those orbitals which occupation did not change noticeably from 2 or from zero in the regions of the PES explored of the states considered. The result was an active space of 10 electron in 8 orbitals, composed of two π and two π^* orbitals of the benzenes, the π and π^* of the azo group and the orbitals of the lone pairs of the nitrogen atoms. In the case of phenylazopyridine, the lone pair orbital of the pyridine nitrogen was also added so the final active space was formed by 12 electrons in 9 orbitals. Test calculations in both cases showed that bigger active spaces do not give noteworthy differences. A Pople d-polarized split-valence basis set 6-31G (d) was used for all calculations.^[50]

The reference wavefunctions and the molecular orbitals were obtained by state average CASSCF calculations. In order to explore all the possibilities of the mechanism, symmetry constraints were not used although *trans*-azobenzene presented C_{2h} geometry. Topography of the PES between critical points of interest was explored using the linear interpolation of internal coordinates strategy (LIIC). Minimum energy paths (MEP) were also computed. An imaginary shift of 0.1 a.u. was added for the zero order Hamiltonian in the MS-CASPT2 calculations in order to preclude the inclusion of intruder states. The CAS state interaction (CASSI) protocol was used to compute the transition oscillator strengths in order to compare transition probabilities among the different studied states. Frequency calculations were also run to determine the nature of the stationary points. These calculations and the MS-CASPT2 optimizations were done numerically due to the lack of implementation of analytical gradients with this protocol. To make these calculations affordable, Choleksy decomposition of the two-electron integral matrix was used.^[51] All calculations were performed using MOLCAS 7.6 package.

Conical intersections and transition states were optimized using the algorithm implemented in Gaussian 09. For the first, state averaged orbitals were used and the orbital rotation derivative correction to the gradient (which is usually small) was not computed. Full diagonalization method was suppressed in order to afford these calculations that will provide the lowest energy point of the crossing.

In spectroscopic terms, due to the fact that static calculations do not take into account the thermal vibrations that occur in real systems, the computational reproduction of experimental absorption spectra is a big challenge. The basic problem is that in the “idealized” and simplified determination of the PES, the deformations of the stationary geometries due to the thermal energy are not contemplated. Consequently, for systems with structural symmetry, the transition dipole moment between states of different symmetry is zero, predicting a null probability of transition between those electronic states. But in experimental conditions, the geometry deformations due to the thermal energy break the symmetry of the system, making possible those transitions. Consequently, in the experimental spectra there appear more bands than those predicted computationally. This is the case of the systems studied here, because the minimum energy geometry is planar in both cases. For this reason, they are good candidates to calibrate a strategy developed in our group to address this issue, and for this reason the experimental spectrum of the 3-PAPy was reproduced.

For this, molecular dynamics was used as a consistent geometry generator to statistically represent 3-PAPy in a real spectroscopic environment at room temperature (298K). In these dynamical calculations, a 100 ps simulation was carried out, using Amber 99 as force field and methanol as solvent. After obtaining up to 400 geometries, using a code designed in our group,^[52] the vertical energies were statically computed using the CASSCF/CASPT2 protocol introducing the effect of the solvent (methanol) with the polarizable continuum model (PCM). All molecular dynamics calculations were performed using periodic boundary conditions in GROMACS 4.5.4.

4.4. AZOBENZENE RESULTS

The study of any photochemical process can be separated in distinct stages: initial excitation, subsequent possible relaxations, and secondary processes. This sequential structure is going to be followed in the exposition of these results. In the first subsection we collect the results for the absorption spectrum. In the second part we analyse the initial relaxation on each excited state surface through the accessible pathways. Finally, we expose the information concerning all the possible subsequent competitive processes. All this information will allow us to propose a comprehensive mechanism for the photoisomerization of azobenzene.

4.4.1 Franck-Condon Region

The first step in any computational study is to optimize the structural parameters for the ground state to obtain the minimum energy geometry. In this case, the optimization was carried out at CASSCF (10, 8) level for *trans* and *cis* isomers. The optimized structure of the *trans* isomer is a planar geometry, while in the *cis* isomer both benzenes rings show a conrotatory twist around the C-N=N-C moiety. In fact, the central link is not completely planar, given that the dihedral angle C-N=N-C is 3.2 degrees. The most relevant parameters of these structures are shown in Figure 4.4. Symmetric values in each benzene moiety are omitted. It must be pointed out that the geometry of the *trans* isomer belongs to the C_{2h} group of symmetry, although no symmetry restrictions were imposed.

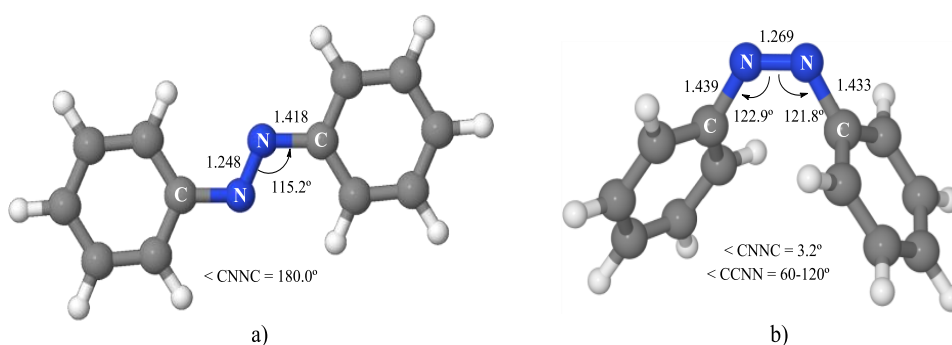


Figure 4.4 - a) Ground state global minimum b) *Cis* isomer minimum. Both optimized at CASSCF level.

In energetic terms, the *trans* isomer is 14.3 kcal·mol⁻¹ more stable than the *cis* isomer. This relative stability is in agreement with the experimental evidences.^[53] The relative energies of the excited states at the Frank Condon geometry will provide a prediction for the absorption spectrum of *trans*-azobenzene. In principle, only the states involved in the photoisomerization are of interest in this study but, given the methodology used to compute the relative energies, a wider initial study must be performed.

At the MS-CASPT2 level, the CASSCF states are mixed in the perturbed modified CAS configuration interaction functions (PM-CAS-CI). States higher than those strictly involved in the mechanism studied can get coupled with the lower energy ones and modify their description and energies. For this reason, it is convenient to perform a preliminary study to determine the minimum number of states that

should be included in the MS-CASPT2 procedure. In this particular case, this preliminary study showed that it was necessary to include 10 roots to obtain a good description of the spectrum. The composition of the PM-CAS-CI functions in terms of CASSCF states is shown in Table 4.2. The results of the calculation at different levels of theory of the vertical excitations for the *trans* isomer are collected in Table 4.3.

Table 4.2 - Eigenvectors of the SA10-MS-CASPT2 effective Hamiltonian matrix diagonalization in the *trans* ground state optimized geometry for the lowest energy states of azobenzene.

States	(GS) PM-CI	$^1(n\pi^*)$ PM-CI	$^1(\pi\pi^*)$ PM-CI	$^1(n^2\pi^{*2})$ PM-CI
GS	-0.9922	0.0000	0.0001	-0.0577
2	0.0000	0.9972	-0.0005	0.0002
3	-0.0004	0.0000	-0.0006	0.0110
4	-0.0001	-0.0004	-0.9448	0.0002
5	0.0591	0.0000	0.0008	0.2494
6	0.0000	0.0751	0.0010	-0.0020
7	-0.0088	0.0000	0.0000	0.7583
8	0.0000	0.0001	-0.0002	-0.0505
9	0.0000	-0.0001	-0.3276	-0.0003
10	-0.1092	0.0000	-0.0001	0.5973

Table 4.3 – Relative energies of the three lowest excited states relative to the *trans* and *cis* ground state geometries (in kcal·mol⁻¹) calculated at CASSCF and CASPT2 levels. Oscillator strengths calculated at CASPT2 level. In parenthesis, the experimental values are presented.^[9]

State	<i>Trans</i> -azobenzene				<i>Cis</i> -azobenzene	
	CASSCF	SS-CASPT2	MS-CASPT2	Osc.	MS-CASPT2	Osc.
GS	0.0	0.0	0.0	-	0.0	
$^1(n\pi^*)$	71.5	64.4	65.9 (64.0)	<10 ⁻⁴	67.3 (65.0)	0.56·10 ⁻¹
$^1(\pi\pi^*)$	142.0	101.3	96.3 (90.5)	1.27	109.8 (110.0)	0.21
$^1(n^2\pi^{*2})$	157.6	150.1	151.3	<10 ⁻⁴	143.0	0.20·10 ⁻¹

The analysis of the wavefunctions indicates that the excitations that give place to the lowest energy states have $n\pi^*$ and $\pi\pi^*$ character. Higher singlet excited states have oscillator strengths that are negligible compared with that of the lowest ($\pi\pi^*$) excited state. Therefore, it could be reasonable to assume that they will not be populated at the initial excitation. However, due to the rotation of the orbitals during isomerization, it is expected that the double excited state $n^2\pi^{*2}$ will decrease

its energy and cross with the lower states, so it was also included in the study. Figure 4.5 shows the molecular orbitals involved in the excitations described.

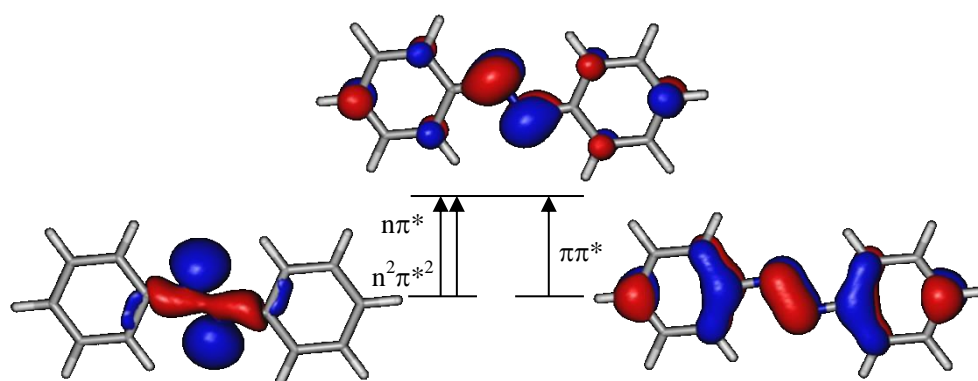


Figure 4.5 - Molecular orbitals of the active space that are involved in the excitations that describe the electronic character of the lowest energy excited states of *trans*-azobenzene.

The PM-CAS-CI wavefunctions indicate that the first excited state has $n\pi^*$ character and it is located $65.9 \text{ kcal}\cdot\text{mol}^{-1}$ above the ground state. This state is described by an excitation from one n orbital of the azo group to a delocalized π^* orbital and do not interact with any other state. This feature is made clear by the composition of the PM-CAS-CI wavefunctions given in Table 4.2, and by the similarity between SS and MS-CASPT2 energies. Comparison with CASSCF results, though, show that the dynamic electron correlation effect, included as a perturbation in CASPT2 results, is not negligible for this state. The computed value for the oscillator strength is very low due to the different symmetry between this and the ground state (for planar geometries), which results in a low transition probability. Experimentally, the spectrum shows a band that is usually assigned to this state, but it is predicted computationally only when dynamic calculations allow a loose of symmetry when the molecule leaves planarity (as it will be seen in the study performed for PAPy).

The second excited state has $\pi\pi^*$ character and it is the one that gets mainly populated after the initial excitation, as the large value of the oscillator strength indicates. This excited state is generated by promotion of one electron from the π orbital of the azo group to the same delocalized orbital as before. The description of this state at MS-CASPT2 level, shown in Table 4.2, mixes several CASSCF states in

such a way that, to be properly described at MS-CASPT2 level, 9 CASCSF states must be included in the calculation. It should be pointed out also the large difference between the excitation energy calculated for this state at CASSCF and SS/MS-CASPT2 levels. It indicates that the dynamic correlation included by the perturbation is also essential to study this state because the CASSCF method does not provide an accurate enough description. It means that the description of the PES of this state will not be accurate enough at CASSCF level either, so the geometry optimization looking for the minima of this state will be performed at CASPT2 level. Due to this fact, in what follows only MS-CASPT2 energies will be taken into account.

The third and last excited state considered consists in a double-excited state similar to the first one because it is described by excitations between the same couple of orbitals. The energy of this state is very high at Frank-Condon, but the doubly occupied π^* orbital reduces the N=N bond order. It is expected therefore that the rotation coordinate will decrease the energy of this state, making that it could be relevant in the rotational mechanism of isomerization. In the same way as for the first excited state, the effect in the energies of perturbation and mixing is not large, although in this case the perturbation is more important.

4.4.2 Minimum energy points on excited state surfaces

Geometry optimizations were carried out for the excited states, starting at the *trans* FC geometry, to localize the minimum energy points of the PES of the lower excited states of azobenzene, that is, for states $^1(n\pi^*)$, $^1(\pi\pi^*)$ and $^1(n^2\pi^{*2})$. The optimizations were run without symmetry constraints, not even those imposed by symmetry, in order to avoid limitations in the areas of the PES explored. Moreover, the different coordinates proposed in the literature to be the driving force of the isomerization mechanism have been explored explicitly.

$^1(n\pi^*)$ state

CASSCF optimization shows a planar minimum energy structure for the S_1 ($n\pi^*$) state (Figure 4.6 a), approximately 55.0 kcal·mol⁻¹ above the ground state minimum, and 11.0 kcal·mol⁻¹ more stable than the excitation energy to this state. In this structure, the C-N bonds are shortened, but there is almost no change in the N=N one, which keeps the double bond character, in spite of the occupation of the

π^* azo orbital with one electron (1.04) from the n orbital. The NNC angle is slightly larger than in S_0 . This is in circumstantial agreement with the initial hypothesis about the isomerization mechanism, which proposed inversion for isomerization on the S_1 state, but this agreement could be due to a cancelation of errors, as will be shown later. The probability of emission from this species is very low as the small oscillator strength indicates (see Table 4.4).

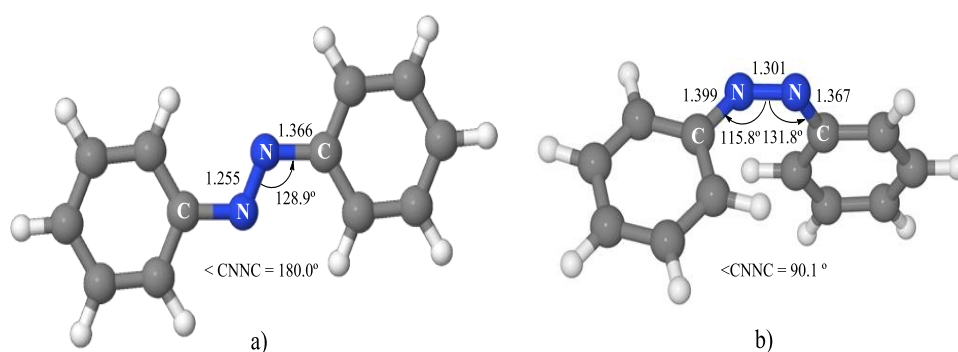


Figure 4.6 - Minimum energy geometries of the lowest excited state of azobenzene, $1(n\pi^*)$, obtained at a) CASSCF level and b) MS-CASPT2 level for S_1 .

Single point energy calculations at MS-CASPT2 level showed that the energy of $n\pi^*$ was lower at non-coplanar geometries, pointing out again the poor description of this potential energy surface at CASSCF level. The minimum of $n\pi^*$ was, therefore, reoptimized at MS-CASPT2 level. A more stable minimum was found with a CNNC dihedral angle of 90.1° . The relaxation path from FC to this minimum is barrierless. This structure is presented in Figure 4.6 b) and Table 4.4 compares the results obtained at CASSCF and CASPT2 level. This result is in disagreement with the traditional view established that rule out the rotation for this state due to the presence of large energy barriers. However, this minimum is in agreement with more recent computational studies, although in these works the stabilization of the $n\pi^*$ reported is almost negligible^[54] in disagreement with our results, where the relaxation decreases the energy in more than $15 \text{ kcal}\cdot\text{mol}^{-1}$ (see Table 4.4). At this geometry, the symmetry is lost. The enlargement of the N=N distance is also very relevant to explain the rotation, given that the double bond must be broken in order to carry out this process. These structural changes enable a significant approach between $n\pi^*$ and the ground state PESs that should be taken into consideration.

Table 4.4 - MS-CASPT2 energies (in kcal·mol⁻¹) relative to the ground state minimum, for the lower states of azobenzene at the minimum energy geometries optimized at CASSCF and CASPT2 level for the nπ* state.

<i>State</i>	<i>CASSCF opt.</i>	<i>Osc. strength</i>	<i>CASPT2 opt.</i>	<i>Osc. strength</i>
GS	19.7		46.8	
¹(nπ*)	55.2	< 10⁻⁸	49.4	0.12·10⁻²
¹ (ππ*)	112.6	1.16	161.6	0.44
¹ (n ² π* ²)	119.6	< 10 ⁻⁸	69.3	0.76·10 ⁻²

¹(ππ*) state

Although it was clear that the dynamic correlation is crucial in the description of the ¹(ππ*) state, the first attempt to find the minimum energy geometry was also done at CASSCF level. With this method, a planar minimum (Figure 4.7 a) 76.3 kcal·mol⁻¹ above the ground state minimum was located by optimizing the fourth excited state since it is the largest contributor to the composition of the MS-CASPT2 absorbing state (see Table 4.2). This structure shows noticeably shortened C-N distances and a clear lengthening of the N=N distance, turning it into a single bond. This is an expected consequence of the promotion of one π electron to an antibonding π orbital that will weaken the π double bond. The MS-CASPT2 energies calculated at this geometry show that the nπ* and the ππ* states are almost degenerate, indicating that this structure can also be a crucial point of deexcitation in the isomerization mechanism. The oscillator strength from this state at this point is large, what could explain a fast deactivation from this structure.

When the geometry is reoptimized at MS-CASPT2 level, the minimum is located at the geometry shown in Figure 4.7 b. Comparison of CASSCF and CASPT2 results are shown in Table 4.5. Contrary to expectations generated by the N=N elongation, the minimum does not correspond to a rotated geometry, unlike the traditional view had predicted,^[15,22] nor to a very fast deactivation to n²π*² ^[23,29,38] but to an out-of-plane concerted distortion of the CCNN and NNC'C' dihedral angles.

Fourth chapter: Azobenzene and Phenylazopyridine

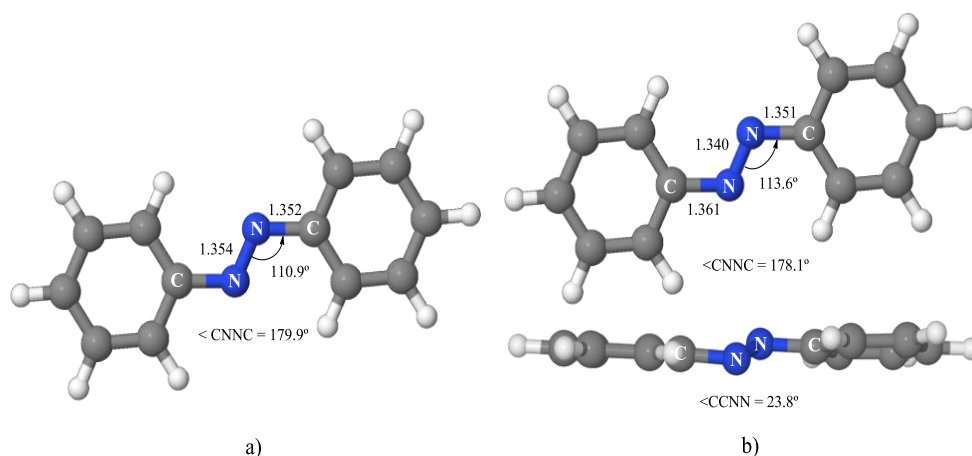


Figure 4.7 - Minimum energy geometries of the ${}^1(\pi\pi^*)$ state of azobenzene obtained at a) CASSCF level and b) MS-CASPT2 level.

Table 4.5 – MS-CASPT2 energies (in kcal·mol $^{-1}$) relative to the ground state minimum, for the lower states of azobenzene at the minimum energy geometries optimized at CASSCF and CASPT2 level for the $\pi\pi^*$ state.

State	CASSCF opt.	Osc. strength	CASPT2	Osc.
GS	7.6		3.9	
${}^1(n\pi^*)$	74.9	$0.59 \cdot 10^{-2}$	66.7	0.72
${}^1(\pi\pi^*)$	76.3	1.29	70.3	0.38
${}^1(n^2\pi^{*2})$	106.3	$0.17 \cdot 10^{-7}$	122.4	$0.80 \cdot 10^{-1}$

In this case, the benzene rings are kept in parallel planes in a pedal-like motion structure. Energetically, this state is located 70.3 kcal·mol $^{-1}$ above the global minimum and, therefore, 6.0 kcal·mol $^{-1}$ lower than the planar CASSCF minimum. The CASPT2 minimum does not match any of the prevalent mechanisms previously proposed in the literature for the isomerization of azobenzene. Although this coordinate has been mentioned in previous works,^[35,36] its description is different from the one provided by our results. In this geometry, ${}^1(n\pi^*)$ and ${}^1(\pi\pi^*)$ states are degenerated, so it could be the case that this geometry does not, in fact, correspond to a minimum for the $\pi\pi^*$ state but to a minimum on the S_2 surface due to a nearby S_2/S_1 conical intersection. It is difficult to determine the exact point of crossing given that the n and π atomic orbitals of the N atoms are mixed in this distorted geometry. Nevertheless, a search in this zone did not locate any minimum of $\pi\pi^*$

character on S_1 . This degeneration will be taken into consideration in the next section.

$^1(n^2\pi^{*2})$ state

CASSCF optimization of the $^1(n^2\pi^{*2})$ state, unlike the other cases at this level, led to a rotated minimum geometry, showed in Figure 4.8, with a CNNC dihedral angle of 94.1° , very close to the value for the $n\pi^*$ MS-CASPT2 minimum. However, comparisons end there because this minimum presents a clearly shorter N=N distance and the benzene moieties are symmetric, unlike in the $^1(n\pi^*)$ minimum. The energy of this state is $61.7 \text{ kcal}\cdot\text{mol}^{-1}$ above the global minimum, $70.0 \text{ kcal}\cdot\text{mol}^{-1}$ more stable than at the Franck Condon geometry (see Table 4.6). At this geometry, this state is the second excited state, what means that a crossing with the $\pi\pi^*$ must have happened along the relaxation path, dominated by the rotation coordinate, favoured by the doubly occupation of the original π^* orbital that results indistinguishable from orbitals of n character due to the rotation. In contrast with the other states, the rotated $^1(n^2\pi^{*2})$ minimum was confirmed at MS-CASPT2 level indicating that CASSCF gives a good description for the surface of this state.

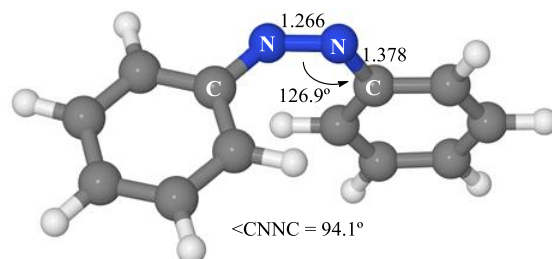


Figure 4.8 - Minimum energy geometry of the $^1(n^2\pi^{*2})$ state of azobenzene obtained at CASSCF level.

Table 4.6 – MS-CASPT2 energies (in $\text{kcal}\cdot\text{mol}^{-1}$) relative to the ground state minimum, for the lower states of azobenzene at the minimum energy geometry optimized for the $^1(n^2\pi^{*2})$ state.

State	SCF optimization	Osc. strength
GS	47.1	
$^1(n\pi^*)$	53.7	$0.30\cdot 10^{-3}$
$^1(\pi\pi^*)$	151.6	0.77
$^1(n^2\pi^{*2})$	61.7	$0.55\cdot 10^{-3}$

MS-CASPT2 results showed that at this geometry the gap with $^1(n\pi^*)$ and the ground state is significantly reduced to 8.0 and 14.6 kcal·mol⁻¹ respectively. The oscillator strength calculations indicate that the probability of emission from this mentioned minimum is negligible.

4.4.3 Reaction mechanisms

Once the minimum energy structures for each studied state are located, it is necessary to figure out how these points are connected. It means that it is necessary to determine points along surfaces where the states can interact and a transfer of population can take place effectively. These funnels become essential for any photochemical process. A scheme of the different processes that will be explored in this section (together with the most relevant energies) is shown in Figure 4.9.

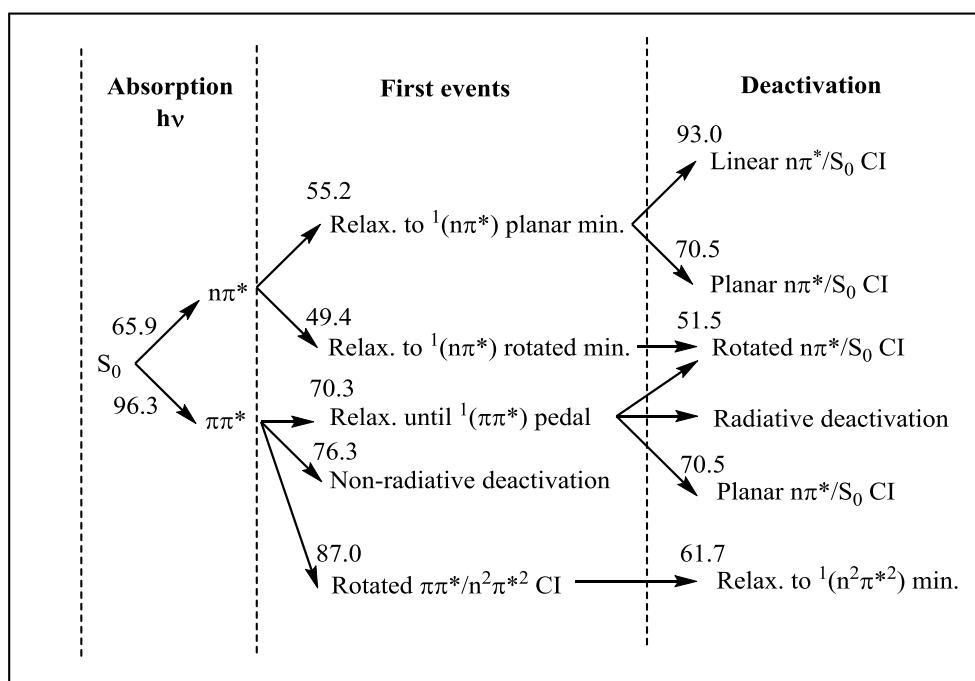


Figure 4.9 – Schematic representation of the possible photoprocesses of azobenzene. Energies in kcal·mol⁻¹.

The energies of the lowest states on the main critical points of the isomerization mechanisms of azobenzene are collected in Table 4.7.

Table 4.7 – MS-CASPT2 relative energies (in kcal·mol⁻¹) of the lowest states of azobenzene at the critical points located on the ground state and lowest energy excited state surfaces.

Geometries					
	S ₀ -min	S ₁ (nπ*)-min	S ₂ (ππ*)-min	S ₃ (n ² π* ²)-min	Cis
State					
GS	0.0	46.8	3.9	47.1	14.3
nπ*	65.9	49.4	66.7	53.7	81.6
ππ*	96.3	161.6	70.3	151.6	124.1
n ² π* ²	151.3	69.3	122.4	61.7	157.3
Geometries					
	TS	S ₁ (nπ*)/S ₀ Rotated CI	S ₁ (nπ*)/S ₀ Planar CI	S ₁ (nπ*)/S ₀ Linear CI	S ₂ (ππ*)/S ₃ (n ² π* ²) CI
State					
GS	45.3	50.5	69.4	93.0	13.3
nπ*	71.3	51.5	70.4	93.9	54.1
ππ*	127.0	144.5	123.9	128.6	85.8
n ² π* ²	174.6	75.5	102.7	144.9	88.6

Isomerization along the ground state

On the ground state surface, a transition state between both isomers was located at a geometry where the NNC angle of one of the benzene moieties is 180°. This ring is perpendicular the rest of the molecule (azo + phenyl), as shown in Figure 4.10 a). This transition state is 45.3 kcal·mol⁻¹ above the global minimum, higher than expected, although it is probable that polar solvents will decrease this barrier. The barrier for the back isomerization, from the *cis* isomer, is 31 kcal·mol⁻¹. This height is consistent with the slow rate of this thermal process that confers long lifetimes to the *cis* isomer. Based on these results, we conclude that the inversion mechanism is an appropriate way to carry out the thermal back-isomerization.

The rotation of the phenyl ring is a relatively inexpensive process, requiring only 5 kcal·mol⁻¹ at the *cis* isomer (the isomer with the strongest steric repulsions). When this planarization is imposed on the TS, the energy of the stationary point optimized (shown in Figure 4.10 b) is 10 kcal·mol⁻¹ higher than the previous one due to the steric repulsion of the rings.

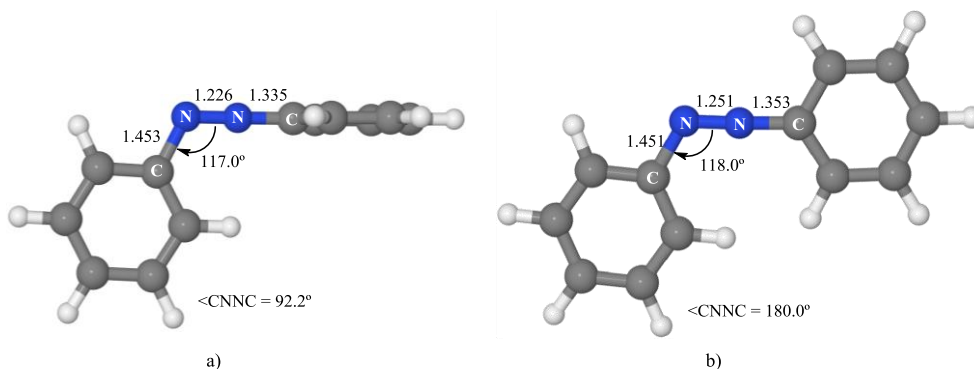


Figure 4.10 – a) TS on S_0 along the inversion coordinate, b) TS on S_0 constrained at planar geometry. Both optimized at CASSCF level.

Isomerization along the $n\pi^*$ state

Although a direct excitation to this state is forbidden by orbital symmetry restrictions in a first level of approximation, experimental evidences show that this state absorbs when azobenzene is in solution. This feature can be, in fact, predicted computationally, but it is necessary a specific strategy to get a better approximation of the experimental absorption spectra to reproduce “forbidden” bands. This subject is going to be specifically treated at the end of this chapter, for the 3-PAPY azobenzene derivative.

When the system is excited to the ${}^1(n\pi^*)$ state ($65.9 \text{ kcal}\cdot\text{mol}^{-1}$), the relaxation on this surface leads to the 90° rotated minimum, located $49.4 \text{ kcal}\cdot\text{mol}^{-1}$ above the ground state minimum, where a crossing with the ground state is nearby. The profiles of the PES of the lowest energy states along the LIIC connecting FC and the ${}^1(n\pi^*)$ minimum were calculated and are represented in Figure 4.11. As it can be seen in this figure, the relaxation on the ${}^1(n\pi^*)$ surface is almost barrierless, with a non-significant barrier of $0.5 \text{ kcal}\cdot\text{mol}^{-1}$. The path along the ${}^1(n\pi^*)$ surface shows that a slight rotation is favourable for this state, although its absolute minimum is planar. On the other hand, the profile of the ${}^1(n^2\pi^{*2})$ surface shows that the rotation coordinate stabilises strongly this state, that locates its minimum at a geometry similar to the ${}^1(n\pi^*)$ one.

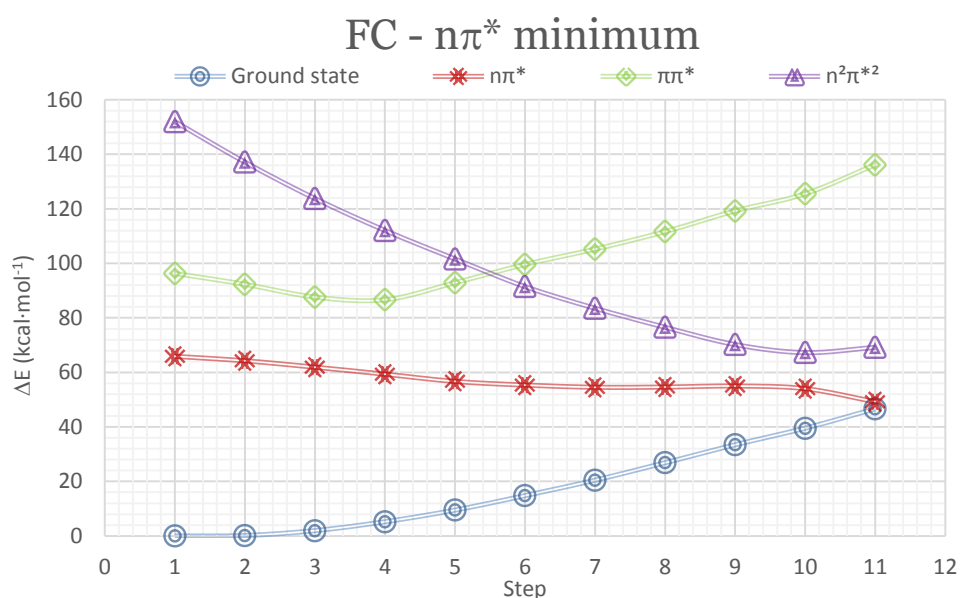


Figure 4.11 – MS-CASPT2 profiles of the PESs of the lowest energy states of azobenzene along the LIIC from FC to the $^1(n\pi^*)$ surface minimum.

A conical intersection with the ground state was located at CASSCF level near the $^1(n\pi^*)$ minimum (and confirmed at MS-CASPT2 level), with very similar geometry except by the shortened N=N distance, as indicated in Figure 4.12, and with an energy only 2.1 kcal·mol⁻¹ higher than the minimum. The closeness of the $^1(n\pi^*)$ minimum ensures that the system will remain enough time in this region. The low energy of the crossing makes it very accessible, taking into account the inertia accumulated from the initial excitation. These two reasons indicate that the funnel to the ground state through this crossing will be very efficient. However, this crossing point is available only if the rotation is chemically not hindered.

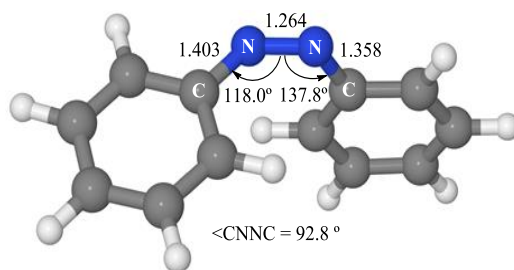


Figure 4.12 – Minimum energy point of the $n\pi^*/S_0$ conical intersection optimized at CASSCF level.

Fourth chapter: Azobenzene and Phenylazopyridine

We also looked for structures that would be involved in the inversion mechanism along the ${}^1(n\pi^*)$ state, but no critical points of these characteristics were located at accessible energies. Nevertheless, two S_1/S_0 conical intersections related with the concerted inversion mechanism were located. In this mechanism, both CNN and NNC' angles increase at the same time, in such a way that a structure with a linear CNNC moiety could be reached. In fact, a S_1/S_0 crossing point with such a structure was found, but its high energy (27.1 kcal·mol⁻¹ above the excitation energy to S_1) indicates that it could only be involved in the isomerization mechanism, although unlikely, when the system is excited to S_2 .

The other $n\pi^*/S_0$ crossing point of similar characteristics was also located at CASSCF level. The geometry of this point is also planar and has a symmetric NNC bending of 153.3° combined with a short N=N distance close to the one corresponding to a triple bond (Figure 4.13 a). Due to the poor description of the ${}^1(n\pi^*)$ state at CASSCF level, when the energies of the ${}^1(n\pi^*)$ and S_0 states are recalculated at this geometry at the MS-CASPT2 level, the energy gap between them is found to be 9.4 kcal·mol⁻¹. Scanning the area around the CASSCF conical intersection point, an extended crossing area at MS-CASPT2 level was found. Exploring the branching space provided by the CASSCF calculations, the lowest energy crossing point in that region at MS-CASPT2 level was determined (Figure 4.13 b). Decay can then occur at this point without rotation.

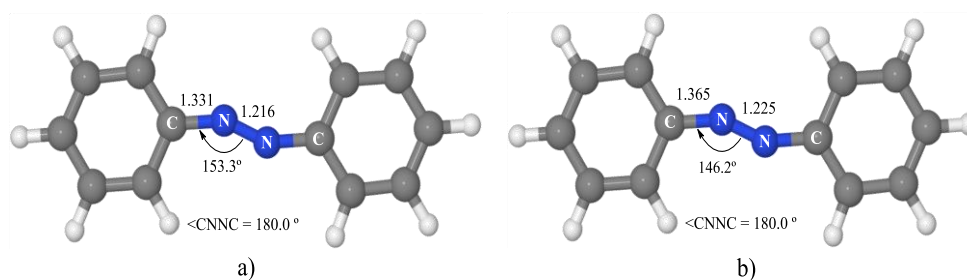


Figure 4.13 – Planar $n\pi^*/S_0$ conical intersection a) optimized at CASSCF level and b) located at MS-CASPT2 level.

However, once the system is on the S_0 PES, given the geometry of the crossing point it does not seem evident that the system will evolve along the S_0 surface to the *cis* isomer. To explore this possibility, the profiles of the lowest excited states along the LIIC from *trans* geometry to the S_1/S_0 planar-CI and from here to *cis* geometry

were calculated and represented in Figure 4.14. In this LIIC, after the S_1/S_0 CI the phenyl groups rotate step by step to reach the orientation they have at the final *cis* structure, keeping the C-N-N-C moiety in plane.

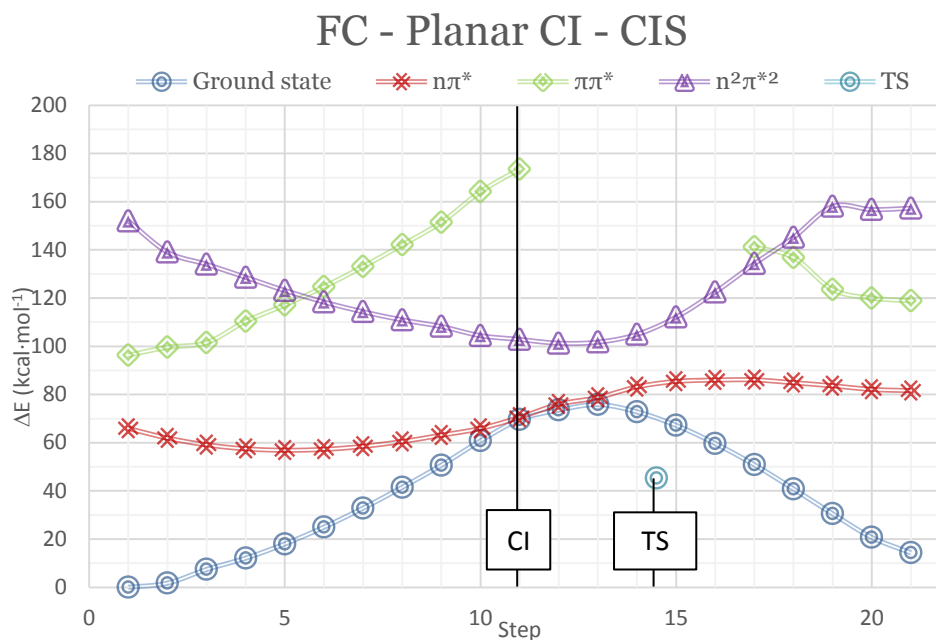


Figure 4.14 – MS-CASPT2 profiles of the PESs of the lowest energy states along the LIIC from FC to planar $n\pi^*/S_0$ CI and to *cis* isomer. TS energy of the ground state at FC geometry used as reference.

In this figure, therefore, two reaction coordinates are represented. From steps 1 to 11 (from *trans* to CI), the CNN and NNC' angles open simultaneously. From step 11 to 21 (from CI to *cis*), the phenyl groups rotate step by step to reach the orientation they have at the final *cis* structure, keeping the C-N-N-C moiety in plane. These profiles indicate that the evolution of a system with restricted rotation from Franck-Condon along the $^1(n\pi^*)$ state leads the system to a shallow minimum that is consistent with the CASSCF optimized structure. From this geometry, a barrier of $13.6 \text{ kcal}\cdot\text{mol}^{-1}$ must be overcome to reach the CI, which can be a bottleneck for the isomerization. This fact can explain the lower quantum yields for isomerization along the $^1(n\pi^*)$ state when the rotation is blocked.^[14]

Once the conical intersection is reached, this linear interpolation shows a downhill profile on the surface of S_0 from the crossing to the *trans* isomer as expected and a

Fourth chapter: Azobenzene and Phenylazopyridine

small barrier of 6.0 kcal·mol⁻¹ in the direction of the *cis* isomer. However, the analysis of this feature indicates that it is an artefact of the route described by the LIIC strategy. To understand it, we must recall as an example the thermal isomerization path along the ground state surface. The transition state found for the ground state path corresponds to the pure inversion mechanism with a linear NNC angle and the benzene rings perpendicular to each other. If the rings are forced to be coplanar, the energy of the structure increases in around 10 kcal·mol⁻¹ (Figure 4.10).

In the aforesaid LIIC, the S₁→S₀ decay geometry (planar CI), has an N-N-C angle of 148°, and the phenyl rings are coplanar. In the next 3 steps of the LIIC the N-N-C angle opens to 180°, and the phenyl rings rotate step by step, but they do not reach a perpendicular orientation until later on along the LIIC. This non-perpendicular orientation of the rings, artificially fixed by the LIIC procedure, increases “unnecessarily” the energy of the S₀ profile. The slightest relaxation of the dihedral angle between phenyl rings will decrease the energy of the system on the S₀ state making the barrier of Figure 4.14 disappear. In fact, a trial calculation was performed on point 13th, the one with the highest energy, which showed that a twist of less than 10° on one the phenyl rings yielded a stabilization of more than 15 kcal·mol⁻¹. Therefore, even a small relaxation of the dihedral angle between phenyl rings decreases enough the energy of the system to make the barrier showed in the path disappear. Unfortunately, it is not possible to reproduce the constraints imposed in the experiments for flatten systems in our calculations, but the obtained results are enough to show that, if the planar nπ*/S₀ CI is reached, the system can evolve towards the *cis* isomer without further barrier.

Isomerization along the ¹(ππ*) state

In section 4.4.2, the minimum energy point of the ¹(ππ*) PES was localized (the pedal-like minimum, 70.3 kcal·mol⁻¹ above the ground state minimum). But to predict the role of this structure in the photoisomerization of azobenzene on this state, it is necessary to know if this region of the surface is accessible after the excitation to this state, and which are the channels that could give place to the isomerization reaction from this region. Starting from the vertical excitation on the S₂ PES at the FC geometry, 96.3 kcal·mol⁻¹ more energetic than the ground state minimum, the calculated gradient on the S₂ surface points toward the pedal-like minimum. In order to check if this relaxation path was barrierless, the profiles of

the PESs of the lowest energy states along the LIIC between Franck-Condon and the ${}^1(\pi\pi^*)$ minimum were computed (Figure 4.15). The barrierless path obtained on S_2 indicates that the system will relax easily to the pedal-like structure.

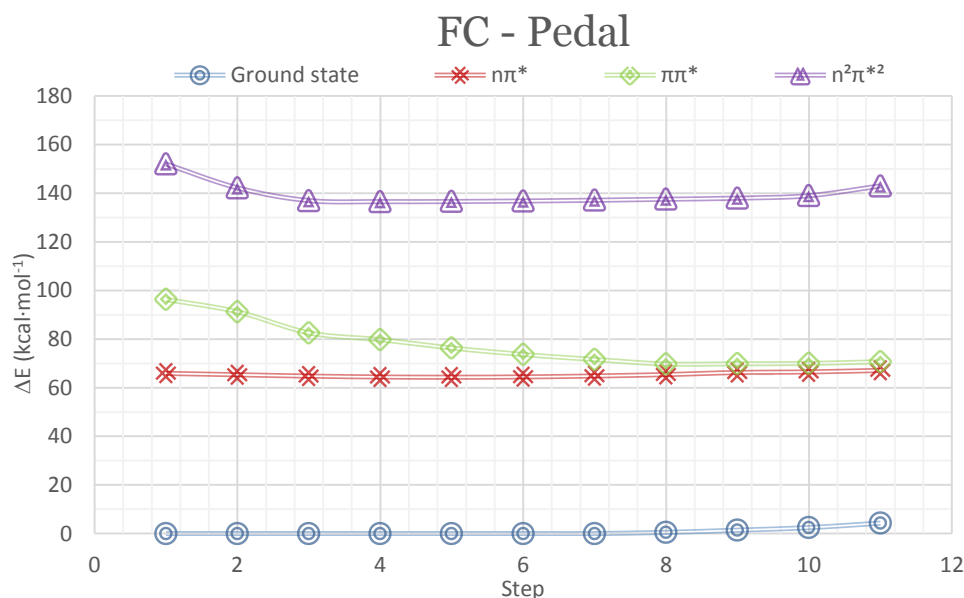


Figure 4.15 – MS-CASPT2 profiles of the PESs of the lowest energy states of azobenzene along a LIIC from FC geometry to the minimum energy point of $\pi\pi^*$ (pedal-like).

Given that the ${}^1(n\pi^*)$ and ${}^1(\pi\pi^*)$ states are degenerated in this final geometry and in the close surroundings, it is expected that the transfer of population to the S_1 ($n\pi^*$) state will be fast and efficient since the population could remain in the area enough time to favour the transfer. After the crossing, the process will continue on the ${}^1(n\pi^*)$ surface. To check if from this geometry the $n\pi^*/S_0$ CIs are accessible, we calculated the profiles of the S_1 surface along the LIICs between the $\pi\pi^*/n\pi^*$ CI and both the rotated and planar $n\pi^*/S_0$ CIs.

As shown in Figure 4.16 (upper panel), the path to the rotated $n\pi^*/S_0$ CI is barrierless, and do not differ substantially from the ones explored above starting at the FC geometry, what is consistent with the close similarity of those geometries. In the case of the relaxation to the rotated CI, the ${}^1(n\pi^*)$ surface is fairly flat in a wide area in the middle of the reaction coordinate although the CI could be reached

because there is not any barrier to stop the process. On the lower panel of Figure 4.16, the LIIC from the pedal-like minimum to the $n\pi^*/S_0$ planar CI shows that there is a local minimum on S_1 , 56.3 kcal·mol⁻¹ above the global minimum, what generates a barrier of 14.2 kcal·mol⁻¹ to reach the planar intersection. In this case, unlike from the FC geometry, the inertia accumulated from the excitation to the $\pi\pi^*$ state can be crucial in order to make this crossing affordable. After reaching the $n\pi^*/S_0$ intersections, the evolution of the system is the same than when excited to S_1 ($n\pi^*$) state.

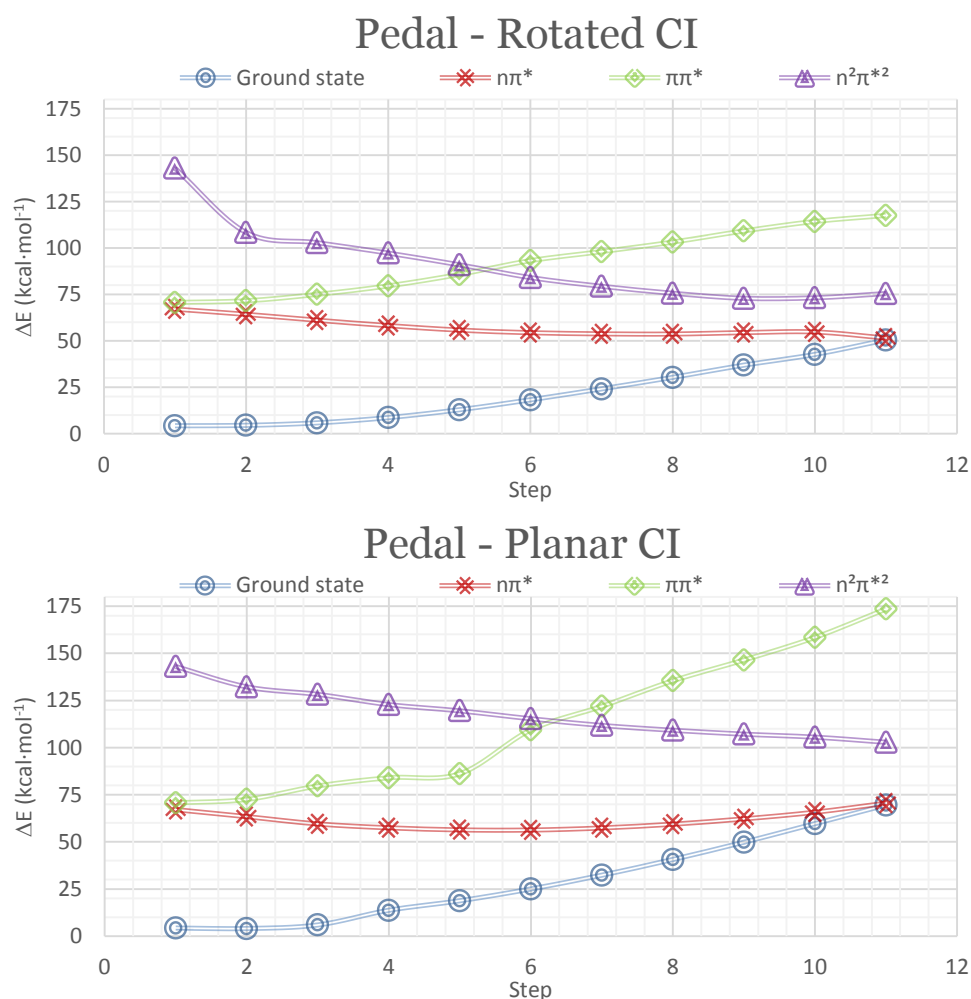


Figure 4.16 – MS-CASPT2 profiles of the PESs of the lowest energy states of azobenzene along the LIICs from the $\pi\pi^*/n\pi^*$ crossing point to both planar and rotated $n\pi^*/S_0$ conical intersections.

After examining these profiles and those shown in Figure 4.14, a common feature that can open up a third pathway of isomerization is observed. It consists in a crossing point between the ${}^1(\pi\pi^*)$ state and the double-excited ${}^1(n^2\pi^{*2})$ state. In this case, this CI could not be optimized due to the poor description of the ${}^1(\pi\pi^*)$ state at CASSCF level, but a low energy point of the S_3/S_2 crossing subspace was found by exploring the area around the crossing points localized in the LIICs. Its geometry shows a CNNC dihedral angle of 141.4° and an elongated N=N distance (Figure 4.17). The shortened C-N distances and NNC angles present asymmetric values. In energetic terms, this crossing point is $87.0 \text{ kcal}\cdot\text{mol}^{-1}$ above the global minimum and, therefore, $9.3 \text{ kcal}\cdot\text{mol}^{-1}$ lower than the initial excitation energy to the $\pi\pi^*$ state.

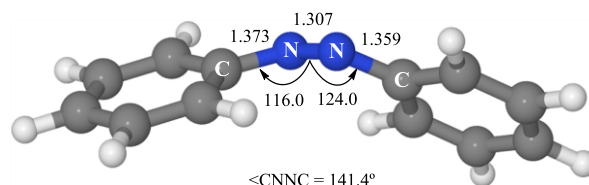


Figure 4.17 – $(\pi\pi^*) / (n^2\pi^{*2})$ crossing point geometry located at MS-CASPT2 level.

The path of accessing this crossing was studied using the LIIC strategy as usual from the Franck-Condon geometry. The profile of the ${}^1(\pi\pi^*)$ surface (Figure 4.18) shows that the energy of this state decreases with the rotation of the CNNC dihedral angle until a twist of around 160° , where a local minimum is placed. This small twist brings the system closer to the crossing, but a relatively small barrier of $6.2 \text{ kcal}\cdot\text{mol}^{-1}$ must be overcome to reach it.

From the energetic point of view, the accessibility of this crossing is given by this energy barrier, but another factor to take into account is the probability that the system decay along this path after the initial excitation. As we have shown before, the gradient on S_2 at the FC geometry points to the pedal-like minimum but, although this will be the preferential stabilization path, a percentage of the wavepacket can relax towards the local minimum of rotated geometry and finally access the $\pi\pi^* / n^2\pi^{*2}$ CI. Once this crossing is reached, the system can populate the ${}^1(n^2\pi^{*2})$ surface minimum showed in Figure 4.8 that present a dihedral angle of 94.1° slightly shifted toward the *trans* isomer. At this minimum, this state is only $10 \text{ kcal}\cdot\text{mol}^{-1}$ higher in energy than the ${}^1(n\pi^*)$ state but the gap is maintained in the surroundings of this minimum and, although a point of degeneration was looked

for, none was found in this area. However, the PM-CAS-CI functions obtained at MS-CASPT2 level for this and the ground state show a strong mixing between the CASSCF wavefunctions of these states, what can indicate that the topography of the S_0 and S_2 surfaces in this area can be given by a strongly avoided crossing between these states.

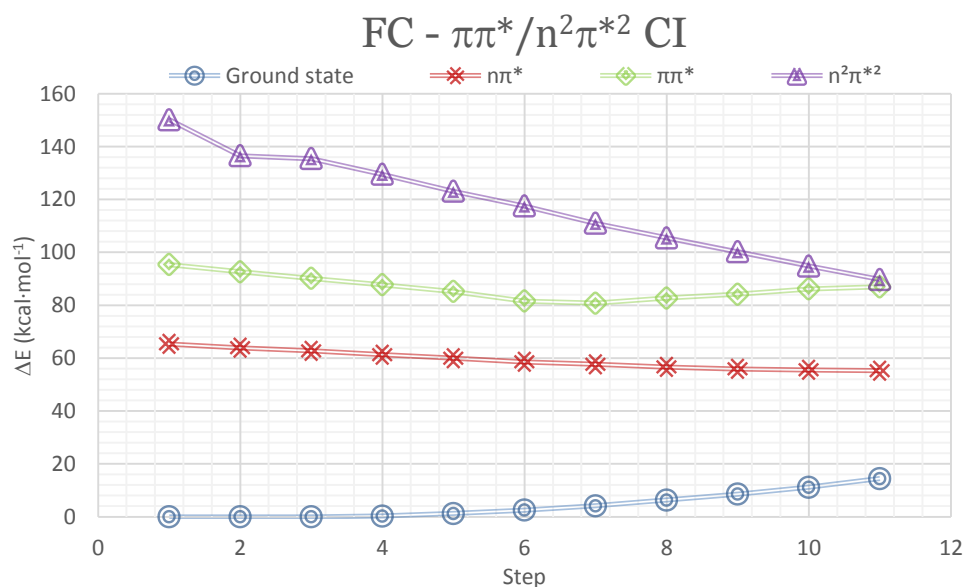


Figure 4.18 – MS-CASPT2 profiles of the PESs of the lowest energy states of azobenzene along the LIIC from the FC geometry to the $\pi\pi^*/n^2\pi^{*2}$ CI.

4.4.4 Global description of the proposed mechanism

The mechanisms suggested by the analysis of the potential energy surfaces is summarize in the cartoon scheme shown in Figure 4.19.

In systems with free rotation, the minimum energy point of the excited S_1 ($n\pi^*$) state has a rotated geometry (optimized for the first time, to our knowledge, in this work), what favours the rotational mechanism for photoisomerization along this state. This fact is in agreement with most of the recent computational studies.^[38-40] Our suggested mechanism includes a crossing point with the ground state located near the S_1 minimum, where the CNNC coordinate reaches the critical value of 90° . On the other hand, for S_2 , a new coordinate of relaxation is detected, where the driving force is the out-of-plane concerted distortion of CCNN and NNC'C' dihedral

angles in a pedal-like motion. At this distorted geometry S_2 and S_1 are degenerate, so this feature could easily explain the fast deactivation from S_2 to S_1 in planar structures (CNNC=180°), given that this critical point is not far from the ground state geometry of the *trans* isomer, in agreement with the high quantum yields of $S_2 \rightarrow S_1$ internal conversion reported from experimental works.^[21] From this deactivation point, the most favourable and barrierless pathway goes through the same rotated S_1/S_0 CI used in the S_1 pathway. But the S_2 PES has another downhill coordinate at the FC geometry, less favoured but still possible. It leads to a local minimum with a slightly rotated geometry (CNNC dihedral angle of 165°) and to the nearby crossing with the S_3 state of double-excited $n\pi^*$ character. The possible bifurcation of the relaxation on the S_2 PES could explain the lower quantum yield of photoisomerization when azobenzene is excited to the S_2 ($\pi\pi^*$) state.

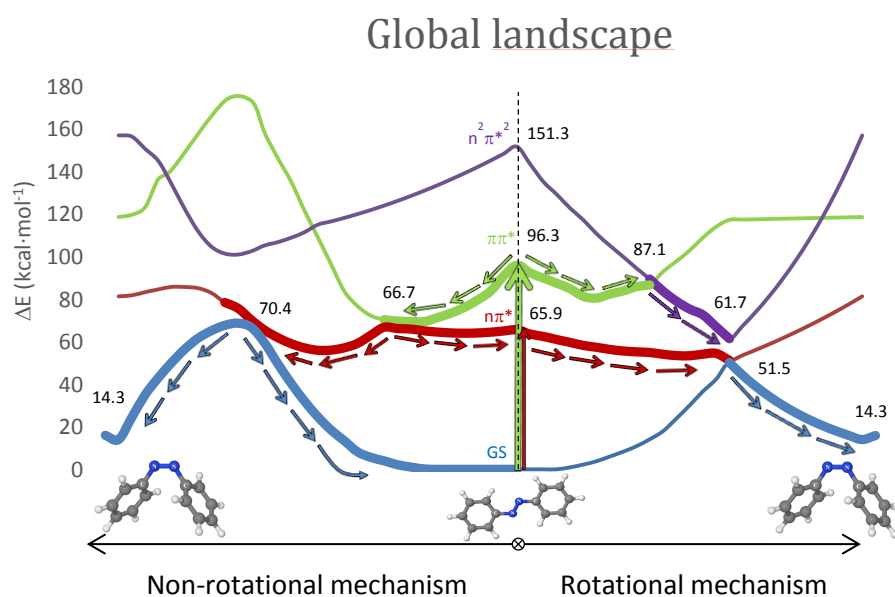


Figure 4.19 – Global scheme of the profiles of the paths for the photoisomerization of azobenzene along S_1 ($n\pi^*$) and S_2 ($\pi\pi^*$) states for free-rotation and restricted-rotation azobenzene derivatives (energies, in kcal·mol⁻¹, not in scale).

In a constrained environment, when the system is excited to S_2 , the relaxation towards the rotated local minimum (at 160° approx.) and the crossing with the S_3 state (at 140° approx.) will be more or less hindered, depending on the rigidity imposed to the system by the constraint. If the rigidity is large, the quantum yield

Fourth chapter: Azobenzene and Phenylazopyridine

of isomerization through S_2 will increase, given that all the relaxation on this surface will lead towards the pedal-like minimum and deexcitation to S_1 . Such an observation was reported by Rau.^[11] If the constraint allows certain rotation, rotational relaxation will compete with direct deexcitation to S_1 and this quantum yield will hardly change, as reported in Bortolus.^[14]

Once on the S_1 ($n\pi^*$) state, reached by deactivation from S_2 or from direct excitation to S_1 , deactivation to the ground state must take place. Again, depending on the strength of the imposed constrain, the decay will take place at more or less rotated geometries of the conical intersection seam. It means that the internal conversion can occur at any point of a subspace of geometries with different energies depending on the environment of the system, and making difficult the prediction of the quantum yield of this isomerization pathway. In the less favoured case, for planar geometries, the barrier to reach the CI is 14 kcal·mol⁻¹, but the accumulated inertia of the system after the initial excitation should be enough to overcome it. From the planar S_1/S_0 CI, the system can relax towards the *trans* or the *cis* isomers. To evolve towards the second one, phenyl rings must twist to reach the final geometry of the *cis* isomer. This movement makes disappears the barrier on the S_0 surface shown in the LIIC of Figure 4.14. Nevertheless, given that the *trans* isomer is favoured thermodynamically, the probability of formation of this isomer is larger. These circumstances would explain the low yield of the *trans*→*cis* photoisomerization of azobenzene.

Finally, the thermal back isomerization *cis*→*trans* that takes place along the ground state potential energy surface, will follow a pure inversion path that shows a barrier of approximately 30 kcal·mol⁻¹. This energy makes this back reaction slow enough to confer long lifetimes to the *cis* isomer. From the computational point of view, our results show that to determine properly the topography of the potential energy surfaces of the excited states of azobenzene, it is necessary to include in the geometry optimization procedure the dynamic electron correlation, in order to describe accurately enough the electronic distribution of this excited states. This special feature of our computational methodology has allowed us to locate more accurately than in previous works the critical points crucial to describe the mechanism of photoisomerization of azobenzene.

4.5. PHENYLAZOPYRIDINE RESULTS

In this part, our comparative study is going to point out the similarities between azobenzene and phenylazopyridine although we are going to focus our attention on the differences that the calculations show up.

4.5.1 Franck-Condon Region

Like in the previous case, the optimization of the structural parameters for the ground state minima is the first step of this study. The asymmetry of the pyridine ring gives place to two possible conformers for each isomer. Only the more stable one will be considered in this work. The minima for the *trans* and *cis* isomers obtained (Figure 4.20) are very similar to those of azobenzene, except for the asymmetry between phenyl and pyridine moieties. In *trans*-3-PAPy, NC bonds and NNC angles are slightly smaller in the pyridine moiety than in the phenyl one (1.419 Å and 114.7° in the first versus 1.423 Å and 115.0° in the second). In *cis*-3-PAPy, the structural parameters are remarkably similar to those of azobenzene, except for the CNN angles, which are almost equal in the first compound. From the energetic point of view, the *cis* isomer is 11.3 kcal·mol⁻¹ above the global *trans* minimum, being this energy difference 3.0 kcal·mol⁻¹ smaller than in azobenzene.

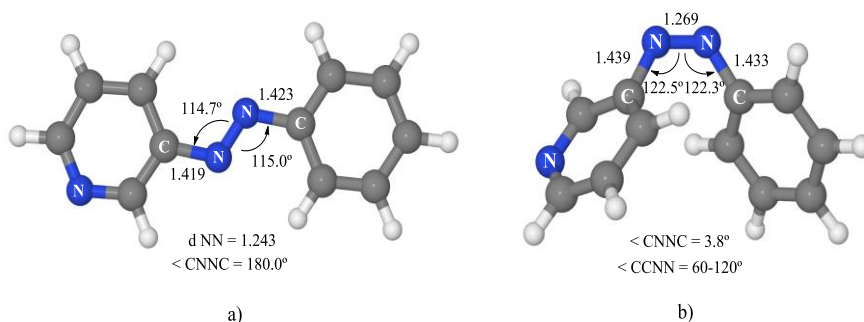


Figure 4.20 – a) Ground state global minimum b) *Cis* isomer minimum. Both optimized at CASSCF level.

The analysis of the wavefunctions points out the main difference with azobenzene, which is the appearance of a ¹(n_{py}π*) state in between the lowest energy states of nπ* and ππ* character (Table 4.8). The relative energies of the other states are close to the results obtained in azobenzene. The lowest excited states are usually the ones that are involved in the photochemistry of a system, so the influence of n_{py}π* has to

Fourth chapter: Azobenzene and Phenylazopyridine

be explored. The orbitals involved in the excitations of the ${}^1(n\pi^*)$, ${}^1(\pi\pi^*)$ and ${}^1(n^2\pi^{*2})$ are similar to those of azobenzene. The ${}^1(n_{py}\pi^*)$ state is described by an excitation from the lone pair of the pyridine nitrogen to the same delocalized π^* orbital where the transitions of the other excited states takes place, although a small contribution from the π^* of pyridine is also present. Similarly to ${}^1(n\pi^*)$, the band of the excitation to the ${}^1(n_{py}\pi^*)$ state is also visible in the experimental spectra despite the low oscillator strength calculated for it (see Table 4.8). The reason of this disagreement has already been commented, and it is going to be addressed later in this section. At CASSCF level, this state is the eighth root, but the dynamic electron correlation included as a perturbation in the CASPT2 treatment strongly affects its relative energy to lower it to the third position.

Table 4.8 – MS-CASPT2 energies (in kcal·mol⁻¹) relative to the ground state minimum, for the five lowest energy states of 3-PAPy at *trans* and *cis* ground state minima. Experimental values in parenthesis.^[45]

State	<i>Trans-3-PAPy</i>		<i>Cis-3-PAPy</i>	
	MS-CASPT2	Osc. strength	MS-CASPT2	Osc. strength
GS	0.0	-	11.3	-
${}^1(n\pi^*)$	65.6 (64.3)	$< 10^{-5}$	78.9	$0.36 \cdot 10^{-1}$
${}^1(n_{py}\pi^*)$	92.6 (123.8)	$0.15 \cdot 10^{-3}$	133.8	$0.92 \cdot 10^{-2}$
${}^1(\pi\pi^*)$	94.3 (90.5)	0.99	114.9	0.12
${}^1(n^2\pi^{*2})$	153.5	$< 10^{-4}$	154.0	$0.10 \cdot 10^{-1}$

As it can be seen in Table 4.8, the experimental energy for $n_{py}\pi^*$ state is quite different compared to the calculated value. The disagreement shown is mainly due to the flexibility of the CNNC dihedral rotation coordinate in solution (explored in the absorption spectrum section) and to the fact that the modifications of this coordinate are extremely unfavourable for the $n_{py}\pi^*$ state.

4.5.2 Minimum energy points on excited state surfaces

The PES of the states ${}^1(n\pi^*)$, ${}^1(n_{py}\pi^*)$, ${}^1(\pi\pi^*)$ and ${}^1(n^2\pi^{*2})$ have been examined. Each studied state has been optimized following the protocol previously used in order to identify and quantify the existing differences between azobenzene and 3-PAPy to determine the effect that these changes could bring to the photoisomerization mechanism. Although major structural changes are not expected, the involvement

of the $n_{py}\pi^*$ state and changes in relative energies can modify the balance between states that eventually lead to different photochemical processes.

$^1(n\pi^*)$ state

The CASSCF minimum of this excited state is located $52.5 \text{ kcal}\cdot\text{mol}^{-1}$ (Table 4.9) above the global minimum and, therefore, $13.1 \text{ kcal}\cdot\text{mol}^{-1}$ lower than the vertical excitation energy to this state. In comparison with azobenzene, the same geometrical modifications of the internal coordinates are present in general: this minimum has a planar structure with shorter C-N_{azo} distances and larger CNN angles (Figure 4.21, to be compared with Figure 4.6). Taking into account the incapacity of the CASSCF to properly describe this state (as observed in azobenzene), the geometry was also reoptimized at MS-CASPT2 level.

Table 4.9 – MS-CASPT2 Energies (in $\text{kcal}\cdot\text{mol}^{-1}$) relative to the ground state minimum of the five lowest energy states of 3-PAPy at the $^1(n\pi^*)$ state minimum.

State	SCF optimization	Osc. strength	PT2 optimization	Osc. Strength
GS	16.3		42.4	
$^1(n\pi^*)$	52.5	$< 10^{-7}$	48.4	$0.91\cdot 10^{-3}$
$^1(n_{py}\pi^*)$	100.5	$0.31\cdot 10^{-3}$	-	-
$^1(\pi\pi^*)$	106.1	1.11	110.7	$0.43\cdot 10^{-1}$
$^1(n^2\pi^{*2})$	117.6	$0.28\cdot 10^{-3}$	62.0	$0.73\cdot 10^{-3}$

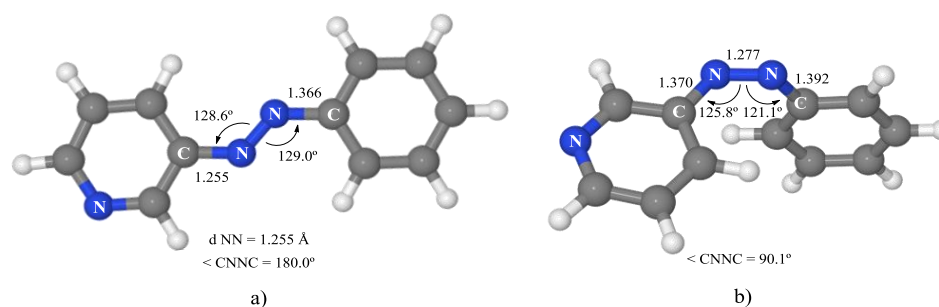


Figure 4.21 - Minimum energy geometries of the S_1 ($n\pi^*$) excited state of 3-PAPy obtained at a) CASSCF level and at MS-CASPT2 level.

As before, a deeper minimum was detected with a twisted geometry where the CNNC dihedral angle is the same than in azobenzene, but the CNN angles are not symmetric, unlike it was in the parent system, and the NN distances are clearly

shortened. This CASPT2 minimum is placed 48.4 kcal·mol⁻¹ above the ground state minimum and, therefore, indicates that in 3-PAPy the difference between planar and rotated minima is smaller.

¹(n_{py}π*) state

When the same protocol was applied to this state, the CASSCF optimization results show a minimum where ¹(n_{py}π*) is 75.7 kcal·mol⁻¹ above the ground state minimum (Table 4.10), and located on the S₁ PES indicating that it is quite probable that this state will be involved in the photoisomerization mechanism of 3-PAPy. The relative stabilization of this state is mainly due to the strong deformation that occurs in the pyridine ring, where the C-N_{py}-C angle enlarges from 117.7° in the FC geometry to 136.1° in this one (Figure 4.22). This modification can be understood in the context of the valence-bond theory where the N is expected to have sp² hybridization in the ground state while, due to the delocalization of one electron of the lone pair of the N in the ¹(n_{py}π*) state, the hybridization of this atom is closer to sp in character and, consequently, the C-N_{py}-C angle opens. Even though these changes are noticeable, the structure continues being planar, with an elongated N-N distance and a much shorter N_{azo}-C_{py} bond, while the N_{azo}-C_{bz} distance hardly changes.

This minimum is also confirmed at MS-CASPT2 level. We must point out that, before reaching the minimum, this state becomes the first excited state and, therefore, there must be a crossing with the ¹(nπ*) state during the in-plane relaxation process.

Table 4.10 – MS-CASPT2 energies (in kcal·mol⁻¹) relative to the ground state minimum of the five lowest energy states at the n_{py}π* state minimum.

<i>State</i>	<i>CASSCF opt.</i>	<i>Osc. strength</i>
GS	23.4	
¹ (nπ*)	83.9	< 10 ⁻⁷
¹(n_{py}π*)	75.7	< 10⁻⁵
¹ (ππ*)	95.1	0.87
¹ (n ² π* ²)	144.4	< 10 ⁻⁴

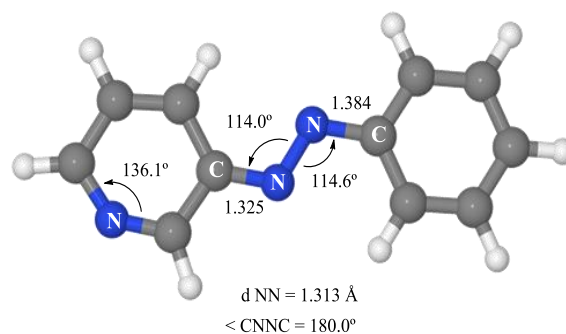


Figure 4.22 - Minimum energy geometry of the ${}^1(n_{py}\pi^*)$ excited state of 3-PAPy obtained at CASSCF level.

${}^1(\pi\pi^*)$ state

Taking into account the results on azobenzene, we expect that the description of this state at CASSCF level will not be very accurate but this method can be useful to obtain a first approximation to low-energy structures. However, in this case all attempts to achieve a CASSCF minimum have failed due to the close proximity of a dark ${}^1(n\pi^*)$ state which prevents the calculation to end successfully. On the other hand, when MS-CASPT2 optimization was used, the geometry obtained (Figure 4.23) presents a slightly twisted dihedral angle of 165° and an elongated N-N distance that corresponds to a single bond. This structure is similar to the ${}^1(\pi\pi^*)$ local minimum of azobenzene placed on the relaxation path along the torsional coordinate, as shown in the LIICs presented in Figure 4.11 and 4.18. In energetic terms, this $\pi\pi^*$ minimum is located $53.9 \text{ kcal}\cdot\text{mol}^{-1}$ above the ground state minimum on the S_1 PES, over $15 \text{ kcal}\cdot\text{mol}^{-1}$ more stable than azobenzene $\pi\pi^*$ minimum (Table 4.11). A local minimum for this state was also found on S_1 at a geometry similar to the pedal-like structure found for azobenzene at $58.8 \text{ kcal}\cdot\text{mol}^{-1}$ indicating a probable competition between both species.

A crucial difference is observed between these two systems since, in the case of 3-PAPy, ${}^1(\pi\pi^*)$ state is lower in energy than the ${}^1(n\pi^*)$ state in the minima located (rotated and pedal-like) with a gap between them of 19.8 and $11.6 \text{ kcal}\cdot\text{mol}^{-1}$ respectively. On the other hand, in azobenzene, at the equivalent structures the ${}^1(n\pi^*)$ state was 3.6 and almost $25 \text{ kcal}\cdot\text{mol}^{-1}$ more stable than the ${}^1(\pi\pi^*)$ one.

Fourth chapter: Azobenzene and Phenylazopyridine

Table 4.11 – MS-CASPT2 energies (in kcal·mol⁻¹) relative to the ground state minimum of the five lowest energy states at the ¹(ππ*) state minimum.

State	CASPT2 opt.	Osc. strength	Pedal-like local minimum	Osc. strength
GS	6.6		7.7	
¹ (nπ*)	73.7	0.10·10 ⁻¹	70.4	0.34·10 ⁻²
¹ (n _{py} π*)	108.6	0.69·10 ⁻²	105.3	0.50·10 ⁻²
¹ (ππ*)	53.9	0.45	58.8	0.48
¹ (n ² π* ²)	146.2	0.22·10 ⁻²	139.1	0.49·10 ⁻²

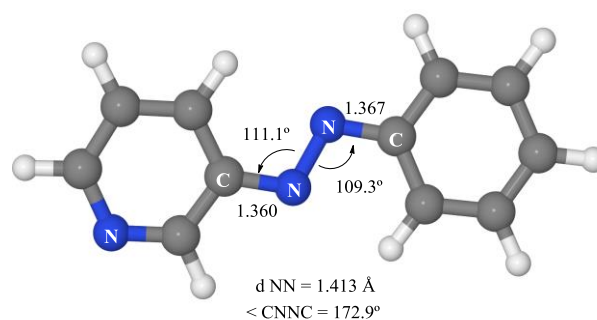


Figure 4.23 – Minimum energy geometry of the ¹(ππ*) excited state of 3-PAPy obtained at MS-CASPT2 level.

¹(n²π*²) state

The optimization procedure at CASSCF level of the doubly excited state found a minimum on this surface located at a very similar geometry to the one found for azobenzene (see Figure 4.24 and Table 4.12). Like before, this minimum was also confirmed at MS-CASPT2 level. The energy of this species is 62.3 kcal·mol⁻¹ relative to the ground state minimum, very similar to azobenzene. The gap with the ¹(nπ*) state at this geometry is also very similar to that found for azobenzene, around 10 kcal·mol⁻¹. The oscillator strength is also small, so the probability of radiative transition to the ground state is predicted to be very low. As can be seen in Table 4.12, the values for the ¹(n_{py}π*) state in rotated geometries are not present because it represents a highly unfavourable coordinate for this state, so high that it does not correspond to any of the roots calculated. In comparison to azobenzene, 3-PAPy shows two ππ* states of low energy in rotated geometries, corresponding to excitation of an electron from a molecular orbital located on the phenyl or on the pyridine rings. In each case, the lower excited state has been selected.

Table 4.12 – MS-CASPT2 energies (in kcal·mol⁻¹) relative to the ground state minimum, for the five lowest energy states of 3-PAPy at the ¹(n²π^{*2}) state minimum.

State	CASSCF opt.	Osc. strength
GS	46.0	-
¹ (nπ [*])	52.8	0.14·10 ⁻³
¹ (n _{py} π [*])	-	-
¹ (ππ [*])	113.3	0.44·10 ⁻¹
¹(n²π^{*2})	62.3	0.75·10⁻³

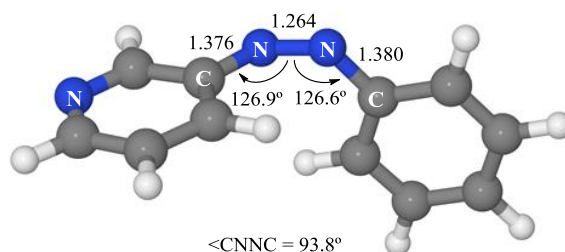


Figure 4.24 – Minimum energy geometry of the ¹(n²π^{*2}) state of 3-PAPy obtained at CASSCF level.

4.5.3 Reaction mechanisms

Isomerization along the ground state

Different from azobenzene, the asymmetry of phenylazopyridine gives place to two possible paths for the thermal isomerization along the ground state surface corresponding to the pure inversion mechanism, depending on which NNC angle is inverted. For both paths, the transition states correspond to structures where one of the rings inverts and rotates onto itself due to the steric repulsion, leaving the plane of the molecule (see Figure 4.25 and Table 4.13). If this is the phenyl ring, the TS energy is 42.9 kcal·mol⁻¹ above the global minimum while when it is the pyridine ring the one leaving the planarity the energy of the barrier is 39.0 kcal·mol⁻¹. This difference means that this last path will be more probable for the thermal isomerization of 3-PAPy. No second order saddle point connecting both TS was found.

Table 4.13 - MS-CASPT2 energies relative to the ground state minimum for the five lowest energy states of 3-PAPy at the transition states geometries.

State	TS1	Osc. strength	TS2	Osc. strength
GS	39.0	-	42.9	-
$^1(n\pi^*)$	67.7	$0.30 \cdot 10^{-3}$	66.3	$0.23 \cdot 10^{-2}$
$^1(n_{py}\pi^*)$	145.6	0.51	152.4	$0.71 \cdot 10^{-2}$
$^1(\pi\pi^*)$	133.9	0.25	137.1	$0.65 \cdot 10^{-2}$
$^1(n^2\pi^{*2})$	120.1	$0.23 \cdot 10^{-1}$	123.2	$0.75 \cdot 10^{-2}$

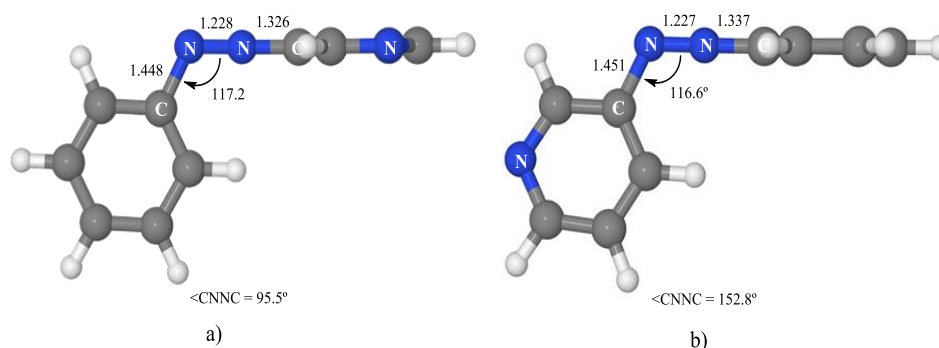


Figure 4.25 – Optimized geometries for the transition states of the isomerization of 3-PAPy along the ground state following different reaction paths: a) TS1 for inversion of the pyridine ring, b) TS2 for inversion of the phenyl ring. Both geometries optimized at CASSCF level.

Isomerization along the $n\pi^*$ state

The critical points that determine the photoisomerization mechanism along this state for 3-PAPy are analogous to those found for azobenzene. We have located rotated and planar $n\pi^*/S_0$ conical intersections (see Figure 4.26 and Table 4.14) with geometries very similar to those of azobenzene. The rotated crossing point is near the $^1(n\pi^*)$ minimum and located $50.6 \text{ kcal}\cdot\text{mol}^{-1}$ above the ground state minimum. It means that it is $15.0 \text{ kcal}\cdot\text{mol}^{-1}$ below the vertical excitation to this state, what makes it easily accessible. On the other hand, the energy of the planar CI is $71.4 \text{ kcal}\cdot\text{mol}^{-1}$, only $6 \text{ kcal}\cdot\text{mol}^{-1}$ above the vertical excitation to this state, making this crossing accessible if the initial absorption populates the $^1(n\pi^*)$ state with some extra thermal energy. The consequence is that our results predict that 3-PAPy can also undergo isomerization on the $n\pi^*$ surface if rotation is blocked. This hypothesis could be tested experimentally.

Similarly to azobenzene, another crossing point was located for 3-PAPy. However, this was a high-energy nearly linear structure, higher than the excitation to the S_2 state ($100.8 \text{ kcal}\cdot\text{mol}^{-1}$) and, therefore, discarded as a probable channel for the isomerization mechanism.

Table 4.14 – MS-CASPT2 energies relative to the ground state minimum, for the five lowest energy states of 3-PAPy at the rotated and planar $n\pi^*/S_0$ conical intersections optimized at CASSCF level.

State	$S_1(n\pi^*)/S_0$	Osc. strength	$S_1(n\pi^*)/S_0$	Osc. strength
GS	48.0	-	71.1	-
$^1(n\pi^*)$	50.6	$0.11\cdot 10^{-2}$	71.4	$0.27\cdot 10^{-5}$
$^1(n_{py}\pi^*)$	133.1	$0.11\cdot 10^{-1}$	152.8	$0.20\cdot 10^{-3}$
$^1(\pi\pi^*)$	120.0	$0.29\cdot 10^{-2}$	141.0	$0.30\cdot 10^{-2}$
$^1(n^2\pi^{*2})$	76.7	$0.21\cdot 10^{-2}$	105.0	$0.55\cdot 10^{-4}$

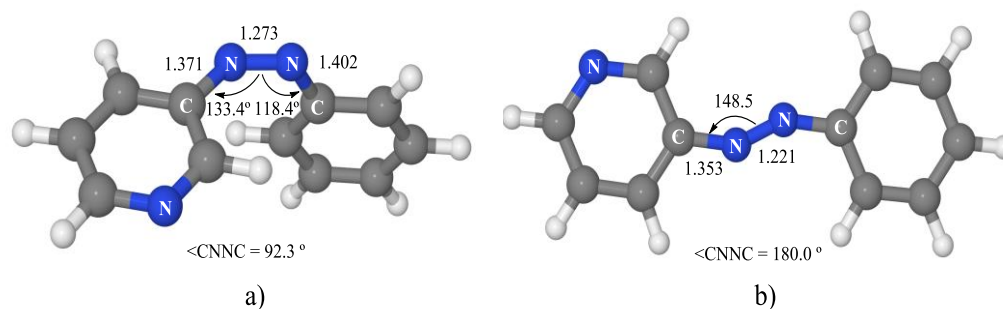


Figure 4.26 – Optimized geometries of $n\pi^*/S_0$ conical intersection a) rotated minimum optimized at CASSCF level, b) planar minimum located at MS-CASPT2 level.

Isomerization along the $^1(\pi\pi^*)$ state

At the FC geometry, the topography of the PES of the $\pi\pi^*$ excited state indicates that there are two possible relaxation coordinates that lead to stable structures, the slightly rotated global minimum and the pedal-like local minimum. To confirm the preferential relaxation path, a MEP was run from FC geometry on this state. Unlike for azobenzene, this path leads to the rotated minimum instead to the pedal-like one. These results mean that this minimum is favoured thermodynamically and kinetically, so just the rotated one should be considered possibly involved in the reaction mechanism along the $^1(\pi\pi^*)$ state for free-rotating systems. In both cases, minima are located on the S_1 PES so crossings with $^1(n_{py}\pi^*)$ and $^1(n\pi^*)$ states must occur along the relaxation path.

Fourth chapter: Azobenzene and Phenylazopyridine

The analysis of the results of the MEP from the FC geometry on the ${}^1(\pi\pi^*)$ surface also provides the geometry of the crossing point between this state and the ${}^1(n\pi^*)$ one. The structure obtained is very similar to the rotated minimum except for a shorter N-N distance (1.351Å versus 1.413Å) with an energy of 66.1 kcal·mol⁻¹. In the case of 3-PAPy, different from azobenzene, the existence of the S_1 ($\pi\pi^*$) minimum in the neighbourhood of the crossing will make that the quantum yield of the ${}^1(\pi\pi^*) \rightarrow {}^1(n\pi^*)$ intersystem crossing at this point will be different from one. On top of this, the strong oscillator strength for transition from this minimum to the ground state indicates that emission from the S_1 ($\pi\pi^*$) species is possible. The internal conversion from the ${}^1(\pi\pi^*)$ state to the ${}^1(n_{py}\pi^*)$ state also could be possible through the crossing of these surfaces but, given the higher energy of the ${}^1(n_{py}\pi^*)$ minimum, this path is not probable.

For analogy with azobenzene, the conical intersection of the ${}^1(\pi\pi^*)$ state with the $n^2\pi^{*2}$ state was also looked for along the rotation coordinate. The crossing point was located, but its energy, 106.3 kcal·mol⁻¹, discarded it as an easily accessible channel. Therefore, its involvement in the isomerization mechanism is not probable. On the other hand, the LIIC path calculated between FC geometry and the pedal like minimum for azobenzene provides another $\pi\pi^*/n^2\pi^{*2}$ crossing point, which is placed 69.7 kcal·mol⁻¹ above the global minimum in a very similar region than the analogous crossing in azobenzene. This crossing and the corresponding pedal-like minimum may become relevant in constrained systems and, therefore, should not be discarded. The prediction of the efficiency of the quantum yield of decay at this point is difficult to predict and it would be necessary to perform dynamic studies to provide an accurate prediction.

4.5.4 Global description of the proposed mechanism

Figure 4.27 shows a cartoon scheme (not in scale) that summarizes the results obtained for 3-PAPy.

If the system is excited to the S_1 ($n\pi^*$) state (weak absorption) in systems with free rotation, the mechanism of photoisomerization will be similar to that predicted for azobenzene: the relaxation on this surface leads to the minimum energy structure on this surface, along the rotational coordinate, and to a conical intersection with the ground state in a neighbouring geometry. After decay, the system can go back to reactants or to the photoproduct, less stable, but favoured by the inertia of the

movement of the nuclei. If this kind of systems are excited to the ${}^1(\pi\pi^*)$ state (strong absorption), unlike in the case of azobenzene, it will relax towards the global rotated minimum, favoured thermodynamically and kinetically, although a local pedal-like minimum can also be partially populated. In both relaxation paths there are crossing points with the ${}^1(n\pi^*)$ state. The decay to this state is predicted to be slow in the surroundings of the pedal-like minimum, as well as when following the rotational coordinate. As a whole, the quantum yield of the photoisomerization along the $\pi\pi^*$ state is expected to be smaller than along the $n\pi^*$ state.

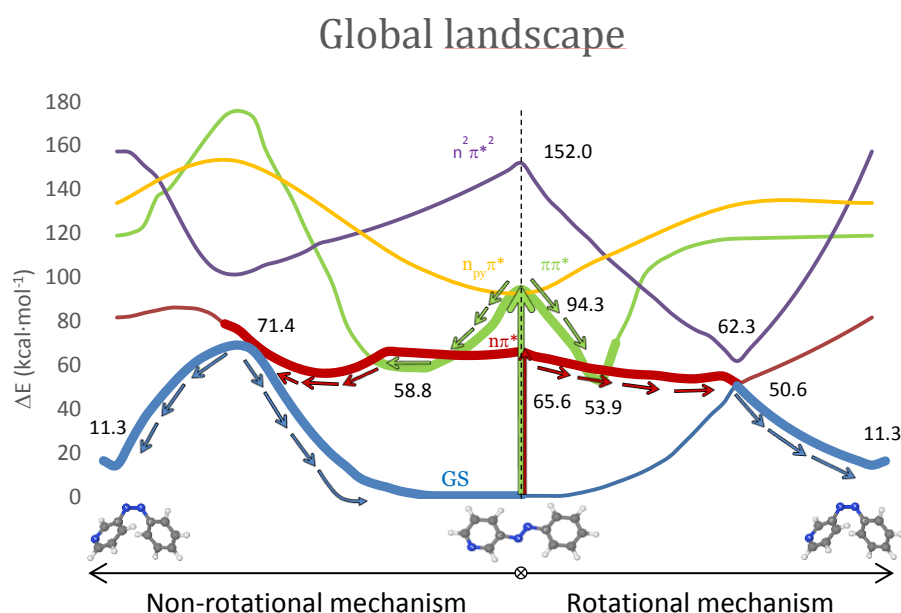


Figure 4.27 – Global scheme of the profiles of the paths for the photoisomerization of 3-PAPy along S_1 ($n\pi^*$) and S_2 ($\pi\pi^*$) for free-rotation and restricted-rotation 3-PAPy derivatives (energies, in kcal·mol⁻¹, not in scale).

For systems with constrained rotation, our results indicate that the quantum yield of photoisomerization along the ${}^1(n\pi^*)$ state will be only slightly smaller for 3-PAPy than for azobenzene, given that the planar $n\pi^*/S_0$ conical intersection is located at energies only slightly higher in 3-PAPy. On the other hand, when the system is excited to the ${}^1(\pi\pi^*)$ state, it only can relax to planar geometries, so in the direction of the pedal-like minimum. If it is reached, the system can decay radiatively from the pedal-like species. Along this relaxation path it can also cross to the ${}^1(n\pi^*)$ state. In this case, the kinetic energy accumulated from the initial absorption can be

enough to reach the planar conical intersection with the ground state that will give place to the *cis* photoproduct. Although the quantum yield of this process will not be very high, it is expected to be larger than that for the $^1(n\pi^*)$ photoisomerization in rigidized systems.

4.5.5 Simulation of the absorption spectrum

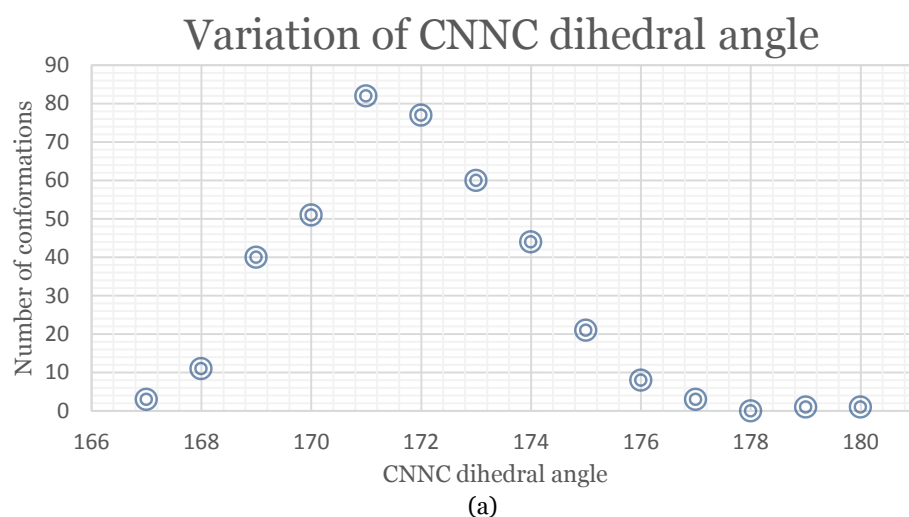
The simulation of the absorption spectrum has been carried out in order to test the computational protocol employed by our group to provide theoretical information about spectra. In this study, we compare the spectrum computed for 3-PAPy with the scarce experimental spectroscopic data available for this system. In order to generate this spectrum, the vertical energies and oscillator strengths of a number of structures have been computed using MS-CASPT2. These geometries were selected from a large dynamical calculation after gathering a statistical representation of the molecular behaviour of a sample of 3-PAPy at room temperature. The number of conformations was decided after several tests, looking for the minimum number which provided stable peak energy, which in this case proved to be 400.

The first step in these calculations is creating a box large enough to fit the target molecule inside. The optimal parameters for this box were chosen by leaving enough space between the last atom in each direction and the edge of the box once the molecule is centred to avoid the interaction between 3-PAPy molecules since we work with periodic boundary conditions. This approach resulted in a rectangular prism of 28 x 31 x 38 Å and adjusted, therefore, to a viable experimental concentration of 0.05 M. Then, this box is “filled” with a particular amount of solvent molecules, depending on the molecular volume of the solvent and the box. In our case, 513 methanol molecules were introduced due to the large box and small size of the solvent molecule and after screening the bibliography for the most suitable solvents.^[45] Afterwards, before starting molecular dynamics calculations, a short energy minimization was run in order to ensure that the system had no steric clashes and possible structure distortions since the aim is not to reach a local energy minimum.

The next step was to perform an equilibration run where 3-PAPy is restrained to the starting position while methanol is relaxing around the structure. These calculations were almost identical to the previous one but controlling the temperature and pressure with the Berendsen coupling algorithm where the

reference temperature and pressure were established to 298 K and 1 bar respectively. The equilibration phase was conducted in two phases: First, a 100 ps NVT ensemble equilibration where the number of particles (N), the volume (V) and the temperature (T) were constant. This ensemble is also referred to as “isothermal-isochoric” and finishes when the temperature is stabilized to the desired value. Second, a 100 ps NPT equilibration was also conducted wherein the pressure is constant instead of volume. This ensemble is also called “isothermal-isobaric” and it continued the simulation from the NVT phase to resemble experimental conditions. The pressure converged more slowly than the temperature but this behaviour was not unexpected. The density values were also checked and they indicated that the system was well-equilibrated.

Upon completion of the two equilibration phases, a final 100 ps MD simulation was run where the position restraints on 3-PAPy were released and the pressure coupling was turned off. The initial positions along with its trajectories were calculated in order to randomly obtain the aforementioned geometries. In order to be sure that we were not cherry-picking the geometries that seemed to give the expected results, the variability of some relevant coordinates were observed. These coordinates were the CNNC dihedral angle, CNN angle and NN distance. Their distribution on the set of conformations that forms the sample is represented in Figure 4.28, which indicates that the geometries selected represent properly the variability of the structural modifications in a real system.



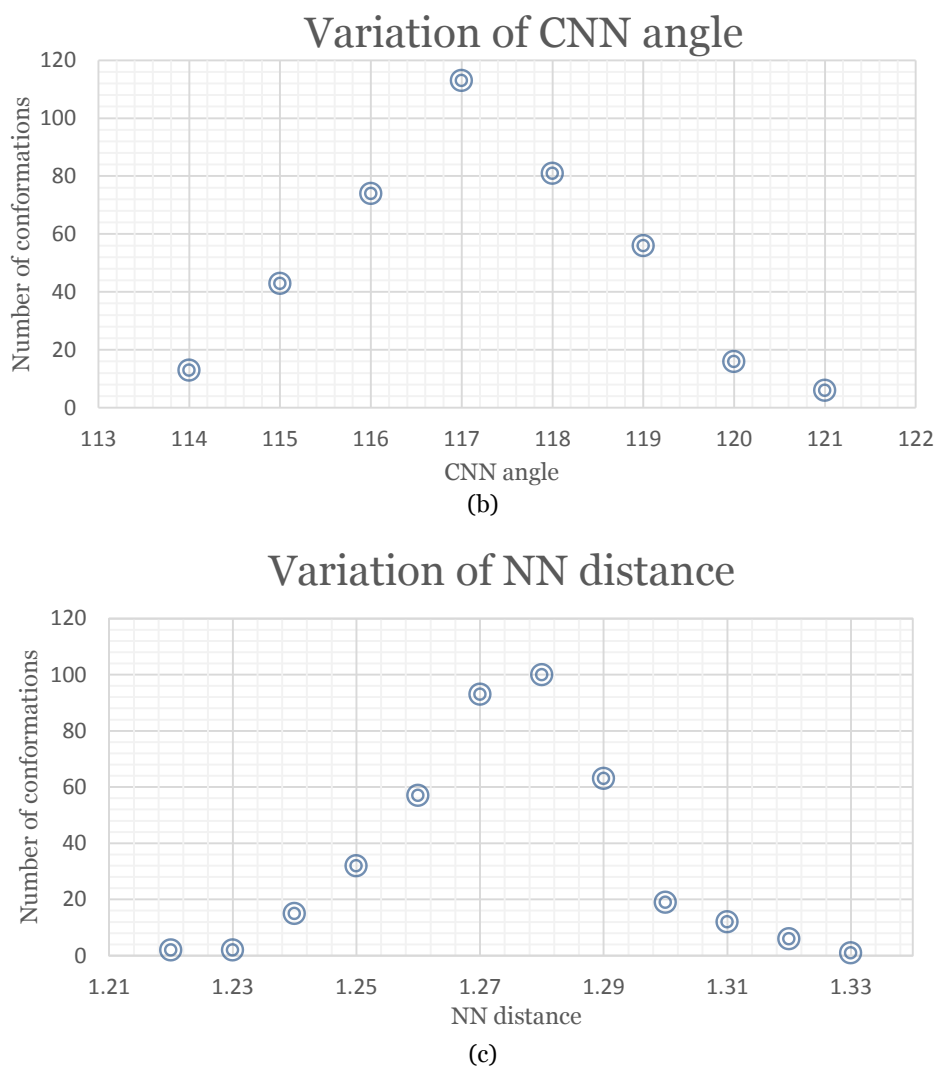


Figure 4.28 – Distribution, in the geometries selected to reproduce the absorption spectrum of 3-PAPy, of the values of a) the CNNC dihedral angle, b) the CNN angle and c) the N-N distance.

It should be pointed out that panel (a) shows that most of the selected geometries are not planar (dihedral angle different from 180°). This deformation breaks the symmetry of the system, so the selection rules does not apply any longer and the transitions that for planar geometries are “forbidden” and consequently little probable, become possible.

At each geometry, the energy of the 10 states more stable together with the transition dipole moment from the ground state were calculated taking into account the solvent environment using the PCM method. Each one of these calculations provides, then, the energy gap and oscillator strengths for 9 transitions for each geometry. The representation of the oscillator strength (proportional to the experimental intensity of the transition) versus the transition energy should reproduce the experimental spectrum. This result is shown in the upper panel of Figure 4.29. Each point represents one of the 3600 transitions ($400 \times (10-1)$ states). The black data correspond to the theoretical value of the maximum of each peak, which should be compared to the respective experimental values (showed below in orange). In order to sum up the data obtained, an R code is used to build the Gaussian curves using the accumulated intensities of each transition. The bands are labelled with the excited states involved in the transition, except for the last band since there is lack of spectroscopic information at high energies. The Figure 4.29 also reproduces the experimental spectrum of 3-PAPy reported in ref [45].

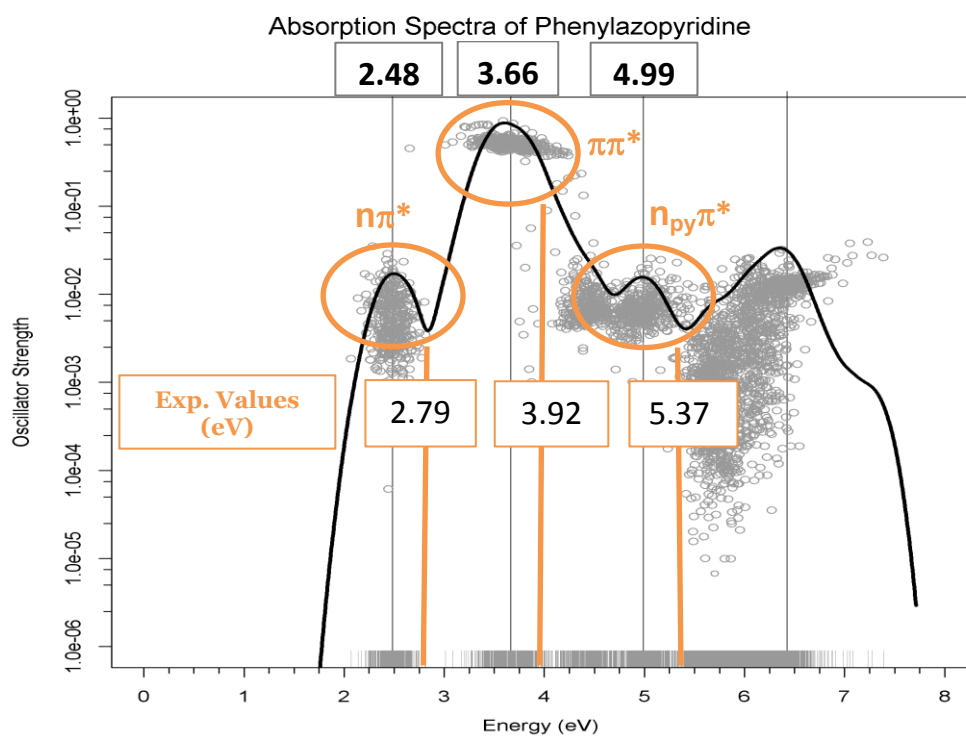


Figure 4.29– Theoretical simulation of the absorption spectra of 3-PAPy. The resulting energies and the experimental comparable values are shown in eV.

Three aspects should be highlighted.

- 1) The three-band shape of the experimental spectrum is reproduced.
- 2) The theoretical spectrum shows a regular shift of 0.3 eV in the position of the maxima of the bands, in comparison to the experimental spectrum. To analyse if this difference was due to the modelization of the solvent as a continuum, test calculations were performed including explicit methanol molecules in the model described at quantum level. The small change of the maxima of the bands showed that this was not the reason of the gap.
- 3) It is interesting to compare the absorption energies predicted computationally in section 4.5.1 (single point calculation by vertical excitation, Table 4.8) with those given by the band maxima in this section, and with the experimental values. These values are collected in Table 4.15. For the $n\pi^*$ and $\pi\pi^*$ transitions, the computed vertical excitations are larger than the computed band maximum, while it is the opposite for the $n_{py}\pi^*$ transition.

Table 4.15 – Comparison between different approaches to the experimental absorption values via vertical excitations of a) single-point MS-CASPT2 calculation and b) ensemble MS-CASPT2 calculation.

State	MS-CASPT2 (single-point)	MS-CASPT2 (ensemble)	Experimental
$^1(n\pi^*)$	65.6	57.2	64.3
$^1(n_{py}\pi^*)$	92.6	115.1	123.8
$^1(\pi\pi^*)$	94.3	84.4	90.5
$^1(n^2\pi^{*2})$	153.5	-	-

The reason of these different trends can be the trend of the variation of the energy with the main deformations from the equilibrium geometry of the geometries of the sample. In fact, we have already seen that in general the internal coordinate that affects most the energy is the dihedral angle CNNC. In the ground state minimum this angle is 180° (planar structure), but the distribution of values of this parameter in the collective that reproduces the experimental sample (Figure 4.28 panel a), show that in a large percentage of geometries the deviation is more than 5° , being the mode around 170° . For the $^1(\pi\pi^*)$ and $^1(n\pi^*)$ states, this variation in the dihedral angle leads to a decreasing of the energy, while for $^1(n_{py}\pi^*)$ the effect is the opposite and more pronounced. Consequently, the average excitation energy of the

collective to the first states will be lower than for the planar ground state minimum, while it will be higher for the ${}^1(n_{py}\pi^*)$ state, and will show a larger difference.

If we compare the energies predicted computationally with the experimental ones, the disagreement found between the computational and experimental data for the $n_{py}\pi^*$ transition can be explained then by the simplification made when considering a single geometry to calculate the excitation and compare it with the maximum of the band, together with the strong dependence of the energy on a geometrical parameter (the dihedral angle in this case).

4.6. CONCLUSIONS

4.6.1 Azobenzene

The photoisomerization of azobenzene was studied by ab initio calculations to elucidate the details of the reaction mechanisms that explain the experimental evidences compiled in the literature. The mechanisms proposed here are based on the topography of the potential energy surfaces determined computationally, using the CASSCF/CASPT2 methodology.

The results obtained lead to the following conclusions.

- Agreement between computed vertical excitations and experimental data from absorption spectra are quite satisfactory (63.5 kcal·mol⁻¹ versus 65.9 kcal·mol⁻¹ for ${}^1(n\pi^*)$ state; 96.3 kcal·mol⁻¹ versus 90.5 kcal·mol⁻¹ for the ${}^1(\pi\pi^*)$ state).^[9]
- For systems with free rotation, photoisomerization from the ${}^1(n\pi^*)$ state (weak absorption) follows a rotational mechanism. The system relaxes along ${}^1(n\pi^*)$ surface to the rotated minimum, and decay to the ground state through a conical intersection located nearby. The barrier to reach this CI is only 2.1 kcal·mol⁻¹ high from the ${}^1(n\pi^*)$ minimum. Once on the ground state surface, the system can evolve back to the more stable *trans* isomer, or forward to the *cis* isomer following the inertia of the movement of the nuclei.

Fourth chapter: Azobenzene and Phenylazopyridine

- If in this kind of systems the excitation leads to the ${}^1(\pi\pi^*)$ state (strong absorption), there are two possible relaxation coordinates on this surface. The main one leads to a pedal-like minimum. This is the first time that this species has been reported. At this geometry ${}^1(\pi\pi^*)$ and ${}^1(n\pi^*)$ states are almost degenerate, so the deactivation to the ${}^1(n\pi^*)$ state will be fast and efficient. The subsequent evolution of the system will continue along the latter surface, following the paths explained before.
- The second possible relaxation coordinate on the ${}^1(\pi\pi^*)$ surface leads to a local slightly rotated minimum, near which a crossing with the ${}^1(n^2\pi^{*2})$ is located, only 6.2 kcal·mol⁻¹ higher in energy. The possible bifurcation of the relaxation on the ${}^1(\pi\pi^*)$ surface can explain the lower quantum yield of photoisomerization in rotation-free environments when the excitation populates this state.
- For systems with restricted rotation, the photoisomerization along the ${}^1(n\pi^*)$ surface follows a concerted inversion pathway. Along this path, a planar conical intersection with the ground state is found. Like in the previous case, deactivation to the ground state can lead back to reactant or to the photoproduct. This path is less accessible than the rotational one, given that the planar $n\pi^*/S_0$ conical intersection is located at higher energies than the rotated $n\pi^*/S_0$ one.
- The relaxation followed on the ${}^1(\pi\pi^*)$ surface by a rotationally constrained system will depend on the degree of the restriction. If the system cannot rotate at all, only relaxation to the pedal-like minimum will be possible. From here, after internal conversion to the ${}^1(n\pi^*)$ state, the system will decay to the ground state through the planar $n\pi^*/S_0$ CI. This funnel will be accessed more easily after an excitation to the ${}^1(\pi\pi^*)$ state than when the system is excited to the ${}^1(n\pi^*)$ state since the absorbed initial energy and consequently the residual energy are larger than when excited to the ${}^1(n\pi^*)$ state. The quantum yield of photoisomerization in that case will be larger than in systems with free rotation.

-
- If the constrain allows a certain rotation, relaxation to the local rotated minimum can occur, but the possibility of reaching the CI with the ${}^1(n^2\pi^*)$ state will depend on the degree of rigidity of the system. If the system is trapped in the local rotated ${}^1(\pi\pi^*)$ minimum, deactivation by energy transfer to the environment is more probable, what would decrease the photoisomerization quantum yield.

4.6.2 Phenylazopyridine

3-PAPy results indicate that there are some differences in the mechanisms of photoisomerization of this system and azobenzene. The main characteristics of the first are summarize in the following.

- Agreement between computed vertical excitations and experimental data from absorption spectra are quite satisfactory (64.3 kcal·mol⁻¹ versus 65.6 kcal·mol⁻¹ for the ${}^1(n\pi^*)$ state; 94.3 kcal·mol⁻¹ versus 90.5 kcal·mol⁻¹ for the ${}^1(\pi\pi^*)$ state).^[45]
- If 3-PAPy is excited to the ${}^1(n\pi^*)$ state, the system will relax to the rotated minimum of this state. From there, it can decay to the ground state surface through the rotate CI located near this minimum also very close in energy. Once on the ground state surface, the system can evolve towards the *cis* isomer, following the inertia of the nuclei, or go back to the more stable *trans* isomer.
- If the system has the rotation constrained, our results predict that the isomerization will take place through the planar $n\pi^*/S_0$ CI that is localized very close to the analogous CI found in azobenzene. No alternative and viable pathway has been found in order to carry out the isomerization through inversion since the quasi linear CI was localized well above even the excitation energy to the ${}^1(\pi\pi^*)$ state.
- If the initial absorption excites the system to the ${}^1(\pi\pi^*)$ state, the system can follow one of the same two competitive pathways than found for azobenzene, leading to the pedal-like minimum, or to the partially rotated global minimum. However, opposite to azobenzene,

Fourth chapter: Azobenzene and Phenylazopyridine

the preferential path in 3-PAPy leads to the rotated minimum. Another difference with azobenzene is that both minima are located on S_1 , so the quantum yield of the IC from the ${}^1(\pi\pi^*)$ state to the ${}^1(n\pi^*)$ state will be smaller in 3-PAPy than in azobenzene. Relaxation paths to the pedal-like minimum and to the rotated one are considered to be highly competitive especially in rotation-restricted cases.

- The path proposed in azobenzene through a conical intersection with ${}^1(n^2\pi^*2)$ is found much higher in energy in 3-PAPy so it cannot be proposed as an alternative route.
- Eventually, decay from the ${}^1(\pi\pi^*)$ to the ${}^1(n\pi^*)$ state will take place through one of the accessible crossings, rotated or planar, depending on the inertia of the route and the restrictions applied. If the system is free to rotate, it will probably decay to the ground state through the rotated $n\pi^*/S_0$ rotated CI since it has lower energy. If the rotation is constrained, the energy absorbed by the system previously excited to the ${}^1(\pi\pi^*)$ state will be enough to reach the planar $n\pi^*/S_0$ CI while the isomerization after excitation to ${}^1(n\pi^*)$ will take longer due to the larger energy barrier.
- The experimental spectrum of phenylazopyridine has been reproduced satisfactorily. It has been proved relevant to model a realistic environment in order to correctly sample the geometrical deformations from the most stable structure. These deformations are able to modify the selection rules imposed by the symmetry and, therefore, the intensity of the absorption that changes with the geometry. The strategy used by our group to reproduce experimental spectra has been validated with this calculation.
- Finally, the CASSCF/CASPT2 protocol has been proved to be suitable to obtain accurate enough results in the study performed here.

4.7. BIBLIOGRAPHY

1. Hartley, G. S. *Nature*, **1937**, *140*, 281.
2. Mahimwalla, Z., Yager, K. G., Mamiya, J., Shishido, A., Priimagi, A., Barrett, C. J. *Polym. Bull.*, **2012**, *69*, 967.
3. Birnbaum, P. P., Linford, J. H., Style, D. W. G. *Trans. Faraday Soc.*, **1953**, *49*, 735.
4. Beveridge, D. L., Jaffé, H. H. *J. Am. Chem. Soc.*, **1966**, *88*, 1948.
5. Jones, L. B., Hammond, G. S. *J. Am. Chem. Soc.*, **1965**, *87*, 4219.
6. Dyck, R. H., McClure, D. S. *J. Chem. Phys.*, **1962**, *36*, 2326.
7. Fischer, E. *J. Am. Chem. Soc.*, **1968**, *90*, 796.
8. Ronayette, J., Arnaud, R., Lebourgeois, P., Lemaire, J. *Can. J. Chem.*, **1974**, *52*, 1848.
9. Griffiths, J. *Chem. Soc. Rev.*, **1972**, *1*, 481.
10. Bortolus, P., Monti, S. *J. Phys. Chem.*, **1979**, *83*, 648.
11. Rau, H., Lueddecke, E. *J. Am. Chem. Soc.*, **1982**, *104*, 1616.
12. Nerbonne, J. M., Weiss, R. G. *J. Am. Chem. Soc.*, **1978**, *100*, 5953.
13. Rau, H. *Journal of Photochemistry*, **1984**, *26*, 221.
14. Bortolus, P., Monti, S. *J. Phys. Chem.*, **1987**, *91*, 5046.
15. Monti, S., Orlandi, G., Palmieri, P. *Chem. Phys.*, **1982**, *71*, 87.
16. Biswas, N., Umaphathy, S. *Chem. Phys. Lett.*, **1995**, *236*, 24.
17. Nägele, T., Hoche, R., Zinth, W., Wachtveitl, J. *Chem. Phys. Lett.*, **1997**, *272*, 489.
18. Lednev, I. K., Ye, T. Q., Hester, R. E., Moore, J. N. *J. Phys. Chem.*, **1996**, *100*, 13338.
19. Lednev, I. K., Ye, T. Q., Matousek, P., Towrie, M., Foggi, P., Neuwahl, F. V. R., Umaphathy, S., Hester, R. E., Moore, J. N. *Chem. Phys. Lett.*, **1998**, *290*, 68.
20. Fujino, T., Tahara, T. *J. Phys. Chem. A.*, **2000**, *104*, 4203.
21. Fujino, T., Arzhantsev, S. Y., Tahara, T. *J. Phys. Chem. A.*, **2001**, *105*, 8123.
22. Cattaneo, P., Persico, M. *Phys. Chem. Chem. Phys.*, **1999**, *1*, 4739.

Fourth chapter: Azobenzene and Phenylazopyridine

23. Ishikawa, T., Noro, T., Shoda, T. *J. Chem. Phys.*, **2001**, *115*, 7503.
24. Chang, C. W., Lu, Y. C., W., T. T., Diao, E. W. G. *J. Am. Chem. Soc.*, **2004**, *126*, 10109.
25. Satzger, H., Spörlein, S., Root, C., Wachtveitl, J., Zinth, W., Gilch, P. *Chem. Phys. Lett.*, **2003**, *372*, 216.
26. Schultz, T., Quenneville, J., Levine, B., Toniolo, A., Martínez, T. J., Lochbrunner, S., Schmitt, M., Shaffer, J. P., Zgierski, M. Z., Stolow, A. *J. Am. Chem. Soc.*, **2003**, *125*, 8098.
27. Cembran, A., Bernardi, F., Garavelli, M., Gagliardi, L., Orlandi, G. *J. Am. Chem. Soc.*, **2004**, *126*, 3234.
28. Altoè, P., Bernardi, F., Conti, I., Garavelli, M., Negri, F., Orlandi, G. *Theor. Chem. Acc.*, **2007**, *117*, 1041.
29. Conti, I., Garavelli, M., Orlandi, G. *J. Am. Chem. Soc.*, **2008**, *130*, 5216.
30. Granucci, G., Persico, M. *Theor. Chem. Acc.*, **2007**, *117*, 1131.
31. Yuan, S., Dou, Y., Wu, W., Hu, Y., Zhao, J. *J. Phys. Chem. A.*, **2008**, *112*, 13326.
32. Tiberio, G., Muccioli, L., Berardi, R., Zannoni, C. *Chem. Phys. Chem.*, **2010**, *11*, 1018.
33. Bandara, H. M. D., Burdette, S. C. *Chem. Soc. Rev.*, **2012**, *41*, 1809.
34. Maurer, R. J., Reuter, K. *J. Chem. Phys.*, **2011**, *135*, 224303.
35. Bockmann, M., Marx, D., Peter, C., Site, L. D., Kremer, K., Doltsinis, N. L. *Phys. Chem. Chem. Phys.*, **2011**, *13*, 7604.
36. Weingart, O., Lan, Z., Koslowski, A., Thiel, W. *J. Phys. Chem. Lett.*, **2011**, *2*, 1506.
37. Diao, E. W. G. *J. Phys. Chem. A.*, **2004**, *108*, 950.
38. Gagliardi, L., Orlandi, G., Bernardi, F., Cembran, A., Garavelli, M. *Theor. Chem. Acc.*, **2004**, *111*, 363.
39. Cantatore, V., Granucci, G., Persico, M. *Comp. Theor. Chem.*, **2014**, *1040–1041*, 126.

-
40. Yu, L., Xu, C., Lei, Y., Zhu, C., Wen, Z. *Phys. Chem. Chem. Phys.*, **2014**, *16*, 25883.
 41. Tan, E. M. M., Amirjalayer, S., Smolarek, S., Vdovin, A., Zerbetto, F., Buma, W. J. *Nat. Commun.*, **2015**, *6*.
 42. Gámez, J. A., Weingart, O., Koslowski, A., Thiel, W. *J. Chem. Theory Comput.*, **2012**, *8*, 2352.
 43. García-Amorós, J., Velasco, D. *Beilstein J. Org. Chem.*, **2012**, *8*, 1003.
 44. Venkataramani, S., Jana, U., Dommaschk, M., Sönnichsen, F. D., Tuzcek, F., Herges, R. *Science*, **2011**, *331*, 445.
 45. Bannwarth, A., Schmidt, S. O., Peters, G., Sönnichsen, F. D., Thimm, W., Herges, R., Tuzcek, F. *Eur. J. Inorg. Chem.*, **2012**, *2012*, 2776.
 46. Hirose, T., Helmich, F., Meijer, E. W. *Angew. Chem. Int. Ed.*, **2013**, *52*, 304.
 47. Alcover-Fortuny, G., de Graaf, C., Caballol, R. *Phys. Chem. Chem. Phys.*, **2015**, *17*, 217.
 48. Brown, E. V., Granneman, G. R. *J. Am. Chem. Soc.*, **1975**, *97*, 621.
 49. Wang, L. X., Yi, C. H., Zou, H. T., Xu, J., Xu, W. L. *J. Phys. Org. Chem.*, **2009**, *22*, 888.
 50. Hariharan, P. C., Pople, J. A. *Theor. Chim. Acta.*, **1973**, *28*, 213.
 51. Røeggen, I., Johansen, T. *J. Chem. Phys.*, **2008**, *128*, 194107.
 52. Domingo, A., Rodríguez-Forteza, A., de Graaf, C. *J. Chem. Theory Comput.*, **2012**, *8*, 235.
 53. Rau, H. *Angew. Chem. Int. Ed. Engl.*, **1973**, *12*, 224.
 54. Crecca, C. R., Roitberg, A. E. *J. Phys. Chem. A.*, **2006**, *110*, 8188.

FIFTH CHAPTER:

PHENYLPHENALENONE PHOTOCYCLISATION

5.1 INTRODUCTION

Through evolution, plants have developed a variety of mechanisms to counteract affections of harmful pathogens and adverse environmental conditions. Variety of biological responses is a necessity given the variety of possible harmful agents and the inability of plants to migrate to more favourable locations. In this situation, they have had to tailor each mechanism for a very specific situation, forming a defensive arsenal where one can find programmed cell death, surface-to-air signalling, expression of defence proteins and secondary production of antimicrobial compounds. Related with the last strategy, living organisms can synthesise a great diversity of chemicals (or phytochemicals). Chemists have put much experimental and theoretical effort into understanding how these substances work, because they can be used as a model for developing novel crop protection strategies or medical applications. The work presented in this chapter wants to be a contribution in this direction.

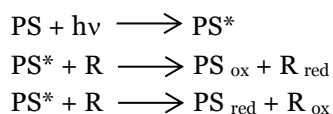
The phytochemicals oriented to defensive activities can be classified in two groups depending on the mechanism that triggers their production: Phytoalexins, which are synthesized *de novo* upon biotic (fungi, bacteria, virus, etc.) or abiotic stress (heavy metal, UV irradiation, cuts or tissue wounding) or phytoanticipins, which

are present in plant tissue prior to the adverse situation. Phytoalexins are usually undetectable in plants before the damaging event happens. However, from that event onwards, experimental results indicate that carbon and energy resources are diverted to rapidly synthesise them in a matter of hours only in focalized affected areas. Due to the broad spectrum of toxicity of these secondary metabolites (not essential metabolites) necessary to be effective against fungal and bacterial pathogens, the focalization on the treated area is essential in order to avoid autotoxicity. In the second case, phytoanticipins represent a group of compounds synthesised by the plant at a constant rate and, therefore, always present in the tissues of the plant. It should be noted that the classification is not based on chemical structure but rather on how the phytochemical is produced and therefore, the same compound can be found in both categories.^[1,2]

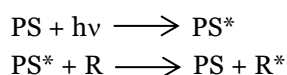
Two mechanisms have been proposed to explain how these phytochemicals accomplish their protective effect. In general, the attack of phytoalexins and phytoanticipins to pathogen agents involves the intervention of highly reactive singlet oxygen, $^1\text{O}_2$, generated from the oxygen present in the air (basically in its triplet state) by the phytochemical after this is excited by light. This process is known as photosensitization and operates through the transfer of energy between two species: the initial receptor of light or photosensitizer agent (PS, in this case the phytochemical) and the secondary receptor (in this case triplet oxygen), that gives place to the final product (in this case $^1\text{O}_2$).

There are two types of photosensitization mechanisms:

- **Mechanism type 1:** Redox photoreaction of the photosensitizer by hydrogen or electron abstraction. The radical species formed oxidizes or reduces the reactant (R).



- **Mechanism type 2:** Electronic excitation and energy transfer through the excited state of the photosensitizer to the reactant, resulting in the deactivation of the PS and the population of the excited state of R.



Focusing on type 2 mechanism for R equal to $^3\text{O}_2$, there are several conditions that have to be fulfilled in order to have an efficient photosensitizer. First, the PS excited state has to be sufficiently long-lived. Computationally, it means that this state must show low oscillator strength of transition to the ground state, what is typically the case for excited states of different multiplicity than the ground state. Most often they are triplet states, so this is the case that we will treat from now on. Second, given that this triplet state will not be easily populated by direct absorption, it has to be efficiently populated by deactivation pathways from the state excited by irradiation. Third, a significant overlap between PS emission and R absorption is necessary.

One of the best examples where the explained mechanism is carried out is in perinaphthenone, also called phenalenone (PN), which is an universal reference for sensitization of singlet oxygen because its quantum yield of this production is close to unity in many solvents.^[3-5] This parameter indicates the number of $^1\text{O}_2$ molecules produced per absorbed quanta of light and measures the efficiency of the whole photochemical process. Phenalenone has been classified as a very efficient phytoalexin since it is only detected in plants when there has been a pathogen aggression to the plant tissue. It is usual that molecules with high photosensitization quantum yields are phytoalexins instead of phytoanticipins, because $^1\text{O}_2$ is very reactive and also attacks the plant tissue, so to produce singlet oxygen continuously is not convenient for the plant.

In order to contribute to the deep understanding of these compounds, our group studied computationally in a previous work the precise mechanism to populate the sensitizer state of phenalenone.^[6] From the mechanistic point of view, the description of the PESs of the states involved in the reaction provides a sound basis to propose a mechanism of the sensitization process, which fulfils the three conditions aforementioned. First, a minimum on the $^3\pi\pi^*$ PES was located. It is predicted to correspond to a long-lived species, given that there are not easily accessible deactivation paths from that point. Second, after screening all possible relaxation paths from the FC geometry after the initial excitation, it has been determined that the pathway that leads to populate the $^3\pi\pi^*$ state is the most probable. Third, the $^3\text{O}_2\text{-}^1\text{O}_2$ energy gap is similar to the energy theoretically calculated of the vertical transition from the $^3\pi\pi^*$ minimum to the ground state of PN. These evidences together with the prediction of the emission energies and

probabilities and spin-orbit couplings, in good agreement with the results of several experimental studies, support the veracity of the mechanism proposed in that study, that is shown schematically in Figure 5.1.

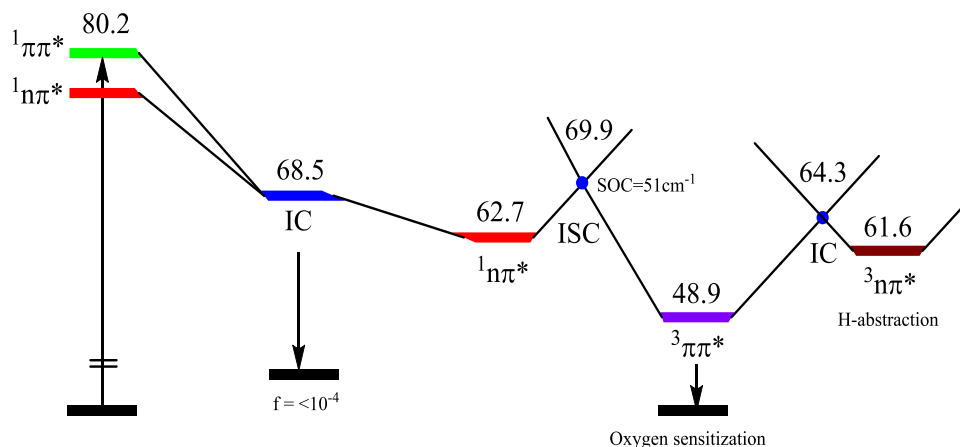
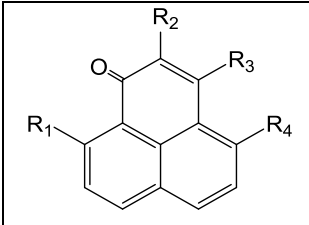


Figure 5.1 – Schematic representation of the mechanism to populate the ${}^3\pi\pi^*$ state of phenalenone. Energies (in kcal·mol⁻¹) relatives to the ground state minimum.

This study confirmed the experimental hypothesis that proposes that the oxygen sensitization occurs from the ${}^3\pi\pi^*$ species, populated through a path that involves the ${}^1\pi\pi^*$ and ${}^1n\pi^*$ states that are connected through an internal conversion first and through an intersystem crossing in a second decay.

Although this study explained why and how phenalenone succeeded in being an efficient singlet oxygen sensitizer, there are some detected peculiarities in some of its derivatives that are convenient to address in order to complete the exploration of the photochemistry of this family of compounds. For a long time, it has been known that not all natural phenalenone derivatives show the same efficiency in the photosensitization process. The reason why the plants synthesise several derivatives has been suggested to be the modulation or regulation of singlet oxygen production according with the needs of the plant, avoiding autotoxicity as much as possible. Phenyl derivatives (PhPN) allow great flexibility in the oxygen sensitization quantum yields (see Table 5.1), so it is worth exploring the factors that modulate their efficiency as singlet oxygen producers.

Table 5.1 – Quantum yields determined experimentally for different phenylphenalenone derivatives in comparison with the parent system phenalenone.^[7]

	R₁	R₂	R₃	R₄	Q. yield
		H	H	H	H
	Ph	H	H	H	0.08
	o-NO ₂ (Ph)	H	H	H	0.51
	H	H	p-MeO(Ph)	H	0.94
	H	MeO	H	Ph	0.72

Within that variability, extreme behaviours are those that have attracted most interest because they require an additional explanation to justify the experimental evidences. It is for this reason that 4-PhPN and 9-PhPN usually stand out as examples of the whole family of derivatives (3-PhPN is also remarkable but it has only a synthetic origin, unlike the previous ones). Like the parent PN, phenyl-substituted phenylphenalenones in the 3- and 4-position generally have large quantum yields of photosensitization in contrast with 9-PhPN that present remarkably low values for the same parameter. To explain this differential behaviour of 9-PhPN is the objective of this study.

The first attempts to synthesise and study 9-PhPN were made by Koelsch in 1941 although he achieved little advance.^[8] Thirty years later, Cooke detected the presence of 9-PhPN compounds in some plant species.^[9-11] However, the function of these compounds was not clear until Luis^[12] and Binks^[13] uncovered a probable relationship between 9-PhPN and phytoanticipin properties. Since then, many other studies have found evidences of this nature in different plants where 9-PhPN is present.^[14-16] In order to confirm their protective function, Opitz^[17] first and Schneider^[18] later measured the amount of 9-PhPN in various parts of the plants (roots, leaves, stems...) of different ages and concluded that the roots contained the highest concentration and preferably in younger areas. The same distribution was known to be followed by other compounds of proven phytoalexin properties and, therefore, 9-PhPN was labelled as such.^[19,20]

In order to prove the antimicrobial properties of 9-PhPN, Quiñones^[21] measured its activity by the effect of the compound on an established fungi colony. The results indicated that this derivative showed slightly reduced activity in comparison with the parent PN although significant compared with other species. Similar results were obtained by Otálvaro several years later in an expanded screening of

derivatives indicating that unmethylated compounds (like the 9-PhPN studied) are potent antifungals.^[22,23] In this direction, Otálvaro^[24] also found a strong positive correlation between 4-PhPN and 9-PhPN concentrations and the resistance to fungal infections although it was not demonstrated to which extent the individual compounds contribute to the combined effect. This work also suggests that 9-PhPN could be the inactive precursor from which the plant usually avoid the production of singlet oxygen and that would be converted in 4-PhPN only when there is a pressing need of defence. These interconversion reactions were explored in natural conditions and an intricate network of connections was found by Opitz^[25].

Flors and Nonell^[7,26] proposed an explanation for the reduction of the quantum yield of photosensitization in 9-PhN. In order to explain this process, they indicate that it was caused by a photoinduced intramolecular charge-transfer (CT) process from the electron-rich phenyl to the PN moiety. This assumption was supported by evidences on systems where electron transfer in 9-PhPN is inhibited (for example by linking a nitro group to the *orto* position of the phenyl) that showed a recovery of the quantum yield. Spectroscopic information also suggested that a different state was populated afterwards, the long-life of which indicated that it should have triplet character. However, the first step of the process (¹9-PhPN* to ¹CT) was not produced in a single step but it had to involve intermediate species, explained in terms of conformational changes of the phenyl ring. These evidences were used to propose a reaction sequence of photocyclisation in order to produce the remarkably stable radical naphthoxanthenyl.^[27]

5.2 SCOPE

In this work, we will determine the factors that make decrease the quantum yield of production of photosensitized singlet oxygen by 9-PhPN in comparison with the parent system PN. The working hypothesis is that sensitization competes with another excited state process that can occur in 9-PhPN but neither in PN nor in 4-PhPN, that has been proposed to be the cyclisation reaction depicted in Figure 5.2. The reaction path of this process has been searched for in the singlet manifold, because the photosensitization process is linked to triplet states, although both, singlet and triplet excited PESs have been examined. The work described in this chapter, therefore, complements the scope of the previous study on PN developed by our group.

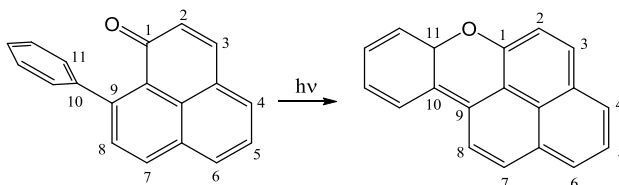


Figure 5.2 – Photocyclisation of 9-PhPN, working hypothesis reaction.

This work has been conducted using the CASSCF methodology and introducing perturbative corrections on the energies through the MS-CASPT2 approach. Using the selected methods, the potential energy surfaces of the ground state and singlet and triplet $n\pi^*$ and $\pi\pi^*$ states have been characterized and minima, crossing points and transition states have been localized. The linear interpolation of internal coordinates has been used in order to properly follow the paths of the reaction between critical points. These results provide accurate information about the competing mechanisms of population of the triplet state manifold versus cyclization along singlet excited states.

5.3 COMPUTATIONAL STRATEGY

The study of the cyclisation reaction of 9-PhPN was performed using the CASSCF/CASPT2 strategy. Nevertheless, like in the study of azobenzene explained in the previous chapter, for those states that are not well described at CASSCF level, geometry optimizations had to be performed at CASPT2 level. This method, though, cannot be used as the standard method for optimization due to its high computational cost. An additional factor that increases the computational cost is the lack of geometrical constraints in the energy calculations. Although the imposition of certain symmetry could be a reasonable approximation at some structures, the reaction coordinates will break it. Consequently symmetry has not been used anywhere, in spite of the additional computational cost that this implies.

The reference wave functions and the molecular orbitals were obtained by state average CASSCF calculations because in this way all states are orthogonal to each other, which is not necessarily true for state specific calculations. The interaction of CASSCF states via dynamic correlation is taken into account by the MS-CASPT2 treatment. The states analysed in this work were the ground state, the singlet $n\pi^*$ and triplet excited states, which are the one formed by the excitation of one

electron of the oxygen lone pair, and the singlet and triplet $\pi\pi^*$ excited states. To get an accurate description of the states of interest at MS-CASPT2 level, it is necessary to take into account all the CASSCF states that interact. This information should be obtained in prospective calculations from the eigenvectors of the MS-CASPT2 effective Hamiltonian that describes the MS-CASPT2 states as a function of the CASSCF states. Table 5.2 show this matrix for the 10 lower singlet states of 9-PhPN at the ground state geometry. It shows that to describe properly the three lowest states at MS-CASPT2 level, it is convenient to take into account the lowest 10 states at CASSCF level. For this reason, 10 states were averaged for the singlet manifold calculations. On the other hand, no state average was used for the triplet states since they do not interact with each other and remain pure in all cases.

Table 5.2 – Eigenvectors of the SA10-MS-CASPT2 effective Hamiltonian at the ground state geometry of 9-PhPN.

<i>States</i>	<i>(GS) PM-CI</i>	<i>¹(nπ^*) PM-CI</i>	<i>¹($\pi\pi^*$) PM-CI</i>	<i>³($\pi\pi^*$) PM-CI</i>
GS	0.9962	0.0000	0.0659	-0.9905
2	0.0094	0.9976	-0.1010	0.0833
3	0.0553	0.0003	-0.6408	-0.0100
4	-0.0373	0.0000	0.6393	0.0933
5	0.0196	0.0000	-0.2200	0.0470
6	-0.0447	-0.0410	0.1571	0.0076
7	0.0006	-0.0009	0.0812	-0.0223
8	0.0155	-0.0303	0.2797	-0.0152
9	0.0144	0.0000	-0.0080	-0.0136
10	-0.0176	0.0469	-0.0903	0.0008

To preclude the inclusion of intruder states, we included an imaginary shift of 0.1 a.u. in the zero order Hamiltonian. To obtain profiles of the PES of the states of interest in the areas of interest, internal coordinates have been scanned. They are more suited than Cartesian coordinates to describe paths where rotation has an important role. The RAS state interaction (RASSI) protocol was used to compute the transition oscillator strengths. MOLCAS 7.6 package was used in all energy calculations. Gaussian 09 package was used for conical intersection optimizations. A Pople d-polarized split-valence basis set 6-31G (d) was used for all atoms and all calculations.^[28]

The problem of the choice of the active space to be used in the calculations requires a more detailed comment. Given the change in conjugation of the double bonds between reactant (9-PhPN) and product (naphthoxanthene), the whole π system of the phenalenone moiety and the phenyl substituent should be included in the active space, together with, at least, the n orbital of the oxygen of the carbonyl group. It would mean to have to work with a (22, 21) active space. The need of inclusion of dynamic electron correlation in the description of some states (as will be shown latter) and the absence of symmetry in some areas of the PES, make this calculations unfeasible, so a reduction of the size of the active space is compulsory.

Test calculations on the geometry of the ground state minimum of 9-PhPN were performed. These exploratory results showed that in this structure, where the phenyl ring is perpendicular to the molecular plane, the low energy excitations are localized exclusively in the phenalenone moiety. Moreover, the π systems of both moieties did not interact due to their different orientations, so the exclusion of the π system of the phenyl group was an obvious and easy simplification, leaving an active space (16, 15) shown in Figure 5.3. Fortunately, the occupation numbers of some of the orbitals of this space were close to 2 or 0 in all the states of interest, what indicated that a further reduction was possible, giving place to a (12, 11) active space, which orbitals are located inside the green box in Figure 5.3. They are the orbital of the lone pair of the oxygen atom, π and π^* orbitals of the carbonyl (where both are obviously essential to explain any process that modifies the connectivity of the oxygen atom) and 8 delocalized orbitals of the phenalenone π system.

However, while this space reproduces accurately the vertical energies of the ${}^1n\pi^*$ state, the energy of the ${}^1\pi\pi^*$ state show a sizable error relative to the experimental value that on the other hand is well reproduced with the (16,15) active space (see Table 5.3). The alternative to be able to afford the computational cost of this study was to use a different active space to describe the ${}^1\pi\pi^*$ state, that was finally reduced to (12, 12), including the orbitals encircled by the red box in Figure 5.3, to get the same accuracy in the calculated energies of all the states of interest.

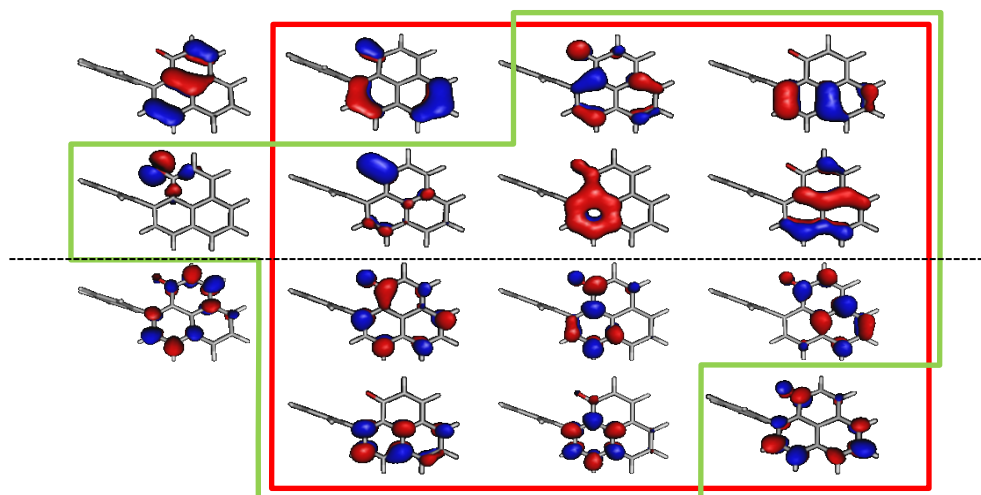


Figure 5.3 – Molecular orbitals of the different active spaces used in the calculations of the Franck-Condon area. Orbitals in the green box form the (12, 11) active space used to describe S_0 and $^1(n\pi^*)$ states. Orbitals in the red box form the (12, 12) active space used to describe $^1(\pi\pi^*)$ and the $^3(\pi\pi^*)$ states.

Table 5.3 – MS-CASPT2 energies (in kcal·mol⁻¹) relative to the ground state for the lowest energy states of 9-PhPN at the ground state minimum, obtained with different active spaces.

State	CAS(16,15) ^a	CAS(12,11) ^b	CAS(12,12) ^c	Exp. ^[7]
$^3(\pi\pi^*)$	-	66.1	65.1	-
$^1(n\pi^*)$	72.9	74.4	-	70.3
$^1(\pi\pi^*)$	84.1	90.8	82.4	80.5
$^3(n\pi^*)$	-	71.7	-	-

^a) Molecular orbitals shown in Figure 5.3 ^b) Molecular orbitals shown in the red box of Figure 5.3 -

^c) Molecular orbitals shown in the green box of Figure 5.3.

Unfortunately this is not the only problem aroused by the reduction of the active space. For the cyclised photoproduct, the set of molecular orbitals needed to properly describe the lower energy states is different than the active space used for the reactant. In the photoproduct, there is only a π system that extends to the whole skeleton of the molecule, what includes the phenyl group of the reactant. On top of this, to study the reaction of interest, the new σ bond formed must be also included in the active space. To form it, the hybridization of the O and C atoms change from reactant to product so, to properly study this process, the active space should be increased even beyond the initial (22,21) size proposed. Facing the unfeasibility of these calculation, we chose the option of using an active space for the product (and

for the transition state of the thermal reaction) equivalent to the (12, 11) and (12, 12) ones used for the reactant, obtained by the progressive change of the orbitals when doing successive calculations following the path that connects reactant and product. Figure 5.4 show the shape of the active orbitals at the product geometry. The use of different active spaces implies that the relative energies of the product and the structures of the zone of the transition state, must be consider only an approximation to provide a qualitative description of these areas of the PESs of 9-PhPN.

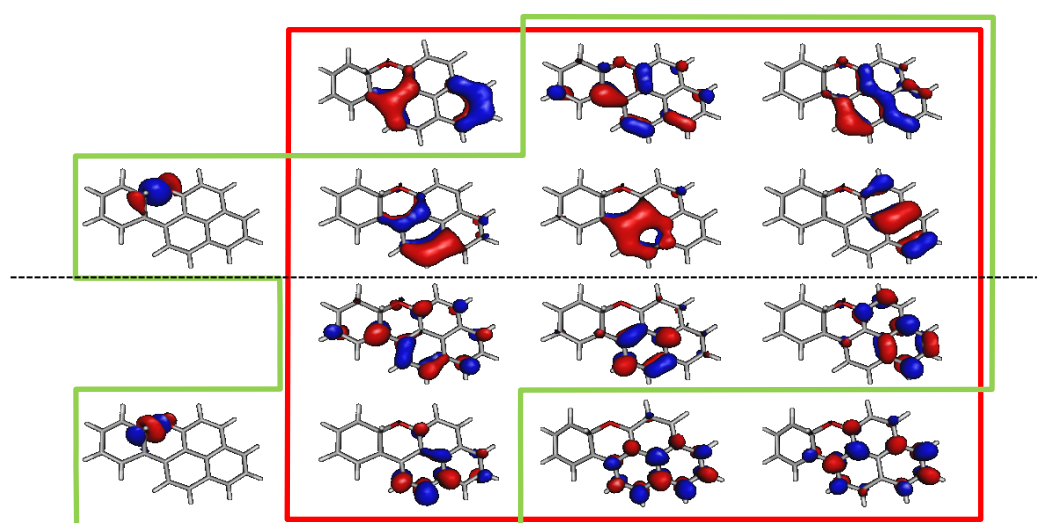


Figure 5.4 – Molecular orbitals of the active space used in the calculations of the photoproduct. Orbital in the green box form the (12, 11) active space used to describe S_0 and ${}^1(n\pi^*)$ states. Orbitals in the red box form the (12, 12) active space used to describe ${}^1(\pi\pi^*)$ and the ${}^3(\pi\pi^*)$ states.

5.4 RESULTS

5.4.1 Ground state minima and vertical excitations

The absorption of a photon initiates the reactivity of the studied system from the geometry of minimum energy of the ground state of the 9-PhPN. The localization of this minimum, therefore, must be the first step of this study. The optimized geometry, depicted in Figure 5.5, shows the phenyl substituent almost perpendicular to the planar phenalenone with a dihedral angle of 92.1° . This structural parameter is essential to describe the reaction of interest. Other relevant parameters are also

shown in Figure 5.5 and relative energies of the lowest singlet and triplet excited states are shown in Table 5.4 together with oscillator strengths.

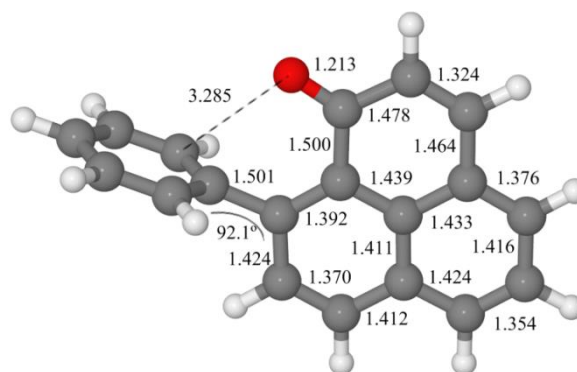


Figure 5.5 – Ground state minimum energy geometry obtained at CASSCF level. Bond distances in angstroms, dihedral angle in degrees.

Table 5.4 – Energies (in kcal·mol⁻¹) relative to the ground state, oscillator strengths (*f*) and dipole moments (*μ*, in D) for the lowest energy states of 9-PhPN computed at several levels, at the ground state minimum.

State	CASSCF	SS-CASPT2	MS-CASPT2	<i>f</i>	<i>μ</i>
GS	0.0	0.0	0.0	-	3.05
³ (ππ*)	61.1	65.8	65.1	0.10·10 ⁻³	2.99
³ (nπ*)	74.2	70.1	71.7	0.26·10 ⁻⁵	0.30
¹ (nπ*)	77.2	73.0	74.4	0.47·10 ⁻³	0.29
¹ (ππ*)	119.4	108.0	82.4	0.21	3.33

The analysis of the wavefunction of the first singlet excited state indicates that it is described by an excitation of an electron of the lone pair of the oxygen atom to a delocalized π anti-bonding orbital of the phenalenone moiety. This nπ* state is located 74.4 kcal·mol⁻¹ above the ground state. Its dipole moment is smaller than that of the ground state as a result of the exocyclic charge transfer. The composition of the PM-CAS-CI function is shown in the second column of the matrix given in Table 5.2. It shows that the ¹(nπ*) CASSCF state do not interact with any other state, as expected by the orbital symmetry of the oxygen lone pair. For this reason, the multi-state perturbative treatment does not introduce a noticeable change in energy from the SS-CASPT2 result. The small value of the oscillator strength indicates a very low probability of transition from the ground state, so this result

predicts that this band will not appear in the absorption spectrum of 9-PhPN. This fact is corroborated by experiments.^[7]

The second singlet excited state has a $\pi\pi^*$ character and it is described by an excitation from a delocalized π bonding orbital on the phenalenone moiety to an antibonding orbital. Its oscillator strength is large what indicates that the probability of transition from the ground state is high. Our results predict that this state will absorb the incident radiation. In energetic terms, the $^1(\pi\pi^*)$ state is located 82.4 kcal·mol⁻¹ above the ground state. This energy value is comparable with the experimental measurements of the maximum absorption wavelength in benzene that locate the state at 80.5 kcal·mol⁻¹. The dipole moment of this state is similar to the ground state one, as expected for an excitation of $\pi\pi^*$ character.

It is noticeable the large differences between the energies obtained for this state at different levels. The large difference between the CASSCF and CASPT2 values indicates that the dynamic electron correlation affects strongly the electronic configuration of this state, which is not described properly at CASSCF level. Consequently, the optimization of critical points cannot be reliably performed by the CASSCF procedure. The MS-CASPT2 results also differ noticeably from the SS-MCSCF one. This difference indicates that the interaction between CASSCF states due to the electron correlation is important. This prediction is corroborated by the description of the PM-CAS-CI state given by the eigenvector of the third column of Table 5.2. The S₂ MS-CASP2 state shows a strong mixing between the S₃ and S₄ CASSCF states with coefficients 0.63 and 0.64 respectively, both of them of $\pi\pi^*$ character.

The first triplet excited state has $\pi\pi^*$ character and it is the lowest-energy excited state, located 66.0 kcal·mol⁻¹ above the ground state. Its description is similar to that of the absorbing state. On the other hand, its PM-CAS-CI function does not show mixing of CASSCF states, so it is expected that the description of this state, and consequently the geometry optimization, will be accurate enough at CACCSF level. The calculated dipole moment is 2.99 Debye, only slightly smaller than in the singlet state of the same character. The second triplet state has $n\pi^*$ character, similar to the one of the lowest singlet excited state. Its energy is similar to that of the singlet state of the same character and, like in that case, its PM-CAS-CI wavefunction does not show any mixing of states.

According to the results obtained for PN in the previous study developed by our group, it is not expected that higher excited states will be involved in the photochemistry of 9-PhPN. In fact, prospective calculations were performed including in the active space molecular orbitals located on the π system of the phenyl substituents, but the 10 lower excited states did not show the involvement of these orbitals in the excitations. For this reason, it is expected that the exclusion of phenyl orbitals in the active space will not introduce noticeably errors in the study of the photochemistry of 9-PhPN.

The geometry of the proposed photoproduct, naphthoxanthene was also optimized. The geometry obtained is depicted in Figure 5.6, where some geometrical parameters are also shown. The energies of the lowest states of naphthoxanthene are collected in Table 5.5. This species is 19.7 kcal·mol⁻¹ less stable than 9-PhPN, so it is not thermodynamically favoured. To predict if it will be long-lived, it is necessary to calculate the energy barrier of the back reaction to phenalenone. If it is low, this photoproduct will be considered an intermediate in the photochemistry of phenalenone, and consequently a species difficult to be observed.

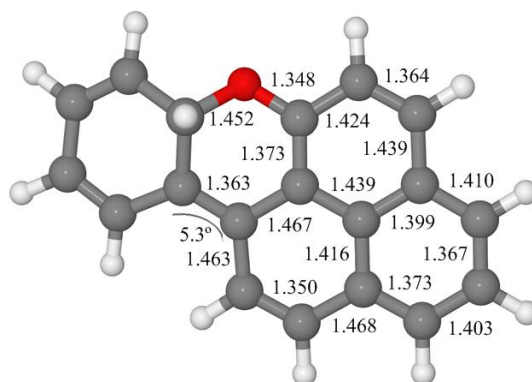


Figure 5.6 – Ground state minimum energy geometry of the product obtained at CASSCF level. Bond distances in angstroms, dihedral angle in degrees.

Table 5.5 – Energies (in kcal·mol⁻¹) relative to the ground state, oscillator strengths (f) and dipole moments (μ , in D) for the lowest energy states of naphthoxanthene at the ground state minimum.

State	MS-CASPT2	f	μ
GS	19.7	-	1.16
$^3(\pi\pi^*)$	64.3	$<10^{-8}$	1.22
$^1(\pi\pi^*)$	87.4	0.56	1.61

Table 5.6 – MS-CASPT2 energies (in kcal·mol⁻¹) relative to the ground state minimum, and oscillator strengths (*f*) of the lower states of 9-PhPN at the minimum energy geometry of the ¹(nπ*) state optimized at CASCSF level.

<i>State</i>	<i>MS-CASPT2</i>	<i>μ</i>	<i>f</i>
GS	14.1	3.20	-
³ (ππ*)	56.3	2.60	0.17·10 ⁻²
¹(nπ*)	58.5	0.98	<10 ⁻⁶
³ (nπ*)	58.8	0.97	<10 ⁻⁷
¹ (ππ*)	76.9	2.63	0.22

In terms of energy (see Table 5.6), the ¹(nπ*) minimum is located 58.5 kcal·mol⁻¹ above the ground state global minimum. It means a relaxation from the Franck Condon zone of 15.9 kcal·mol⁻¹, and a vertical energy gap with the ground state of 44.4 kcal·mol⁻¹. The small value of the oscillator strength predicts a very low probability of emission from this species, what rules out the probability of emission from the ¹(nπ*) state. An exploratory search at CASPT2 level on this PES confirmed the character of a minimum of this structure, indicating that the description of this surface provided by CASSCF is reliable. Table 5.6 shows that at this geometry singlet nπ* and triplet ππ* states are in close proximity. Due to the character of these states, it is expected that the spin-orbit coupling between them will be large. In this case, if the ¹(nπ*) minimum is populated, the transfer between the two states through ISC will be very probable, like in the parent compound phenalenone.

¹(ππ*) state

Third column of Table 5.2 shows the PM-CAS-CI that describe the ¹(ππ*) state at Frank Condon. It can be observed that there is a strong interaction of the 3rd and 4th CASSCF states, what means that neither of those CASSCF wavefunction will describe properly the ¹(ππ*) state, but both will give rough approximation to it. For this reason the optimization of this state had to be performed at CASPT2 level. This is not a trivial calculation, which took 3 months of wall time to be completed, using 12 nodes (with Xeon E5-2630 processors and 64G of memory) in parallel computing.

Figure 5.8 shows the minimum energy geometries obtained for optimization of the 3rd and 4th roots at CASSCF level and 3rd root at CASPT2 level. It can be observed that, while the distances in the phenalenone moiety are similar in all structures, the

dihedral angle of the phenyl ring relative to phenalenone is drastically different, being close to perpendicular at CASSCF level but almost coplanar at CASPT2 level. This geometrical parameter is crucial in the photoreaction of interest. Given that the O-C₁₁ bond must be formed, it is necessary that these atoms get close together, as happens only in the CASPT2 minimum. These results show again that a correct description of the PES that includes the dynamic electron correlation is necessary to correctly determine reaction mechanisms.

Energies (calculated at MS-CASPT2 level) of the CASSCF and CASPT2 minima are collected in Table 5.7. The energy of the minimum optimized at CASPT2 level is much lower than the energy of the CASSCF minima, what confirms the better performance of the CASPT2 optimization, as it was expected. This structure is 24.1 kcal·mol⁻¹ more stable than the FC energy of this state, and it is almost isoenergetic with the ¹(nπ*) minimum. Moreover, at all three minima the ¹(ππ*) state is clearly below the ¹(nπ*) and, therefore, it becomes the lowest singlet excited state. These results together with non-negligible values for the oscillator strengths indicate that emission is possible from these species although improbable if the population do not remain enough time in those minima (short-lived species), what depends on the possible paths of depopulation of the ¹(ππ*) minimum that we will analyse further down. The inversion of the S₁ and S₂ states indicates that there must be a conical intersection between these states and that the CI hyperspace must extend for a large range of values of the phenyl dihedral angle.

Table 5.7 – MS-CASPT2 energies (in kcal·mol⁻¹) relative to the ground state minimum, and oscillator strengths (*f*) of the lower states of 9-PhPN at the minimum energy geometries optimized at CASSCF and CASPT2 level for different roots of ππ* state.

State	3 rd CASSCF root		4 th CASSCF root		3 rd CASPT2 root	
	MS-CASPT2	<i>f</i>	MS-CASPT2	<i>f</i>	MS-CASPT2	<i>f</i>
GS	15.0	-	7.6	-	6.9	-
³ (ππ*)	56.5	0.58·10 ⁻³	53.9	0.43·10 ⁻³	49.0	0.26·10 ⁻³
³ (nπ*)	74.3	< 10 ⁻⁵	70.7	< 10 ⁻⁷	62.2	< 10 ⁻⁴
¹ (nπ*)	74.9	< 10 ⁻⁵	72.5	0.20·10 ⁻⁴	64.8	0.05
¹ (ππ*)	71.0	0.17	68.9	0.19	58.3	0.13

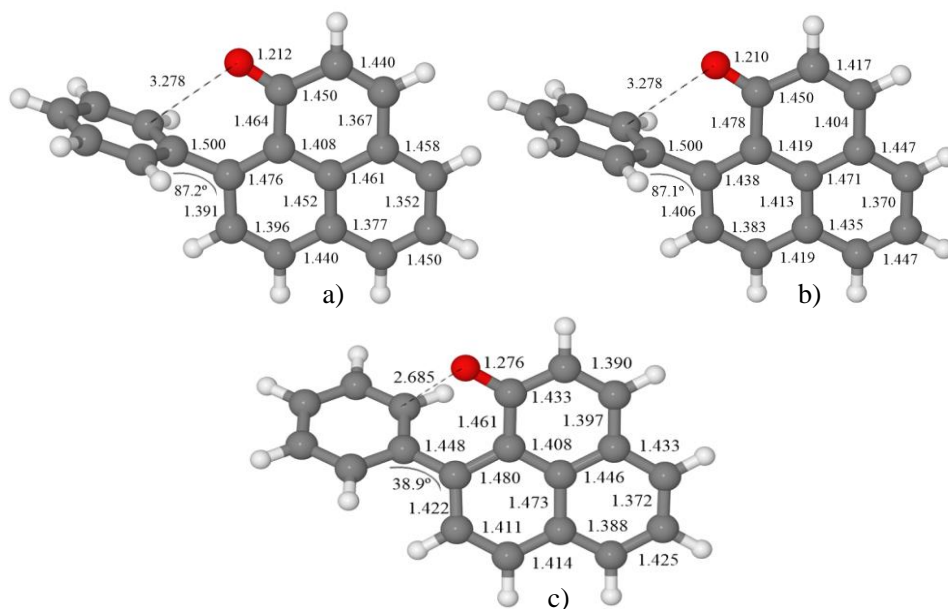


Figure 5.8 – Minimum energy geometries of the ${}^1(\pi\pi^*)$ state of 9-PhPN obtained as a) 3^{rd} root at CASSCF level b) 4^{th} root at CASSCF level and c) 3^{rd} root at MS-CASPT2 level.

${}^3(\pi\pi^*)$ and ${}^3(n\pi^*)$ states

The minimum energy structures of these states were also located at CASSCF level and they are shown in Figure 5.9. As can be seen in this figure, both geometries have the phenyl perpendicular to the molecular plane but present very different CO distances, which is also the main difference between the CASSCF singlet state minima. The vertical energies are exposed in Table 5.8 for both structures. In spite that the composition of the PM-CAS-CI of the ${}^3(\pi\pi^*)$ state does not show a mixing of CASSCF states and, therefore, we could assume that CASSCF level describes properly this state, the minimum located at this level does not seem to be, in fact, the minimum energy point on the ${}^3(\pi\pi^*)$ surface. Having a look at the energies of this state at the geometries of the ${}^1(\pi\pi^*)$ minima in Table 5.7, we observed that the energy of the ${}^3(\pi\pi^*)$ is lower in the geometry where the phenyl group has a dihedral angle of 38.9°, far from the 87.4° predicted at CASSCF level. Given that the exact location of the minimum of this state will not be of crucial interest and the cost of the CASPT2 optimization is high, we will assume that the geometry of the ${}^3(\pi\pi^*)$ minimum will be similar to that of the ${}^1(\pi\pi^*)$ one. What is important is that the

$^3(\pi\pi^*)$ minimum is the most stable one, being around 10 kcal·mol⁻¹ more stable than those of the singlet excited species.

Table 5.8 – MS-CASPT2 energies (in kcal·mol⁻¹) relative to the ground state minimum of the lowest excited states at the $^3(\pi\pi^*)$ and $^3(n\pi^*)$ minima optimized at CASSCF level.

State	$^3(\pi\pi^*)$ state		$^3(n\pi^*)$ state	
	MS-CASPT2	<i>f</i>	MS-CASPT2	<i>f</i>
GS	8.1	-	10.1	-
$^3(\pi\pi^*)$	51.0	<10 ⁻⁶	54.3	<10 ⁻⁵
$^3(n\pi^*)$	71.6	<10 ⁻⁷	57.0	<10 ⁻⁷
$^1(n\pi^*)$	73.4	<10 ⁻⁵	58.9	<10 ⁻⁶
$^1(\pi\pi^*)$	72.1	0.28	77.4	0.25

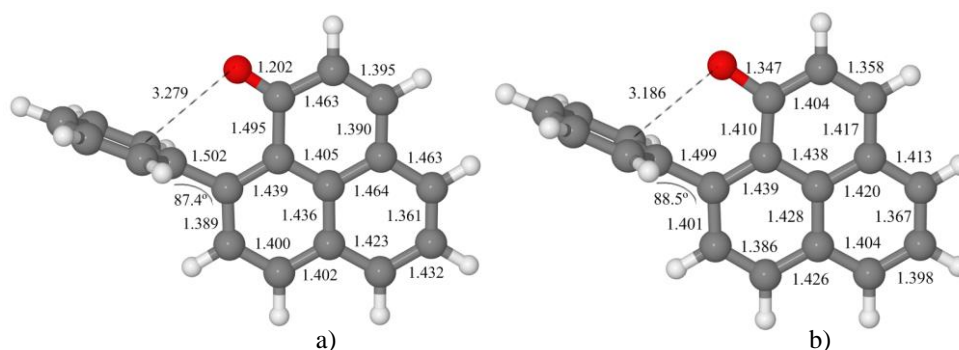


Figure 5.9 – Minimum energy geometries of the a) $^3(\pi\pi^*)$ state and b) $^3(n\pi^*)$ of 9-PhPN obtained optimizing at CASSCF level.

On the other hand, the relative energy of the $^3(n\pi^*)$ state is only slightly lower in its minimum than in the $^1(n\pi^*)$ minimum, which indicates again that the PES of these states must be similar.

5.4.3 Reaction mechanisms

A collection of critical points is not enough to determine a reaction mechanism without reasonable paths that link the proposed structures on the excited states and finally leads to products. These links are explored in the current section through the localization of several conical intersections and real crossings that connect different states and the exploration of paths along surfaces with location of transition states, when necessary, in order to determine the relative affordability of each transformation. The linear interpolation of internal coordinates has been

Photochemical reaction paths.

The only state that shows a certain probability of absorbing the initial irradiation in 9-PhPN is the $^1(\pi\pi^*)$ state. We can assume then that the photochemical process starts at the Franck Condon geometry of the PES of this state, located 82.4 kcal·mol⁻¹ above the ground state minimum. The aforementioned assumption is also validated through the analysis of the available experimental spectra, which indicates that there is no other band present.^[7] From the theoretical point of view, an additional state (dark state) can be located but it will remain dark during the studied reactivity. The probability of absorption of the initial excitation by the $^1(n\pi^*)$ is very low. It could increase if orbital symmetry restrictions are broken by loss of planarity of the phenalenone moiety by vibrational movements, but this is not probable due to the rigidity of this fragment given by the conjugation of its π system.

Once on the $^1(\pi\pi^*)$ state, the energy of the $^1(n\pi^*)$ is not close enough to predict an internal conversion between them, so the most probable process will be relaxation along the $^1(\pi\pi^*)$ PES. In principle this relaxation would lead to the $^1(\pi\pi^*)$ minimum where the bond distances of the phenalenone moiety are slightly changed, and the phenyl ring has rotated approximately 60°. But, although this downhill path is the most favoured thermodynamically because leads to the lowest energy structure, the rotation of the phenyl ring is a drastic geometrical change that can be hindered by the solvent and, in any case, will be slower than the change of bond distances. We cannot discard, then, the population of areas of the $^1(\pi\pi^*)$ PES of geometries similar to the structure given by the CASSCF optimization of this state (where the phenyl ring has hardly rotated).

Given that the $^1(\pi\pi^*)$ and $^1(n\pi^*)$ states are inverted at both geometries (CASSCF and CASPT2 minima) relative to the energetic ordering at FC, these surfaces must cross along the paths that lead from FC to those geometries. Exploring the S_1 and S_2 surfaces by means of LIICs, the crossing points along both paths were located. It would be desirable to find the lowest energy point of these crossings, but this calculation would not give reliable results, given that this optimization can only be performed at CASSCF level, where the $^1(\pi\pi^*)$ state is very poorly described. The structures of the crossings shown in Figure 5.11, then, are not optimized, so the

energies of these points of degeneracy give upper limits of the barriers of internal conversion between the ${}^1(\pi\pi^*)$ and ${}^1(n\pi^*)$ states.

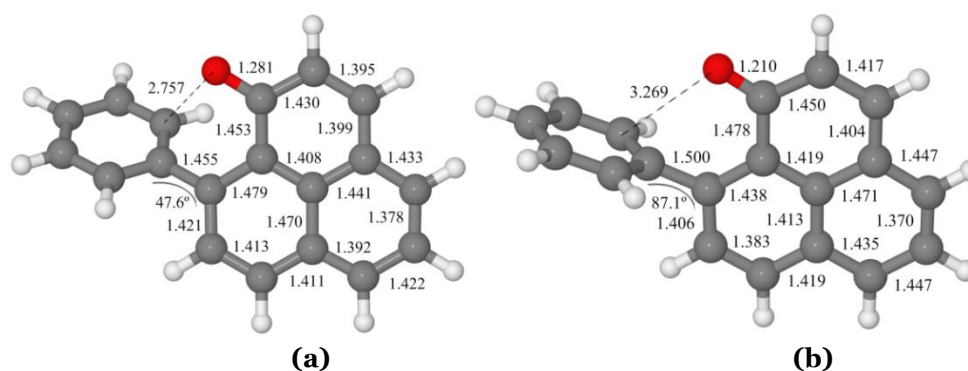


Figure 5.11 – Points of the ${}^1\pi\pi^*/{}^1n\pi^*$ conical intersection hyperspace. Geometries obtained in the LIICs from FC to (a) the CASPT2 minimum (b) the CASSCF minimum.

The structure shown in Figure 5.11 (b), where the phenyl ring is almost perpendicular to the phenalenone moiety (*perp*-CI), is found to be 70.1 kcal·mol⁻¹ above the ground state global minimum, while the structure shown in Figure 5.11 (a) (*rot*-CI) is only 62.4 kcal·mol⁻¹ high. To check if both crossing points are accessible in the relaxation route from FC, the profiles of the lowest energy surfaces along the LIICs from FC to these geometries were calculated. The results, collected in Figure 5.12 in a unique graphic, show that these points are accessible along barrierless paths on the ${}^1(\pi\pi^*)$ surface.

Crossing to the ${}^1(n\pi^*)$ surface can then take place easily, and in this surface the system will continue relaxing towards the minimum energy point of this state. The LIIC paths from the located crossing points to this minimum were also calculated and are shown in Figure 5.13. It should be noted that ${}^1(n\pi^*)$ and ${}^1(\pi\pi^*)$ minima are almost isoenergetic (58.5 kcal·mol⁻¹ and 58.3 kcal·mol⁻¹ respectively) and they are connected through the *rot*-CI that, as explained before, provides an upper limit for the barrier of this interconversion, that is only around 4.0 kcal·mol⁻¹. It means that, independently of the relaxation path followed from FC, and independently of which minimum will be initially populated from the *perp*- or *rot*-CI, the ${}^1n\pi^*$ and ${}^1\pi\pi^*$ species are directly connected. The subsequent relaxation process can then take place from any of both minima.

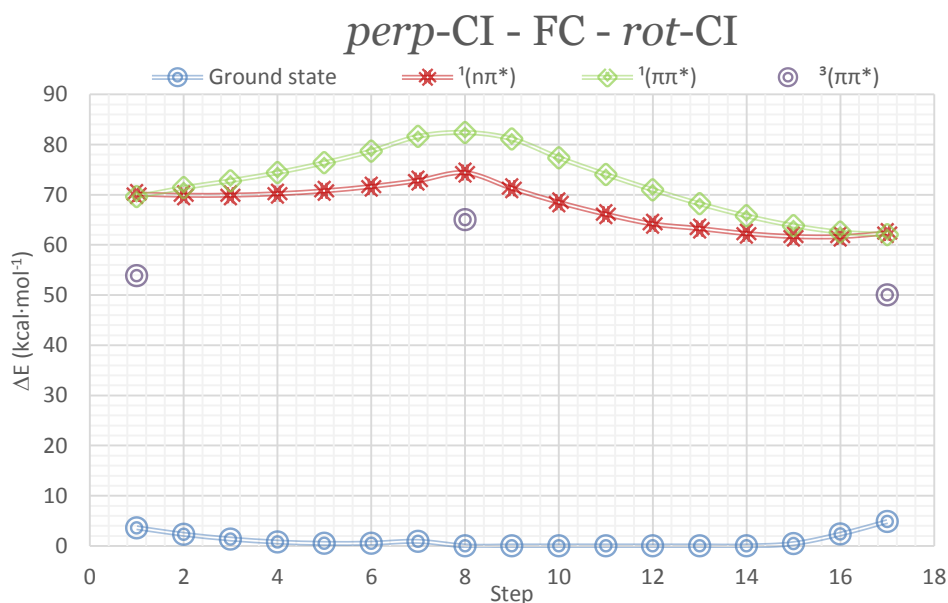


Figure 5.12 – MS-CASPT₂ profiles of the PES of the lowest singlet energy states of 9-PhPN along the LIIC from the FC geometry (step 8) to the ¹ππ^{*}/¹nπ^{*} crossings: *perp*-CI (step 1) and *rot*-CI (step 17). Energy of the ³(ππ^{*}) state at the initial and final points of the LIICs are also represented by single points.

Taking into account that only the ³(ππ^{*}) state and the ground state are lower than S₁ and S₂ in the areas explored, there are only three possible deactivation processes: radiative deactivation (fluorescence) from the ¹(nπ^{*}) or ¹(ππ^{*}) minima; intersystem crossing to ³(ππ^{*}); and internal conversion to the ground state. The probability of fluorescence depends on the oscillator strength for the transition from the studied species and the ground state, and on the live time of the excited species. Oscillator strength has only a non-negligible value at the ¹(ππ^{*}) minimum, so only this species could fluoresce. The live time depends on the other possible channels of depopulation of this minimum, which are analysed in the following points.

ISC to the ³(ππ^{*}) is only probable from the ¹(nπ^{*}) for two reasons: the ³(ππ^{*}) state is always much lower than the ¹(ππ^{*}) state, while is higher in energy (2.2 kcal·mol⁻¹) than the ¹nπ^{*} state at this latter minimum. It means that a real crossing must exist nearby. Moreover, the spin-orbit coupling between ¹(nπ^{*}) and ³(ππ^{*}) is predicted to be large, so intersystem crossing between this states is possible. If the system reaches the ³(ππ^{*}) state minimum, the energy transfer to the triple oxygen is

possible, giving place to oxygen sensitization. This is the most favoured reaction in phenalenone, because the competing processes are less probable than population of the $^3(\pi\pi^*)$.

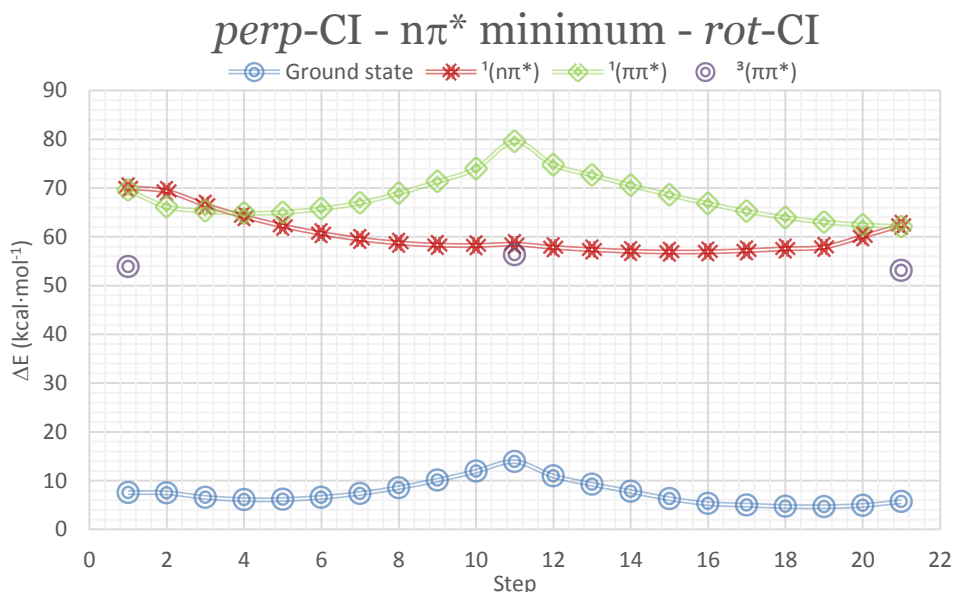


Figure 5.13 – MS-CASPT2 profiles of the PES of the lowest energy states of 9-PhPN along the LIIC from the minimum energy point of $^1(n\pi^*)$ state (step 11) to the *perp*-CI (step 1) and *rot*-CI (step 21). Energy of the $^3(\pi\pi^*)$ state at the initial and final points of the LIICs are also represented by single points.

However, a crossing between the $^1(n\pi^*)$ state and S_0 is possible in 9-PhPN. The minimum energy point of this CI was obtained at CASSCF level, and degeneracy of the states confirmed at CASPT2 level. The geometry of this point is shown in Figure 5.14. At this structure, the dihedral angle of the phenyl ring is still 37° , far from planarity, but the carbonyl double bond can be considered almost broken, while the new σ bond is not completely formed. This CI is located $54.8 \text{ kcal}\cdot\text{mol}^{-1}$ above the ground state minimum, and lower in energy than both $^1(n\pi^*)$ and $^1(\pi\pi^*)$ state minima.

The analysis of the correlation between the states of reactant and product at the valence-bond level, indicates that the ground state of the product correlates with the $^1(n\pi^*)$ state of the reactant. The n orbital of the oxygen is oriented towards the p orbital of the C_{11} of the phenyl group, which are close together at the geometry of

the optimized CI. In the $^1(n\pi^*)$ state, the n orbital is mono-occupied, what allows the formation of a σ bond with the p orbital of C₁₁. This cyclisation is possible in 9-PhPN, but not in PN or in 4-PhPN.

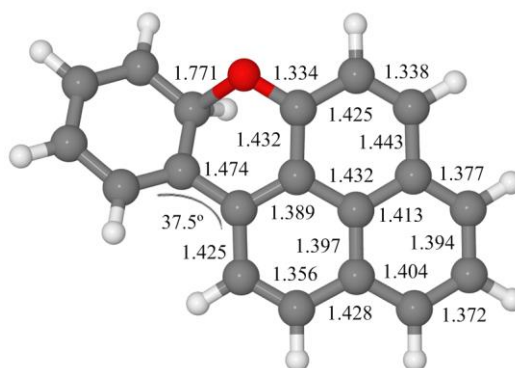


Figure 5.14 - Minimum energy geometry of the S_1/S_0 conical intersection optimized at CASSCF level and confirmed at MS-CASPT2 level.

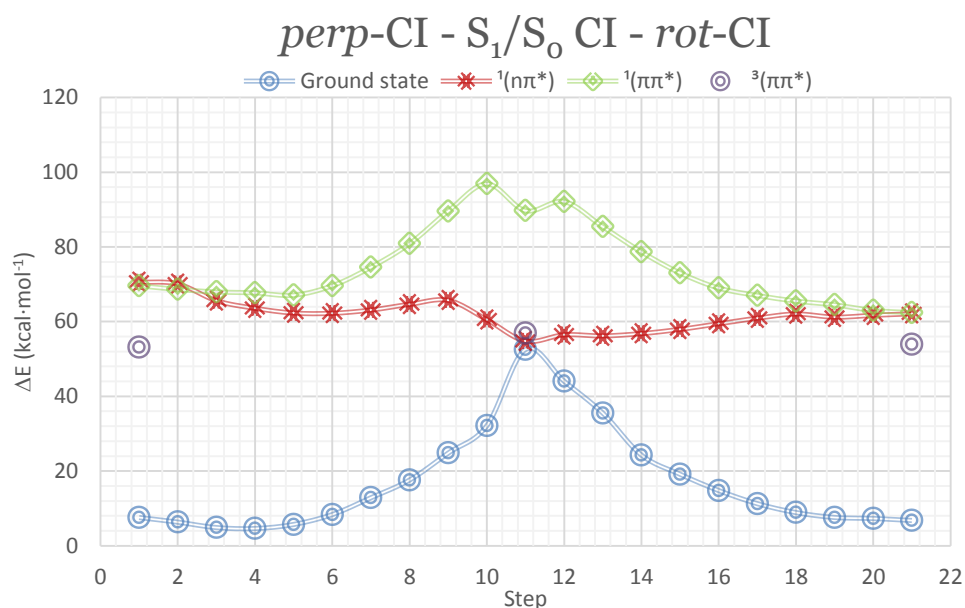


Figure 5.15 – MS-CASPT2 profiles of the PES of the lowest energy states of 9-PhPN along the LIIC from the perpendicular (step 1) and rotated (step 21) $^1n\pi^*/^1\pi\pi^*$ CIs to the S_1/S_0 conical intersection (step 11).

To confirm that this conical intersection is accessible from the deactivation path from the FC geometry, the profiles of the lowest energy surfaces along the LIIC from the ${}^1n\pi^*/{}^1\pi\pi^*$ CIs to the S_1/S_0 CI were calculated (Figure 5.15). In terms of energy, a small energy barrier of $1.0 \text{ kcal}\cdot\text{mol}^{-1}$ is found from the *rot*-CI. On the other hand, from the *perp*-CI, the path is similar but the barrier is $3.5 \text{ kcal}\cdot\text{mol}^{-1}$, due to the higher energy of this latter CI. In any case, these are upper bounds for the energy of the real barrier, and anyway the system will have enough residual kinetic energy from the initial excitation ($82.4 \text{ kcal}\cdot\text{mol}^{-1}$) to surmount these small local barriers and reach the S_1/S_0 CI.

Finally, the relaxation from the conical intersection to the product on the ground state surface has also been analysed, to confirm that this relaxation path is probable, by means of a LIIC path calculated from the S_1/S_0 CI to the photoproduct (shown in Figure 5.16). The results indicate that the final C_{11} -O bond formation follows a barrierless path to the product ground state. At the same time, the S_1 surface increases its relative energy. The reaction cycle would finish with the return via thermal path to 9-PhPN in the ground state.

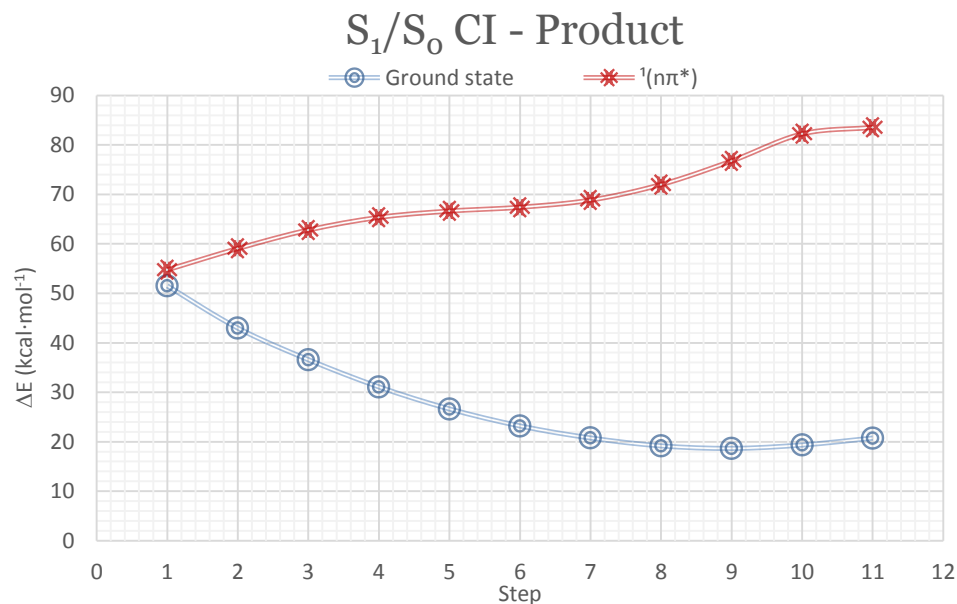


Figure 5.16 – LIIC profiles of the PES of the lowest energy states from the S_1/S_0 CI to the minimum energy geometry of the cyclized product. MS-CASPT2 energies ($\text{kcal}\cdot\text{mol}^{-1}$).

Global description of the proposed mechanism

The global landscape that these results is shown in Figure 5.17.

The initial excitation populates the $^1\pi\pi^*$ state. The computed absorption energy ($82.4 \text{ kcal}\cdot\text{mol}^{-1}$) is in good agreement with the experimental value of $80.5 \text{ kcal}\cdot\text{mol}^{-1}$. Whatever the relaxation direction followed by the system (with or without rotation of the phenyl ring), the two isoenergetic minima of the S_1 surface, which correspond to the $^1(\pi\pi^*)$ and $^1(n\pi^*)$ species will be populated. These minima are connected through a small barrier (of less than $4 \text{ kcal}\cdot\text{mol}^{-1}$) that corresponds to the conical intersection between these surfaces and opens the internal conversion path. The system only can fluoresce from the $^1\pi\pi^*$ minimum but, although this radiative deactivation is probable, it is a process slower that the other ones that compete with it, so the fluorescence quantum yield is expected to be low.

One of the processes competing with fluorescence is intersystem crossing to the $^3(\pi\pi^*)$ surface, which can take place through a real crossing between this triplet state and the $^1(n\pi^*)$ state. This transfer is predicted to be probable because the crossing between these surfaces must be located near the $^1(n\pi^*)$ minimum and close in energy, and because the spin-orbit coupling between the $^1(n\pi^*)$ and $^3(\pi\pi^*)$ states will be large, according to Kasha's rules and similarly to what was found for phenalenone in the previous work of the group on this system.^[6]

The last possible process is internal conversion from the $^1(n\pi^*)$ to the ground state through a conical intersection located between these states. To reach this crossing point, a small barrier of less than $4 \text{ kcal}\cdot\text{mol}^{-1}$ must be overcome, but the energy absorbed in the initial excitation is enough to surmount it. Once on the ground state, the system can return to the initial reactant or to the cyclised photoproduct, which will finally revert to the original 9-PhPN through a thermal reaction along the ground state surface.

This last path seem to be the most favoured thermodynamically and kinetically, because it leads to the most stable minimum and do not involved slow processes as ISC and radiative decay are. Nevertheless, none of these last phenomena are discarded to happen, so population of the $^3(\pi\pi^*)$ minima and emission from the $^1(\pi\pi^*)$ species can also happen to a certain extend.

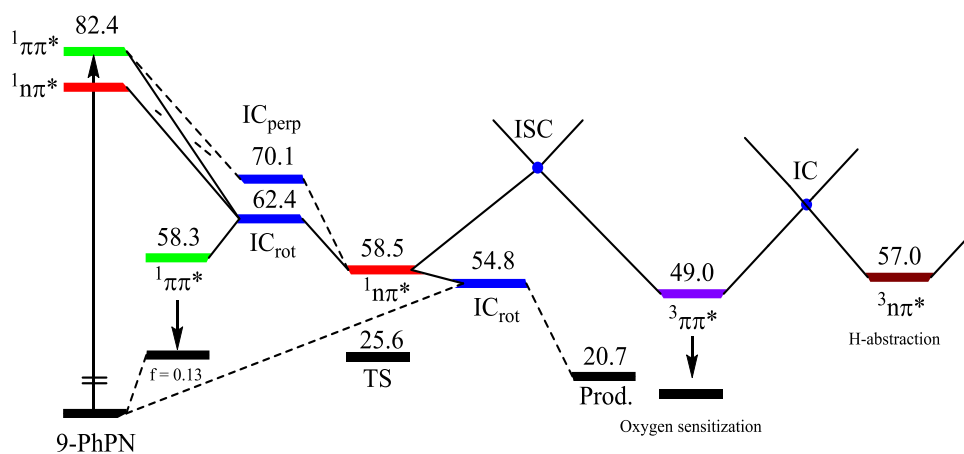


Figure 5.17 – Schematic representation of the processes involved in the photochemistry of 9-PhPN. (Energies in kcal·mol⁻¹, not in scale). Color code: red ¹(nπ*), green ¹(ππ*), purple ³(ππ*), brown ³(nπ*) and blue for interaction region.

5.5 CONCLUSIONS

The photochemistry of 9-PhPN has been studied to understand why the oxygen sensitization efficiency of this compound is much smaller than the one of its parent compound, phenalenone. This study has been performed by means of ab initio calculations, using the CASSCF and CASPT2 methods. Due to the complexity of the reactivity and the large size of the system, reductions in the most adequate active space have had to be performed. The main conclusions derived from this study are summarized in the following points.

- The difference of quantum yield of oxygen sensitization observed experimentally between PN and its derivative 9-PhPN has been explained satisfactorily.
- Both systems show similar topography and energies of the ¹(nπ*), ¹(ππ*), ³(ππ*) and ³(nπ*) surfaces in the areas near the Frank Condon geometry. The processes that take place in these zones, emission from the ¹(ππ*) species and oxygen sensitization from the ³(ππ*) minimum, will be possible in both systems.

- 9-PhPN also has an alternative reaction path, which is cyclisation by a bond formation between the carbonyl oxygen and a carbon atom of the phenyl substituent. This process is predicted to be more efficient than the previous ones, decreasing consequently the quantum yield of oxygen sensitization. On the other hand, emission from $^1(\pi\pi^*)$ species is expected to be more probable since this state becomes the first excited in its minimum unlike in phenalenone where this behaviour is not observed. This emission would agree with weak fluorescence experimentally observed.
- The results obtained agreed satisfactorily with experimental data and observations. The approximations applied in the computational methods seem to have been appropriate.

5.6 BIBLIOGRAPHY

1. Paxton, J. D. *Plant Dis.*, **1980**, *64*, 734.
2. VanEtten, H. D., Mansfield, J.W., Bailey, J.A., Farmer, E.E. *Plant Cell.*, **1994**, *6*, 1191.
3. Schmidt, R., Tanielian, C., Dunsbach, R., Wolff, C. *J. Photochem. Photobiol. A*, **1994**, *79*, 11.
4. Martí, C., Jürgens, O., Cuenca, O., Casals, M., Nonell, S. *Photochem. Photobiol. A.*, **1996**, *97*, 11.
5. Oliveros, E., Bossman, S.H., Nonell, S., Martí, C., Heit, G., Tröscher, G., Neuner, A., Martínez, C., Braun, A.M. *New J. Chem.*, **1999**, 85.
6. Segado, M., Reguero, M. *Phys. Chem. Chem. Phys.*, **2011**, *13*, 4138.
7. Flors, C., Ogilby, R., Luis, J.G., Grillo, T.A., Izquierdo, L.R., Gentili, P-L., Bussoti, L., Nonell, S. *Photochem. Photobiol.*, **2006**, *82*, 95.
8. Koelsch, C. F., Anthes, J.A. *J. Org. Chem.*, **1941**, *6*, 558.
9. Cooke, R., Thomas, R. *Aust. J. Chem.*, **1975**, *28*, 1053.
10. Cooke, R., Dagley, J. *Aust. J. Chem.*, **1978**, *31*, 193.
11. Cooke, R., Edwards, J.M. *Prog. Chem. Org. Nat.*, **1981**, *40*, 153.
12. Luis, J. G., Fletcher, W.Q., Echeverri F., Grillo T.A., Kishi, M.P., Perales, A. *Nat. Prod. Lett.*, **1995**, *6*, 23.

-
13. Binks, R. H., Greenham, J.R., Luis, L.G., Gowen, S.R. *Phytochemistry*, **1997**, *45*, 47.
 14. Luis, L. G., Quiñones, W., Echeverri, F., Grillo, T.A., Kishi, M.P., Garcia-Garcia, F., Torres, F., Cardona, G. **1996**.
 15. Kamo, T., Hirai, N., Iwami, K., Fujioka, D., Ohigashi, H. *Tetrahedron*, **2001**, *57*, 7649.
 16. Kamo, T. K., N., Hirai, N., Tsuda, M., Fujioka, D., Ohigashi, H. *Biosci. Biotechnol. Biochem.*, **1998**, *62*, 95.
 17. Opitz, S., Schneider, B. *Phytochemistry*, **2002**, *61*, 819.
 18. Schneider, B., Paetz, C., Hölscher, D., Opitz, S. *Magn. Reson. Chem.*, **2005**, *43*, 724.
 19. Lazzaro, A., Corominas, M., Martí, C., Flors, C., Izquierdo, L.R., Grillo, T.A., Luis, J.G., Nonell, S. *Photochem. Photobiol. Sci.*, **2004**, *3*, 706.
 20. Echeverri, F., Torres, F., Quiñones, W., Escobar, G., Archbold, R. *Phytochem. Rev.*, **2012**, *11*, 1.
 21. Quiñones, W., Escobar, G., Echeverri, F., Torres, F., Rosero, Y., Arango, V., Cardona, G., Gallego, A. *Molecules*, **2000**, *5*, 974.
 22. Otálvaro, F., Nanclares, J., Vásquez, L.E., Quiñones, W., Echeverri, F., Arango, R., Schneider, B. *J. Nat. Prod.*, **2007**, *70*, 887.
 23. Otálvaro, F., Jitsaeng, K., Munde, T., Echeverri, F., Quiñones, W. Schneider, B. *Phytochemistry*, **2010**, *71*, 206.
 24. Otálvaro, F., Echeverri, F., Quiñones, W., Torres, F., Schneider, B. *Molecules* **2002**, *2002*.
 25. Opitz, S., Hölscher, D., Oldham, N.J., Bartram, S., Schneider, B. *J. Nat. Prod.*, **2002**, *65*, 1122.
 26. Flors, C., Nonell, S. *Acc. Chem. Res.*, **2005**, *39*, 293.
 27. Bucher, G., Bresoli-Obach, R., Brosa, C., Flors, C., Luis, J.G., Grillo, T.A., Nonell, S. *Phys. Chem. Chem. Phys.*, **2014**, *16*, 18813.
 28. Hariharan, P. C., Pople, J. A. *Theor. Chim. Acta.*, **1973**, *28*, 213.

SIXTH CHAPTER:

DEHYDROSQUALENE PHOTOPHYSICS

6.1. INTRODUCTION

Carotenoids are a family of natural organic pigments often present in nature, from fungi to humans, but it is in the plants and other photosynthetic microorganisms where their true nature is revealed. This observation is mainly justified due to the many essential functions they play during the photosynthesis. Some examples are: (1) light harvesting collecting visible light not accessible for chlorophylls and subsequent energy transfer, (2) excess energy dissipation, (3) photoprotection via the quenching of chlorophyll triplet states and (4) protection against oxidation via quenching of singlet oxygen ($^1A_g^-$).^[1] Due to the protective effect against oxidation, carotenoids have attracted interest outside basic research in the fight against the development of cardiovascular diseases, cancer and other serious diseases.^[2,3] Research in this field in order to understand the photophysics and photochemistry that gives them these properties has been intense and fruitful, thanks to the use all the tools available, both experimental and computational.

Focusing on the mechanism involved in the deactivation of singlet oxygen, it is known that the direct excitation and deexcitation between singlet $^1A_g^-$ oxygen and triplet ($^3\Sigma_g^-$) ground state oxygen is highly unlikely given that this kind of transition is forbidden by symmetry, both geometrical and of spin. In fact, the generation of

singlet oxygen is usually assisted by neighbour molecules via sensitization, as described in the previous chapter of this thesis. In photosynthesis, this species is a subproduct of the light-harvesting process of chlorophyll molecules. In cases where singlet oxygen is isolated, the lack of an affordable deactivation mechanism causes a long lived excited state which, if persists in the environment of the organism, can make more harm than good. Therefore, the same mechanism that is used in defence strategies against external attacks, like the ones discussed in chapter 5, can cause fatal tissue damage.

The first evidences of involvement of carotenoids in light-harvesting processes were found more than seventy years ago with the discovering of a constant quantum yield for chlorophyll for a considerable range of wavelengths in some plant species.^[4] These results contrasted with the general trend in organic compounds that show specific absorption bands, so it was suggested that the carotenoids present in those plants acted as intermediaries interacting through their excited states. Their ubiquitous appearance generated further interest for the excited states of carotenoids and, for extension, of polyenes in general^[5]. However, it was not until the seventies that there was a crucial discovery for the understanding of their photophysics. It was discovered that the absorbing state was not the lowest excited state, but an additional lower energy dark state (state that do not absorb or emit because its transition to/from the ground state is forbidden by symmetry) existed.^[6,7] From this point, the elucidation of the role of this state in the mechanisms that explain the photophysics of carotenoids became a major issue by both computational and experimental studies. However, as the research has progressed, more and more intricate excited state structures with other dark states have been found either below or above the absorbing state depending on each particular case. This situation has led to highly complex mechanisms only elucidated in detailed for a few systems.^[8]

In the analysis of dark states, experimental studies have the handicap that forbidden transitions give rise to experimental bands of very low intensity which are very difficult to characterize.^[9] The situation has been changing through the development in the late eighties of new spectroscopic techniques that facilitated the study of excited states in very short timescales and allow locating experimentally also dark states. On the other hand, computational studies can be a very useful tool because they provide information about both bright and dark states with the same

level of precision. In spite of this, the role of the dark state and the detailed mechanism of the deactivation processes have been studied theoretically only for a very few carotenoids, because these systems are a demanding challenge for computational methods, due to their large size, the difficulties of the study of excited states and in this particular case, the complex nature of the dark state. To improve the efficiency of the calculations, conditions are usually idealized, for example by restricting the geometry to a given symmetry. In fact, in carotenoids where the main chain is rigid due to conjugated double bonds, the *all-trans* configuration will be the most stable one and the majoritarian in real samples, due to the high energy necessary for the isomerization that requires the break of a double bond.^[10,11] The few theoretical studies that confront this question confirm this hypothesis,^[10,12,13] but the validity of this approach has to be specifically assessed for each system, especially if the compound presents absence of conjugation in some areas.

Assuming C_{2h} symmetry, the excited states of polyenes have been historically labelled using the irreducible representations of this point group, which are A_g , A_u , B_g and B_u . In addition, a symbol + or - is introduced to indicate if their wavefunctions are expanded on plus or minus combinations of degenerate single excited configurations. This symbol is also related to the character of the states where “-“ states are essentially covalent or neutral while “+” states are mainly described by ionic structures.^[14] Based on this nomenclature and taking into account that the symmetry of the ground state is A_g , the usually lowest singlet excited states of carotenoids are denoted $2^1A_g^-$ and $1^1B_u^+$ where $2^1A_g^-$ is described as a dark or symmetry-forbidden state while the bright state will be $1^1B_u^+$. These states will be the focus of our study, because they are responsible of most of the spectroscopic properties of carotenoids.

$2^1A_g^-$ state consists of a mixture of singly, doubly and other higher excited configurations, which have to be taken into account if a quantitative agreement is wanted while, on the other hand, $1^1B_u^+$ state is described by a single excitation. This latter state gives place to a strong transition that shows a three-peak structure in the absorption spectra of carotenoids corresponding to its three lowest vibrational levels. The different nature of these states is a challenge for computational calculations that should be able to give a balanced description of both of them

because the energy difference between these states can be very small, or even change sign (invert the energetic order of these states) for different systems.

Moreover, it is well-known that this gap depends mainly on the number of conjugated double bonds (represented by the parameter N) so that, in general, for long conjugated chains the dark state is less energetic than the absorbing one and vice versa for small values of N . In this direction, previous studies on open-chain carotenoids have proposed a critical conjugation length of 3 as the boundary for the lowest excited state to be the forbidden state. Anyway, carotenoids with short conjugation chains are not very common, being most abundant those with values of N between 7 and 13.^[15,16]

For the most common cases, where the $1^1B_u^+$ state is more energetic than the $2^1A_g^-$ one, the schematic description of the photophysics of a typical carotenoid will start with the promotion to the absorbing S_2 state. From this state, fast relaxation to the S_1 state is carried out in a short time of the scale of 50 to 300 fs.^[16] Due to the dark nature of S_1 , the determination of the energy and dynamics of this state was not possible until fluorescence detection techniques improved to be sensitive enough to detect the weak S_1 emission, covered up by overlap with the dominating S_2 emission.^[17] These studies found that the S_2 - S_1 internal conversion rate was dependent on the conjugation length because it affects the energy gap between these states and consequently the S_2 lifetime.

As N increases, the absorption energy of S_2 decreases, but not as much as the energy of the S_1 state and, consequently, the energy gap between S_1 and S_2 increases with N . According to this trend, it should be expected that lifetime of S_2 would increase with N and conversion rate decrease, but that was not the case observed, what indicates that the decay mechanism must not be a direct one.^[18,19] For carotenoids with N around 8, it was suggested that a larger gap favours the direct radiative deactivation from the bright state to the ground state, what would be a violation of Kasha's rule.^[20,21] Although absorption and emission spectra are very similar in all carotenoids, what indicates that the states involved in these processes are identical, other hypothesis to explain the experimental observations suggest the involvement of intermediate states or the overlapping of vibrational modes (Figure 6.1).

Raman spectroscopy measurements suggested the existence of a dark state of B_u^- symmetry localized between S_1 and S_2 , that would act as intermediate due to the strong vibronic coupling with S_1 (A_g^-) and a small energetic gap with S_2 (Figure 6.1 B).^[12] However, this gap was finally shown to be too large for carotenoids with $N > 10$, so this hypothesis was discarded in those cases. Other studies report the localization of an additional state of A_g^- symmetry,^[22-24] while others, based on spectroscopic measurements, suggest the involvement of a S^* state of undefined symmetry.^[25] This state would decay independently to the ground state, so it would not act as an intermediate, but opens a different deactivation process in competition with the $S_2 \rightarrow S_1 \rightarrow S_0$ pathway (Figure 6.1 C). Nevertheless, calculations of decay rates indicate a preference for this last path, although the reason is not clear. The origin of the S^* state is not yet established, but some studies propose it to be a vibrationally hot ground state in solution and an independent state in biological environments, where is found consistently higher but very close to S_1 . In spite of this closeness, both states do not interact, which is at least intriguing.^[26]

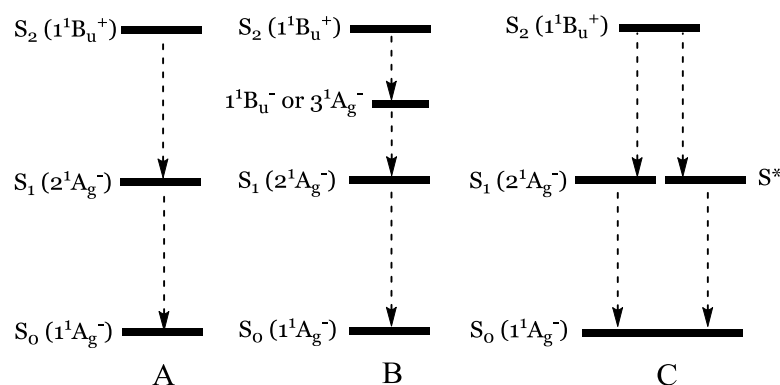


Figure 6.1 – Three possible relaxation pathways that can take place after excitation of a carotenoid into the S_2 state. A) Direct pathway through the main states, B) Indirect pathways through $1B_u^-$ or $3A_g^-$, depending on the conjugation and C) Competitive pathway between S_1 and S^* .

All this accumulated experimental evidences do not resolve, anyway, certain inconsistencies. For example, the extremely fast internal conversion to the intermediate state should prevent the observation of emission since the intermediate state is a dark state. The fluorescence could be produced thanks to a symmetry break that would make the selection rules less restrictive, but this process is impossible in the short time scale of the fluorescence. Another contradictory fact is that the similarity

of the absorption and emission spectra is observed in all carotenoids, irrespective their conjugation length, while the behaviour of the dark states localized changes with N . Thus, although the intermediate state hypothesis would be a suitable solution, further studies are needed to resolve the ultrafast mechanism of deactivation.

Finally, the last S_1 - S_0 relaxation step for carotenoids of large conjugation lengths is the best understood so far. Since in these systems those states have the same symmetry, the coupling between the vibrational totally symmetric stretching modes is possible, opening the internal conversion path.^[27] This effect, confirmed experimentally, was also known for short polyenes where the C=C stretching plays a central role in this process.

The mechanisms invoked so far cannot be applied to carotenoids with low values of N , because in these cases $1^1B_u^+$ and $2^1A_g^-$ states are inverted. For short carotenoids, the vibrational coupling between the totally symmetric tension modes of the S_0 and S_1 ($1^1B_u^+$) states is not possible due to the different symmetry of these states. An alternative hypothesis suggests that the $S_1 \rightarrow S_0$ conversion takes place through a conical intersection, but the required substantial shift of the PES of the states is not supported by experimental data. For internal conversion between S_2 and S_1 , bending vibrational modes of b_u symmetry have been invoked for carotenoids with small S_1 - S_2 gap, where those states can mix.^[28]

It can be concluded that despite the numerous contributions that have made both experimental and theoretical studies over the last and the current century, in-depth knowledge of the mechanisms that dominate the properties of carotenoids is still lacking, especially for short carotenoids.^[29] For this reason the study of the photochemistry of carotenoids is still an active field of research.

6.2. SCOPE

In this work we develop a computational study on the absorption, excited state relaxation and possible deexcitation pathways of dehydrosqualene (DHS). Carotenoids can be classified into two classes depending on whether they present oxygen or other heteroatoms (xanthophyll) or not (carotene) inside the shared basic structure of polyene hydrocarbon type. DHS is a natural carotenoid of the subfamily of carotenes that shows their typical hydrocarbon structure (Figure 6.2).

Its parent system, squalene, is a triterpenic hydrocarbon present in high concentrations in virgin olive oils and it is considered a remarkable bioactive substance as a scavenging agent for singlet oxygen. Anticarcinogenic and antitumor properties have also been attributed to this compound.

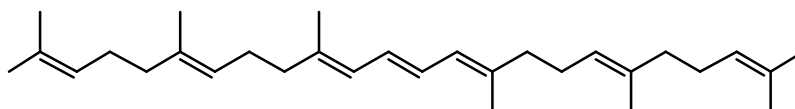


Figure 6.2 – Schematic representation of dehydrosqualene.

DHS has the particular characteristic of a flexible skeleton, given that there are only three conjugated double bonds ($N=3$) in the center of its backbone that connect two symmetrical chains of saturated hydrocarbon. Such a short conjugation length has not been exhaustively studied, not in polyenes nor in carotenoids,^[8,15] so an unquestionable assignment of the order of the excited states is not possible. According to the general trends stated before, it is expected that the bright state $1^1B_u^+$ will be lower in energy than the $2^1A_g^-$ one.

One of the main difficulties for the theoretical study of carotenoids is the size of the systems, which make most of them unaffordable to be studied with high level ab initio methods. One of the reasons why we have chosen dehydrosqualene is its moderate size: it is large enough for being a realistic example, but small enough for allowing high level computational methods, in the limit of their applicability. Our aim is to compare the results obtained for dehydrosqualene using these high level methods with those obtained with some other less demanding methods to establish the computational strategy that provides the best ratio quality/cost. The strategy established here can be used latter on studying larger systems.

The other reason to have chosen dehydrosqualene is the flexibility of its skeleton, although it adds a subsequent difficulty to the study. For carotenoids where the main chain is rigid due to conjugated double bonds, it is sensible to assume that the geometry of the backbone will be planar, keeping the C_{2h} symmetry. This geometrical restriction reduces noticeably the computational costs, so it has been assumed commonly in theoretical studies of carotenoids to make calculations feasible. Opposite to this, dehydrosqualene can have several conformations of low energy connected by low-barrier paths. This fact complicates the study in two

different ways. First, it will be necessary to explore the conformational space to locate low-energy species and analyse the influence of conformation on the photophysics of the system. Second, there is an increase of the computational costs due to the loose of symmetry that will make necessary the search of less demanding methods. They must, though, still offer reliable results of the required precision to describe properly the $2^1A_g^-$ and $1^1B_u^+$ excited states of carotenoids.

In order to carry out this study, we have used several ab initio multireference methods, in particular CASSCF, CASPT2 and the restricted versions of the first two, RASSCF and RASPT2. We have performed this study in gas phase because, due to the low dipole moment of dehydrosqualene, it is expected a negligible influence by the solvent in the photochemistry of this compound, unlike carotenoids with carbonyl end-groups.^[8,30,31] The agreement of our results with the experimental data available indicate that the methodology used is appropriate, and give a solid ground to rely on the mechanistic hypothesis proposed here.

In this work we will explore the potential energy surfaces of the lowest singlet and triplet states to explain the photophysical properties of DHS. For this initial study we will consider only a conformation of C_{2h} symmetry. In a subsequent step, we will determine the influence of the flexibility of the skeleton of DHS in its spectroscopic properties. Given the moderate size of this system, we will use it to test the performance of the RASSCF/RASPT2 methodology in this kind of problem, to optimize the ratio accuracy/cost.

6.3. COMPUTATIONAL STRATEGY

Due to the large size of carotenoids, the computational methods found in the literature used for their study are usually monoreferencial DFT methods alone or combined with multireference ones (MRCI). The first type works well for carotenoid radical cations, but multireference methods are needed to describe properly the excited states of polyenes.^[13,30] In order to decrease computational costs, most of the computational studies assume the maximum symmetry the particular system allows. In this work, the computational strategy used consists mainly in a combination of ab initio multiconfigurational self-consistent (SCF) methods. The most standard procedure we have worked with is the CASSCF/CASPT2 strategy. For the active space of DHS, 14 electrons and 14 active

orbitals were selected to take into account the whole π electron system. Geometry optimizations with C_{2h} point group symmetry restrictions were carried out for planar geometries, but no constrains were imposed for other conformations.

This strategy is hardly affordable for a system of the size of DHS and, more crucially, using such a large active space. For this reason, the CASSCF/CASPT2 methodology was used only for testing purposes, and instead we used restricted active space methods (RASSCF/RASPT2) to perform the general work. The orbitals of the active space (14, 14) that had occupations close to 2 or 0 in the wavefunctions of all the states of interest obtained in the CASSCF (14, 14) test calculations were included in RAS1 and RAS3 respectively. Hence, an active RAS2 (6, 6) subspace was kept containing only the orbitals needed to describe the states of interest while allowing single and double excitations from RAS1 and to RASs3. This reduced active space made the calculations of the averaged lowest excited states much faster. Further details are going to be provided later.

In all calculations, the configuration interaction matrix was selected larger than the calculated number of states to ensure that the selected states are the lowest in energy. In CASPT2 and RASPT2 calculations we employed the imaginary level shift technique in order to prevent intruder states. In this case, a shift parameter of 0.2 a.u. was selected after checking the stability of the excitation energies and the CASSCF wavefunction weights. We also allowed the mixing of SCF states with the multi-state approximation (MS-CASPT2). Oscillator strengths were calculated from these new perturbative wavefunctions using the state interaction method (RASSI). In all calculations we used the d-polarized split-valence basis set 6-31G(d).^[32]

Although the CASPT2 method is well known and widely used, we wanted to compare the results that this perturbative method provides with those of a variational multireference method. For this, we have used the DDCI (difference-dedicated configuration interaction) method described in Chapter 3. We used here the active space defined by RAS2 and considered 300 orbitals (counting occupied and virtual) to develop the configuration interaction space. In symmetry restricted calculations with different state symmetries, two sets of orbitals are generated. In order to be able to use these orbitals in DDCI, we have to generate state averaged SA-CASSCF orbitals independent of the spatial symmetry and spin multiplicity of

the CASSCF states. The iterative procedure (IDDCI) has been used to ensure the independence of the results of the molecular orbital set.

The search for the non-symmetric low energy geometries was conducted using molecular mechanics calculations using the Universal Force Field. The resulting set of minimum energy geometries was refined at DFT level with the B97D functional. The energies of these reoptimized structures were calculated finally at RASSCF/RASPT2 level.

All of these calculations were performed using MOLCAS 7.6 software package and Gaussian 09.

6.4. RESULTS

Strategy of the study

The two main aims of this study (detailed photochemistry of linear DHS and influence of the flexibility in the photochemistry) require different computational strategies, which we will sketch separately in what follows.

Linear DHS belongs to the C_{2h} symmetry point group, which imposes geometrical restrictions that makes computations cheaper allowing the use of more accurate methods. For this reason, we first studied the photochemistry of linear DHS using CASSCF and CASPT2 methods. The same study was performed afterwards at RASSCF/RASPT2 level, to validate this method by comparison with the previous results. The satisfactory agreement between the complete and the restricted methods indicates that the latter one is accurate enough to be used for the study of non-linear conformations of DHS, where the loose of symmetry increases the computational costs.

The large flexibility of the side arms of DHS makes possible the existence of many stable conformations of similar energy. That is, in the ground state potential energy surface there can be many local minima of similar energy. We used molecular mechanics methods to generate several hundreds of configurations to make a final selection of several tenths of low-energy geometries, which were optimized at DFT level. Finally, the lowest energy geometries obtained in this step were the starting points for the photochemical study performed at the RASSCF/RASPT2 level

validated in the first part of our work to obtain reliable ground and excited state energies. A full RASSCF optimization was also performed, but the cost of this procedure preclude using this method as the standard one for the whole study.

In order to organize these results, they are structured in three sections. The first one contains the results of the absorption of DHS restricted to an all-trans C_{2h} ground state equilibrium structure. In this section we will also analyse the nature of the excited states of lower energy and will compare CASSCF/CASPT2 and RASSCF/RASPT2 results. In the second section, we will study the low-energy excited states 2^1A_g , 1^1B_u , 1^3A_g and 1^3B_u , search the geometries of minimum energy for each one, explore their potential energy surfaces and possible interactions among them and propose a comprehensive mechanism of deactivation to explain the photophysics of DHS. In the third section we will present the conformational exploration performed to analyse the influence of the geometric deformations on the spectroscopic properties of this carotenoid.

6.4.1. Franck-Condon Region and calibration of computational methodologies

As usual, the first step has been the optimization of the ground state structure. To begin with, this optimization has been run at CASSCF (14, 14) level, under the C_{2h} symmetry constraint. The bond distances of the central chain are shown in Figure 6.3.

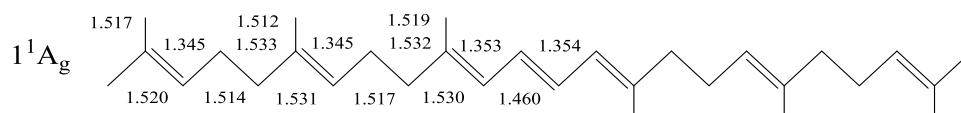


Figure 6.3 – Bond distances (in Å) of the ground state C_{2h} minimum of DHS, optimized at CASSCF (14, 14) level. Symmetric bond distances are omitted.

At this geometry, the relative energies of the lower excited states were calculated. To allow interaction of the CASSCF states at MS-CASPT2 level, more states than the strictly involved in the process of interest have to be included initially in this calculation. For this reason, three A_g states and up to four B_u states were considered for the singlet manifold. On top of this, the CI matrix of the B_u states was expanded to six states. Additionally, we also calculated the lowest triplet state of each symmetry. The results of the vertical excitations obtained in this way are shown in Table 6.1.

Table 6.1 – Absorption energies (in kcal·mol⁻¹) and oscillator strengths (f) for dehydrosqualene at the computed ground state minimum optimized at CASSCF (14, 14) level. Very low oscillator strengths are omitted.

<i>States</i>	<i>CASSCF</i>	<i>f</i>	<i>SS-CASPT2</i>	<i>MS-CASPT2</i>	<i>f</i>
GS	0.0	-	0.0	0.0	-
1 ³ B _u	57.0	<10 ⁻⁷	58.7	59.2	<10 ⁻⁷
1 ³ A _g	91.1	<10 ⁻⁷	94.8	95.2	<10 ⁻⁷
1 ¹ B _u	168.0	1.52	108.2	107.1	0.98
2 ¹ A _g	118.9	<10 ⁻⁷	117.4	117.5	<10 ⁻⁷
2 ¹ B _u	151.7	0.01	146.3	147.4	0.01
3 ¹ B _u	160.2	1.42·10 ⁻⁴	154.7	154.7	< 10 ⁻⁵
4 ¹ B _u	160.8	4.79·10 ⁻²	155.6	155.6	< 10 ⁻⁴
3 ¹ A _g	157.0	<10 ⁻⁷	155.3	155.7	<10 ⁻⁷

It can be seen that the energy difference between the excited states of A_g symmetry is large. The eigenvectors of the MS-CASPT2 effective Hamiltonian show that there is not any interaction between the CASSCF A_g states so the 2¹A_g state is then properly described at CASSCF level without the need of taken into account possible interactions with other states. Consequently, no higher A_g states will be considered in the subsequent calculations on this system. The oscillator strength of this state is negligible, showing that it will not be capable of absorbing or emitting radiation. The wavefunction that describes this dark A_g state is multideterminantal, describe by singly and doubly excited configurations where the latter have half of the total weight.

On the other hand, the effect of the dynamic correlation is crucial in the calculation of the energy of the B_u states. The perturbation stabilized surprisingly differently these states, provoking an order inversion, so that the 4¹B_u state at CASSCF level becomes the first singlet excited state (1¹B_u) at CASPT2 level. For this reason, four B_u states will be systematically included in the calculations, although from now on only the energy of the 1¹B_u CASPT2 state will be reported. This state is especially relevant because it is the absorbing state, as indicated by the large value of its oscillator strength. Its wavefunction is monodeterminantal, defined by an excitation between molecular orbitals localized in the central conjugated area (see Figure 6.4 further down). This result agrees with previous descriptions of the excited states of carotenoids and polyenes that reveal that the bright state is an ionic state, which is poorly described at CASSCF level.^[9,14] This vertical energies

obtained at CASPT2 level predicting that the $1B_u$ state is lower in energy than the 2^1A_g one, indicate that for this carotenoid, with conjugation length of 3, the established rule for the relative energies of the dark and bright states^[8,16] is fulfilled.

The reproduction of the experimental absorption spectrum from a theoretical point of view will help to reveal important information about the states that may be involved in the reactivity of the molecule and, therefore, essential to understand its photophysics. The relative energy of the bright state ($107.1 \text{ kcal}\cdot\text{mol}^{-1}$, 267 nm) can be compared with the experimental spectrum of DHS in n-hexane.^[33] It shows a band of $\pi\pi^*$ character at 287 nm associated with this strongly allowed transition with a three-peaked vibrational structure. The difference between the computational and the experimental data ($7.5 \text{ kcal}\cdot\text{mol}^{-1}$) is satisfactory, but there is also room for improvement. As it will be shown later (subsection 6.4.3, further down), our results indicate that the disagreement is due, not to the computational methodology, but to the approximation done by imposing C_{2h} symmetry to the geometry.

To apply the RASSCF/RASPT2 method, the population of the orbitals had to be inspected in order to include the appropriate ones in the RAS2 subspace. These are those involved in the main excitations that describe the 2^1A_g and 1^1B_u states and that, consequently, have occupation numbers significantly different from 2 and 0 in at least one of the three lowest energy states of DHS. Those orbitals of the CAS that are not involved in these excitations are included in RAS1 or RAS3. The reduction of the active space was done, therefore, including six orbitals and six electrons in RAS2. These orbitals, as shown in Figure 6.4, are localized in the central conjugated moiety of DHS. From the eight external orbitals localized in the non-conjugated moieties, the “arms” of DHS, there are four in RAS1 and four in RAS3. The computational parameters used in the restricted calculations will be the same than those used in the CAS methodology. Table 6.2 shows the energies, obtained with the complete and restricted active spaces, of the lowest singlet at triplet states of DHS calculated at the ground state C_{2h} minimum optimized at CASSCF level. It can be observed that the MS-RASPT2 results reproduce correctly the MS-CASPT2 results for both singlet and triplet states, while reducing the computational cost to a tenth of the original CPU time. This approach proves then to be suitable to study this kind of system, so it will be used to continue studying the PES of DHS outside the Franck-Condon area.

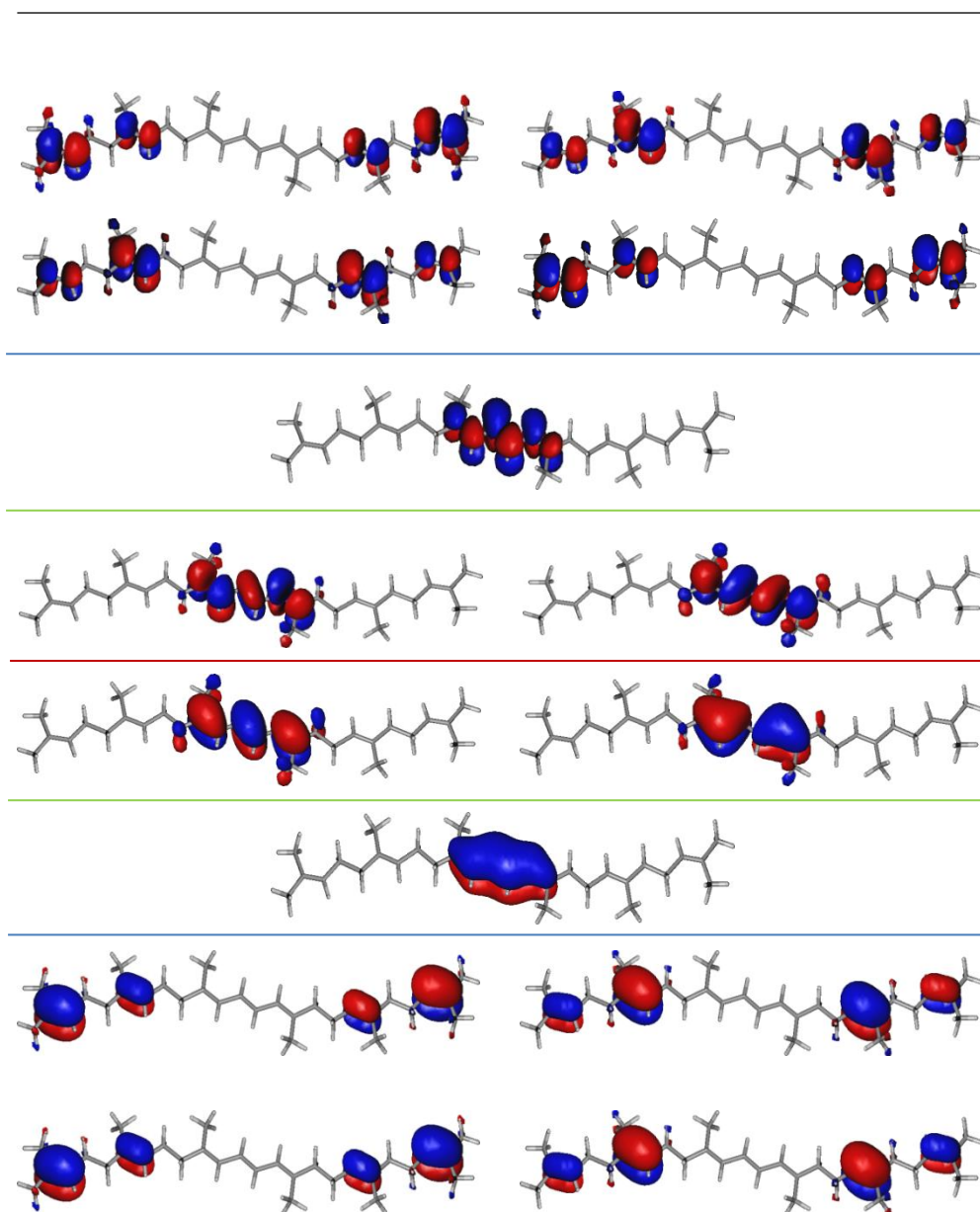


Figure 6.4 – Molecular orbitals of the whole π system of DHS. Orbitals below the red line are occupied in the ground state configuration. Orbitals between blue lines are included in RAS2. The occupation numbers of these orbitals are significantly different from 2 and from 0 in at least one of the three lowest states (S_0 , 2^1A_g and 1^1B_u) of DHS. Orbitals between green lines are the ones included in CAS (4, 4) used in DDCI calculations.

Table 6.2 – Comparison of absorption energies (in kcal·mol⁻¹) and oscillator strengths (*f*) for dehydrosqualene using MS-CASPT2 and MS-RASPT2 methods. Very low oscillator strengths are omitted.

<i>State</i>	<i>MS-CASPT2</i>	<i>f</i>	<i>MS-RASPT2</i>	<i>f</i>
GS	0.0	-		-
1 ³ B _u	59.2	<10 ⁻⁷	58.8	<10 ⁻⁷
1 ³ A _g	95.2	<10 ⁻⁷	94.7	<10 ⁻⁷
1 ¹ B _u	107.1	0.98	107.7	0.97
2 ¹ A _g	117.5	<10 ⁻⁷	117.3	<10 ⁻⁷

It is well known that the dynamic electron correlation can affect in greater or lesser degree to different states, but the large stabilization that provokes in the B_u state of DHS is somehow surprising. To check that this result was not an artefact of the CASPT2 perturbational method, we decided to reproduce these calculations with another method that includes the dynamic correlation in a different way. We chose the IDDCI (difference-dedicated configuration interaction) method, in its iterative version. DDCI is based initially on a small CAS that must contain the electrons and active molecular orbitals required to properly describe the states of interest. In our case it means that the two orbitals involved in the excitation that describes the 1¹B_u state should be included along with the four orbitals involved in excitation of the 2¹A_g state, which altogether represents a (4, 4) active space (see Figure 6.4). Due to this reduction of the active space, the MS-RASPT2 values were recalculated to make the results fully comparable. The IDDCI (4, 4) results obtained are collected in Table 6.3 together with the MS-RASPT2 (4, 4) ones for comparison. The good agreement found confirms that both methodologies are appropriate to describe the system of interest and indicates that the results obtained at MS-RASPT2 level are reliable.

Table 6.3 – Comparison of absorption energies (in kcal·mol⁻¹) for dehydrosqualene using MS-RASPT2 and IDDCI methods, using in both cases a CAS (4, 4).

<i>State</i>	<i>MS-RASPT2</i>	<i>IDDCI</i>
GS		0.0
1 ³ B _u	58.8	58.8
1 ³ A _g	93.7	93.9
1 ¹ B _u	109.3	113.9
2 ¹ A _g	117.3	118.4

6.4.2. Excited state surfaces and reaction paths under C_{2h} symmetry constraint.

To understand the photophysics of DHS, it is necessary to explore the potential energy surfaces of the excited states that could be involved in the deactivation mechanism. We are going to focus our interest on the first singlet and triplet excited states of each symmetry, trying to locate the critical points of these surfaces and the areas of connection between them. Geometry optimizations will be carried out using CASSCF method due to the lack of implementation of analytical gradients for RASSCF calculations, although the vertical energies have been calculated at MS-RASPT2 level. These geometries will be refined performing scans at MS-RASPT2 level along the most representative internal coordinates, given the poor description of some states by CASSCF. All optimizations were run under C_{2h} symmetry constraint.

Excited state minima

Although the 1B_u state is not properly described at CASSCF level, this method can give a first approximation of the minimum energy geometry of this state. The optimized structure obtained in this way (shown in Figure 6.5) only shows noticeable differences from the ground state minimum in the central moiety, given that it is in the conjugated π system where the excitation is localized. The nature of the π^* orbital where the electron is excited, which locates the nodes in the opposite bonds than the ground state, makes that the C-C distance of all C-C bonds becomes the same (C-C distances of this part of the molecule become almost equal), and the same happens with the bond order, that becomes intermediate between single and double bonds. This minimum is located $95.4 \text{ kcal}\cdot\text{mol}^{-1}$ above the ground state one, what means a relaxation energy from the Frack Condon geometry of $11.7 \text{ kcal}\cdot\text{mol}^{-1}$. The substantial change in energy and the small geometry deformation ensure that this relaxation is produced along a barrierless path, so this minimum will be easily reached after the initial excitation that populates this state. At this geometry, the 1B_u state is almost degenerate with the $2{}^1A_g$ one (energy gap: $2.8 \text{ kcal}\cdot\text{mol}^{-1}$, see Table 6.4), but the first one is more stable than the second one, like at FC geometry.

In spite of the poor description of this state at CASSCF level, a scan around the minimum geometry confirmed that it corresponds also to a minimum energy point at CASPT2 level. The oscillator strength calculated for this structure indicates that the emission from this 1B_u species is possible ($f=0.90$). Nevertheless, to predict if

it will take place, it is necessary to analyse the alternative paths that compete with radiative deexcitation.

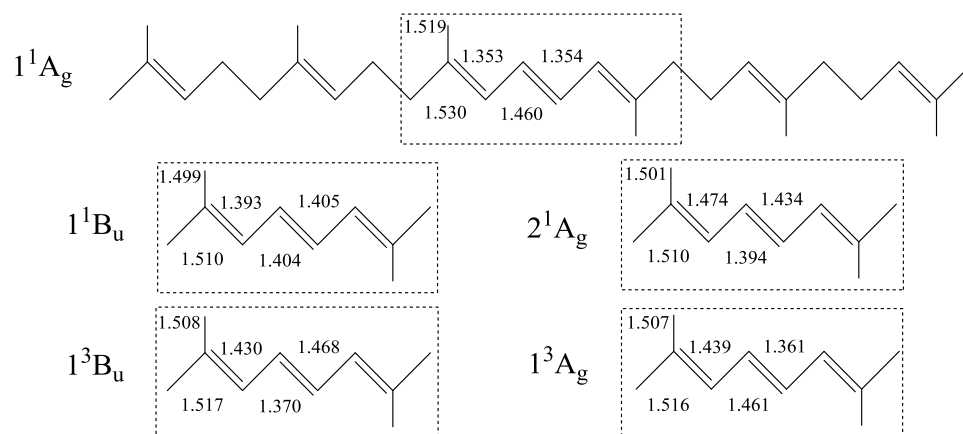


Figure 6.5 – Relevant geometrical parameters of the minima of the lowest energy states of DHS, optimized at CASSCF (14, 14) under C_{2h} symmetry constrain. Distances are in angstroms.

The optimization of the $1A_g$ state at CASSCF level provided a geometry that, like in the case of $1B_u$ state, only shows significant differences from the ground state minimum in the central conjugated moiety (see Figure 6.5). Although the state is mainly described by a double excitation between the same orbitals that describes the excitation of the $1B_u$ state, there are also strong contributions of singly excitations involving other orbitals, which makes that the single/double nature of the bonds of the central moiety are reversed relative to their location in the ground state (see Figure 6.5). Like in the case of the $1B_u$ state, this geometry showed to be a minimum also at the MS-CASPT2 level, 23.8 kcal·mol⁻¹ more stable than the FC energy of this state. Such a large stabilization indicates that the relaxation along this surface must be quite favoured. The relative energies shown in Table 6.4 also indicate that at this geometry the 2^1A_g state becomes the first singlet excited state, and that this is the global minimum of the S_1 PES. This can be a feature that can be crucial in the photophysics of DHS. It should also be pointed out that at this point the $1A_g$ state is degenerate with the triplet state of the same symmetry.

The lowest triplet excited states have also been suggested in some studies to play a role in the mechanisms of deactivation of carotenoids because they have been experimentally found at energies close to the lowest singlet excited states.^[34,35] In

order to check this hypothesis, we also took them into account in this study by localizing their minima and calculating their energy in the critical points found. Their geometries optimized at CASSCF level are also shown in Figure 6.5.

Table 6.4 – State energies (in kcal·mol⁻¹) and oscillator strengths (*f*) for dehydrosqualene at both singlet ¹B_u and ²A_g minima.

State	¹B_u state minimum		²A_g state minimum	
	<i>MS-RASPT2</i>	<i>f</i>	<i>MS-RASPT2</i>	<i>f</i>
GS	3.5	-	16.1	-
¹ B _u	46.0	<10 ⁻⁷	46.2	<10 ⁻⁷
¹ A _g	91.0	<10 ⁻⁷	93.2	<10 ⁻⁷
¹B_u	97.5	0.90	100.3	0.87
²A_g	99.4	<10⁻⁷	93.7	<10⁻⁷

The changes of the ¹³B_u minimum relative to the ground state geometry are similar to those of its singlet counterpart: the lengths of the double bonds increase and those of the single bonds decrease. On the other hand, the ¹³A_g state decreases the length of the central double bond, and increases the length of the other two double bonds. The ¹³B_u state is the lowest excited state in the whole area of the PES explored in this work keeping a large energy gap (around 30 kcal·mol⁻¹) almost constant with the other excited states. The ¹³A_g state also tends to be more stable than the singlet excited states but, having energy similar to them, it crosses with the ¹A_g state and is almost degenerate with the ¹B_u state at some points.

Table 6.5 – State energies (in kcal·mol⁻¹) and oscillator strengths (*f*) for dehydrosqualene at both triplet ¹³B_u and ¹³A_g minima.

State	¹³B_u state minimum		¹³A_g state minimum	
	<i>MS-RASPT2</i>	<i>f</i>	<i>MS-RASPT2</i>	<i>f</i>
GS	13.2	-	7.2	-
¹³B_u	43.6	<10⁻⁷	54.0	<10⁻⁷
¹³A_g	97.2	<10⁻⁷	87.2	<10⁻⁷
¹ B _u	97.9	0.88	98.9	0.92
² A _g	95.5	<10 ⁻⁷	103.6	<10 ⁻⁷

The information obtained up to here for dehydrosqualene, allow us to suggest the photochemical processes that this system undergoes under radiation and that

explain its photophysical properties. We will take into account both radiative and non-radiative decay channels and singlet and triplet manifolds.

The initial irradiation of DHS excites the system to the 1B_u excited state, the only one that shows non-negligible oscillator strength for the transition from the ground state. At FC geometry, this is the first singlet excited state, fulfilling the general rule that predicts that for carotenoids with small conjugation length, the 1B_u state is more stable than the 1A_g one. This could indicate that the later state will not be involved in the photophysics of these compounds but, as we will see, this is not necessarily true in all cases. Once on the 1B_u PES, the system will relax towards the minimum of that surface. To understand the paths that the system can follow afterwards, we have to take into account the interactions between the surfaces of the different low energy states of DHS. Figure 6.6 shows a schematic representation of some critical points of the PES of the low energy states of DHS under C_{2h} symmetry constraint.

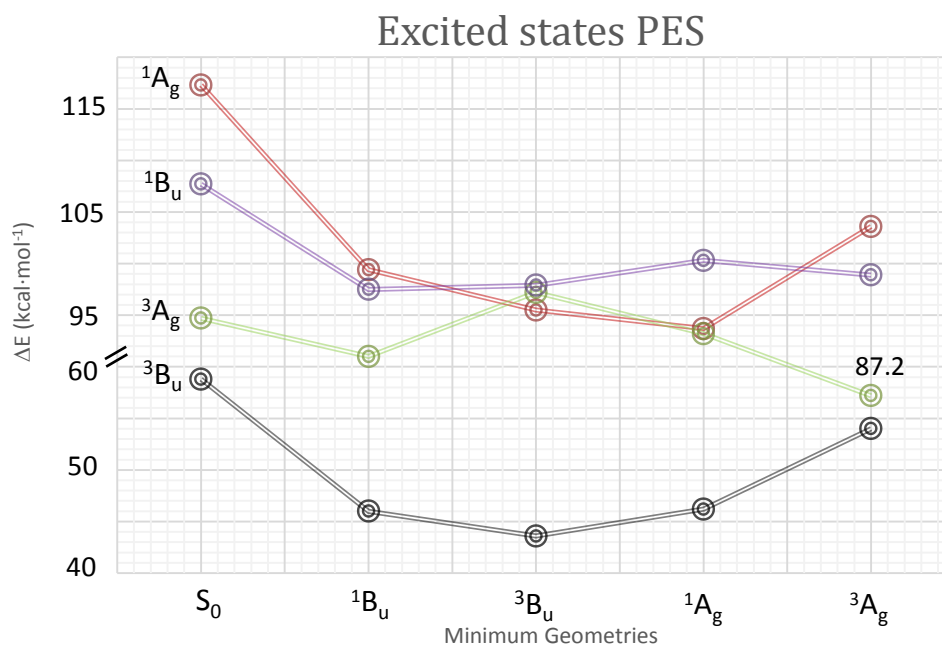


Figure 6.6 – Schematic representation of the relative energies (MS-RASPT2 level) of the lower excited states of DHS, at the minimum energy geometries of the PES of these states, optimized under C_{2h} symmetry constraint.

At the 1B_u minimum geometry, the 1A_g state is just $1.9 \text{ kcal}\cdot\text{mol}^{-1}$ above the 1B_u surface. A crossing between both surfaces has been located by interpolating the coordinates between the minima of the excited states. This crossing is found near the 1B_u minimum, just $0.8 \text{ kcal}\cdot\text{mol}^{-1}$ above it, so it is easily accessible. Under C_{2h} symmetry constraint, given the different spatial symmetry of the states, the crossing is a “real crossing”, what implies that the probability of internal conversion through this topological feature is null. But any deformation that takes the system out of planar geometries (out-of-plane vibrations), will break the symmetry and make of the internal conversion an efficient decay channel. This hypothesis would agree with previous works that suggest that the interaction between S_1 and S_2 states in carotenoids with small values of N is controlled by certain vibrational modes.^[28,36] On the other hand, the oscillator strength of the transition from the 1B_u minimum to the ground state is large, indicating that the probability of radiative deactivation from this species is high. To predict the percentage of the wavepacket that will follow each of these deactivation paths (internal conversion to 1A_g or radiative deactivation) a dynamic study should be performed, what is beyond the scope of this work.

If the system crosses to the 1A_g surface, it will relax on this surface to the minimum energy geometry of this state, which is in fact the global minimum of the S_1 PES (for planar geometries). Here, singlet and triple A_g states are degenerate, but the probability of intersystem crossing is very low, as the Kasha’s rules predict (because of the different spin symmetry and the same spatial symmetry), and the calculation of the oscillator strength between these states confirms it. Radiative deexcitation to the ground state is not probable either because also in this case the oscillator strength between $2{}^1A_g$ state and the ground state is negligible ($f < 10^{-8}$). Our results predict that the only deexcitation channel that can compete with ISC from this minimum is the deactivation to the ground state by vibrational coupling. Experimental evidences suggest that this is the preferential path,^[27] but we cannot discard a certain population of the triplet manifold.

6.4.3 The effect of the flexibility on the absorption

Due to the flexibility of the side arms of DHS, it cannot be assumed that this system will mostly keep the C_{2h} symmetry. It is important, then, to analyse how the deformation of the planar geometry will affect the predicted photophysics of this system. The loose of planarity has already been taken into account qualitatively in

the analysis of the possible paths that the system can follow after the initial excitation, but the quantitative changes in the energies due to the change of conformation must also be assessed, because they could induce drastic qualitative changes. This study has, among others, two problematic points. First, it can be very difficult to find the absolute minimum on the ground potential surface (and of the excited states surfaces) due to numerous stable conformations of similar energy that the flexible arms of DHS can adopt. Second, even if the most stable conformation is found, calculation based only on this species will not necessarily reproduce the experimental results, because experimental samples will be formed by a collective of many different conformers. We have already addressed this problem in Chapter 4, in relation with the reproduction of the experimental absorption spectra of phenylazopyridine. In this case our aim is not so ambitious because the size of the problem does not allow it, so we will limit this study to analyse the influence of the geometric deformations on the excited state energy.

To scan an area as large as possible of the conformational space, we generated initial geometries changing systematically the dihedral angles of one of the saturated arms of DHS, to have the values of 60° , 120° , 180° , 240° and 300° . In this way, we generated 665 geometries that were optimized at the molecular mechanics level using the Universal Force Field (UFF). The distribution of the energies of the conformations obtained is shown in Figure 6.7.

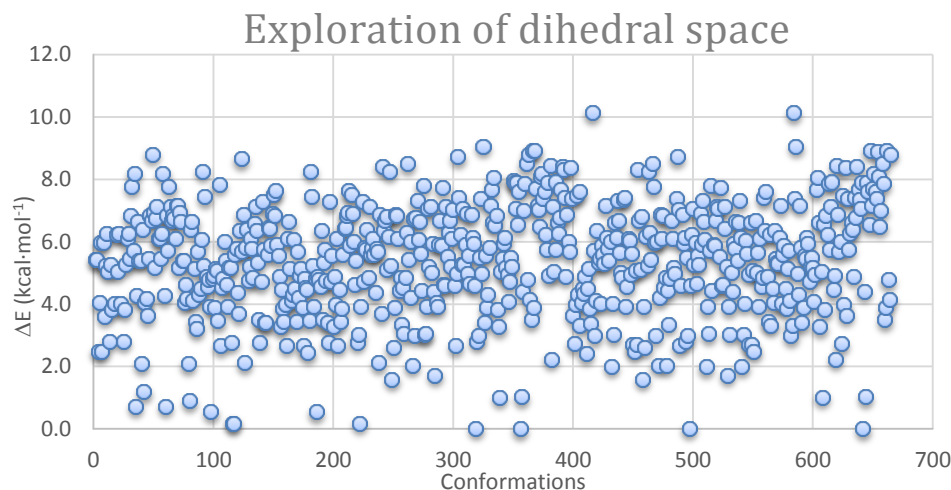


Figure 6.7 – MM energy distribution of the collective of conformations generated by a grid of dihedral angles and subsequent geometry optimization at MM level.

The 16 lowest energy conformations, which energies are in a range of 2.0 kcal·mol⁻¹, were selected and the dihedral angles of the non-linear arm applied to both of them to obtain another 16 conformations. The geometries of all of them were reoptimized at MM and DFT level, using the B97D functional to take into account the long-range interactions. The distribution of energies of these collectives is represented in Figure 6.8. Blue points represent the conformations where one arm keeps linear, while red points stand for conformations where both arms have lost linearity. MM and DFT results agree in showing systematically lower energies for these second conformations than for the first ones.

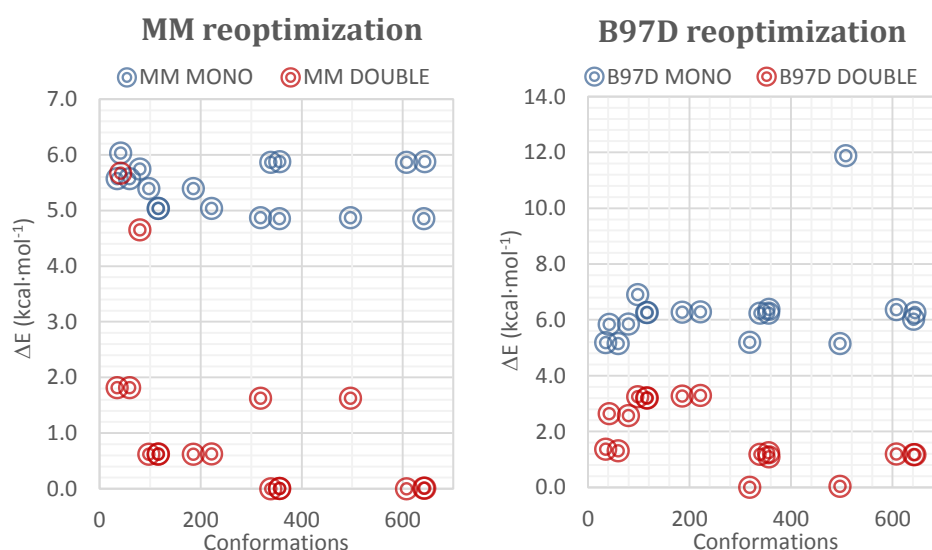


Figure 6.8 – Energy distribution of conformations optimized at (a) MM (UFF) level and (b) DFT (B97D) level. Blue points represent the conformations where one arm keeps linear, while red points stand for conformations where both arm have lost linearity.

The 16 most stable conformations at the DFT level, all of them with both arms non-linear, were selected to calculate at MS-RASPT2 level the energy of their low energy states. The geometry of the most stable conformation obtained in this way is shown in Figure 6.9 a. It is surprising the large deformation from linearity that this conformations show, where the side arms are bent to interact with each other.

An extra calculation was finally performed, to be used as benchmark to compare the results obtained so far: the ground state geometry optimization of DHS was

performed at RASSCF level, without any constraint. This calculation was carried out in a sequential computation and it took four months of wall time (in a Xeon E5-2630 processor with 64G of memory), what makes this procedure unaffordable to be used systematically in a study. The geometry obtained is also shown in Figure 6.9 b. It can be observed that the geometry obtained does differ considerably at first glance from the ones obtained at MM/DFT level but it is worth mentioning that the out-of-plane dihedral angle caused by the tetrahedral sp^3 carbons nearest to the central conjugation is similarly reproduced.

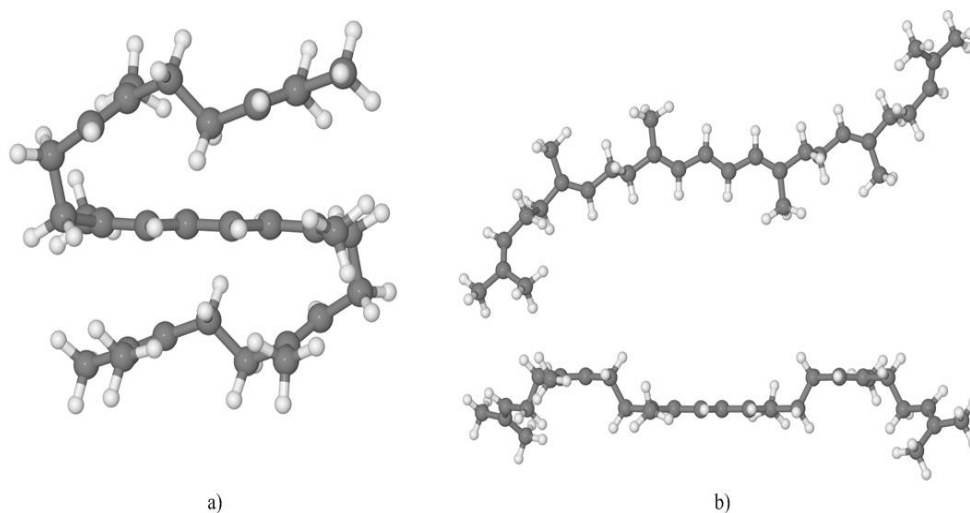


Figure 6.9 – Most stable conformation optimized at a) MM/DFT level from dihedral systematic exploration and b) RASSCF level from the planar FC geometry.

The energies of the lower states of the conformations obtained at C_{2h} -CASSCF, DFT and RASSCF level are represented in Figure 6.10. The representation of the energies of the lowest excited states in the upper part of the chart are related to the corresponding ground state energy and, therefore, are directly comparable to the absorption energy. On the other hand, the ground state (lower part in blue) is compared with the lowest minimum that has been located in order to appreciate the relative stability. The first conclusion that can be drawn is that the energies of conformers located at MM level are considerably higher in energy than the ones located with DFT. This result was already expected since the latter computational level is much more accurate than the first one. Moreover, it is quite surprising that all the structures derived from the conformational study have significantly lower

ground state energy than the planar geometry. In order to address this aspect, the symmetry restrictions are lifted for the RASSCF optimization and the results show a critical improvement in the ground state energy but still not better than DFT geometries. We can assume that the RASSCF optimization reached a local minimum, leading the procedure to a halt.

The conformations with lower energies give also a better description of the absorption energy. Comparing the values obtained for the ¹Bu vertical energies with the experimental value (99.6 kcal·mol⁻¹), the best result is the one encircled in Figure 6.10 (99.4 kcal·mol⁻¹), that corresponds to a MM/DFT optimized conformation, but not to the one with the lowest ground state energy. Although this good agreement can be considered spurious, the average of the absorption energy provided by MM/DFT geometries give a value of 102.5 kcal·mol⁻¹, in a satisfactory agreement with the experimental data, that improves the results provided by the C_{2h} calculation and even for the RASSCF optimization. This result is not unexpected, given that the DFT methods are known to predict accurately ground states geometries, and MS-RASPT2 has proved to give good excited states energies for this system.

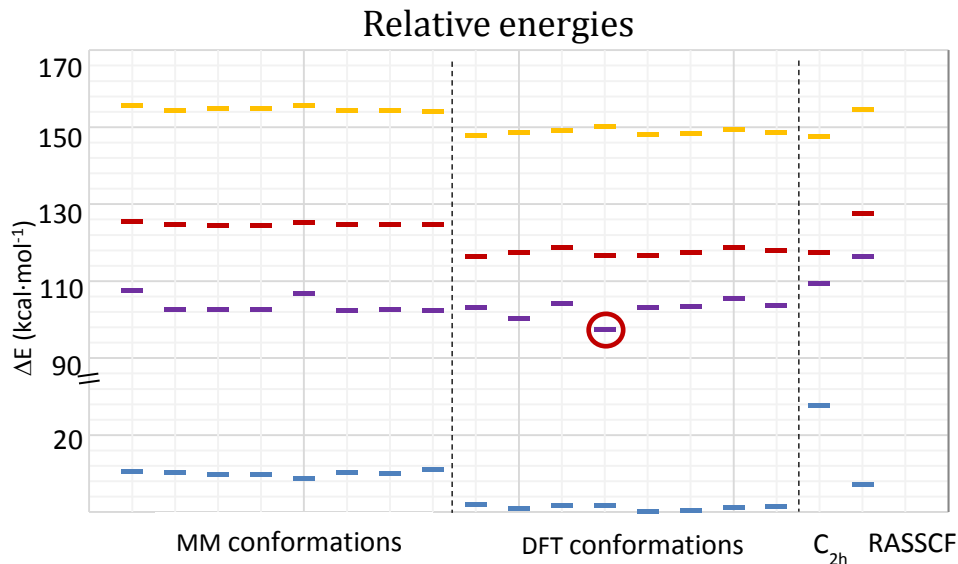


Figure 6.10 – Relative energies of the ground and lowest excited states for the most stable conformational study geometries, the C_{2h} approximation and the resulting geometry from the RASSCF optimization. Ground state energies are relative to the most stable conformation while excited state energies are relative to their corresponding ground state energies.

Comparing the relative energies of the excited states of the C_{2h} geometry with those of the MM/DFT geometries, a good qualitative agreement is observed. This result validates the study of the mechanism of the photochemistry of DHS with the C_{2h} symmetry constraint developed in the first part of this chapter, given that the main arguments were based on the qualitative interplay between the excited states.

6.5. CONCLUSIONS

The photophysics of dehydrosqualene as representative of flexible carotenoids of short conjugation length has been studied by means of ab initio calculations. This system has been chosen to validate the use of approximations relative to the computational method and to the geometry of the compound. The results are summarized in the following.

- The first part of this study has been performed under C_{2h} symmetry constraint (planar geometries). The relative energy of absorption for 1B_u state calculated with this assumption (267 nm/107.1 kcal·mol⁻¹) is comparable to the experimental value (287 nm), but the energy difference between these magnitudes is non-negligible.
- For C_{2h} DHS, the bright 1B_u state is the first excited state at FC geometry. The second excited state there, the dark $^2^1A_g$ state, becomes more stable in other areas of the PES in such a way that the global S_1 minimum has 1A_g character.
- Our results predict that after the initial excitation, DHS relaxes towards the 1B_u minimum on S_1 , where it decays to the 1A_g surface in a crossing located nearby. Subsequent relaxation leads the system to the S_1 1A_g minimum.
- From this species, the most probable path of decay to the S_0 surface is by vibrational coupling with the ground state, as observed experimentally. Nevertheless, ISC to the 3A_g state and radiative deactivation to S_0 are also possible although little probable.

-
- The performance of the RASSCF/RASPT2 methodology has been checked by comparison with the more accurate and expensive CASSCF/CASPT2 strategy. The accuracy of the results obtained and the save of computational costs clearly indicate that the restricted methodology is very suitable to study this kind of problems.
 - The effect of the approximation made by imposing the C_{2h} symmetry constrain in the geometry of the system has been measured, analysing how the loose of planarity affects the vertical energies of the excited states at the FC area. The results indicate that the approximation leads to quantitative changes, responsible of the not very satisfactory agreement between experimental and computational results for absorption energies, but does not change qualitatively the prediction of the mechanisms of deactivation of excited DHS since they are based mainly in the central area of this carotenoid.

6.6. BIBLIOGRAPHY

1. Edge, R., McGarvey, D. J., Truscott, T. G. *J. Photochem. Photobiol. B.*, **1997**, *41*, 189.
2. Nishino, H. *J. Cell. Biochem.*, **1997**, *67*, 86.
3. Warleta, F., Campos, M., Allouche, Y., Sanchez-Quesada, C., Ruiz-Mora, J., Beltran, G., Gaforio, J. J. *Food Chem. Toxicol.*, **2010**, *48*, 1092.
4. Dutton, H. J., Manning, W. M., Duggar, B. M. *J. Phys. Chem.*, **1943**, *47*, 308.
5. Orlandi, G., Zerbetto, F., Zgierski, M. Z. *Chem. Rev.*, **1991**, *91*, 867.
6. Hudson, B. S., Kohler, B. E. *Chem. Phys. Lett.*, **1972**, *14*, 299.
7. Schulten, K., Karplus, M. *Chem. Phys. Lett.*, **1972**, *14*, 305.
8. Polívka, T., Sundström, V. *Chem. Rev.*, **2004**, *104*, 2021.
9. Cerón-Carrasco, J. P., Requena, A. Marian, C. M. *Chem. Phys.*, **2010**, *373*, 98.
10. Ostroumov, E. E., Müller, M. G., Hundsdörfer, C., Stahl, W., Marian, C. M., Holzwarth, A. R. *Chem. Phys.*, **2010**, *373*, 137.

11. Papagiannakis, E., Van Stokkum, I. H. M., Vengris, M., Cogdell, R. J., Van Grondelle, R., Larsen, D. S. *J. Phys. Chem. B.*, **2006**, *110*, 5727.
12. Sashima, T., Nagae, H., Kuki, M., Koyama, Y. *Chem. Phys. Lett.*, **1999**, *299*, 187.
13. Ruiz-Anchondo, T., Glossman-Mitnik, D. *J. Mol. Struct.*, **2009**, *913*, 215.
14. Angeli, C., Pastore, M. *J. Chem. Phys.*, **2011**, *134*, 184302.
15. Tavan, P.; Schulten, K. *Phys. Rev. B.*, **1987**, *36*, 4337.
16. Polívka, T., Sundström, V. *Chem. Phys. Lett.*, **2009**, *477*, 1.
17. Britton, G., Liaaen-Jensen, S., Pfander, H. *Carotenoids, Vol.4: Natural functions*, 2008; Vol. 4.
18. Macpherson, A. N., Gillbro, T. *J. Phys. Chem. A*, **1998**, *102*, 5049.
19. Akimoto, S., Yamazaki, I., Sakawa, T., Mimuro, M. *J. Phys. Chem. A*, **2002**, *106*, 2237.
20. Christensen, R. L., Goyette, M., Gallagher, L., Duncan, J., DeCoster, B., Lugtenburg, J., Jansen, F. J., Van der Hoef, I. *J. Phys. Chem. A*, **1999**, *103*, 2399.
21. Frank, H. A., Desamero, R. Z. B., Chynwat, V., Gebhard, R., Van der Hoef, I., Jansen, F. J., Lugtenburg, J., Gosztola, D., Wasielewski, M. R. *J. Phys. Chem. A*, **1997**, *101*, 149.
22. Furuichi, K., Sashima, T., Koyama, Y. *Chem. Phys. Lett.*, **2002**, *356*, 547.
23. Kurashige, Y., Nakano, H., Nakao, Y., Hirao, K. *Chem. Phys. Lett.*, **2004**, *400*, 425.
24. Fujii, R., Inaba, T., Watanabe, Y., Koyama, Y., Zhang, J-P. *Chem. Phys. Lett.*, **2003**, *369*, 165.
25. Lenzer, T., Ehlers, F., Scholz, M., Oswald, R., Oum, K. *Phys. Chem. Chem. Phys.*, **2010**, *12*, 8832.
26. Gradinaru C. C., K., J. T. M., Papagiannakis, E., Van Stokkum, I. H. M., Cogdell R. J., Fleming G. R., Niederman, R. A., Van Grondelle, R. *Proc. Natl. Acad. Sci. U.S.A.*, **2001**, *98*, 2364.

-
27. Zerbetto, F., Zgierski, M. Z., Orlandi, G., Marconi, G. *J. Chem. Phys.*, **1987**, *87*, 2505.
 28. Woywod, C., Livingood, W. C., Frederick, J. H. *J. Chem. Phys.*, **2001**, *114*, 1645.
 29. Schmidt, M.; Tavan, P. *J. Chem. Phys.*, **2012**, *136*, 124309.
 30. Dreuw, A., Starcke, J. H., Wachtveitl, J. *Chem. Phys.*, **2010**, *373*, 2.
 31. Wild, D. A., Winkler, K., Stalke, S., Oum, K., Lenzer, T. *Phys. Chem. Chem. Phys.*, **2006**, *8*, 2499.
 32. Hariharan, P. C., Pople, J. A. *Theor. Chim. Acta.*, **1973**, *28*, 213.
 33. Takaichi, S. *Photosynth. Res.*, **2000**, *65*, 93.
 34. Bettermann, H., Bouschen, W., Ulrich, L., Domnick, G., Martin, H. D. *J. Mol. Struct.*, **1999**, *480–481*, 101.
 35. Rondonuwu, F. S., Watanabe, Y., Fujii, R., Koyama, Y. *Chem. Phys. Lett.*, **2003**, *376*, 292.
 36. Fuß, W., Haas, Y., Zilberg, S. *Chem. Phys.*, **2000**, *259*, 273.

SEVENTH CHAPTER:

FINAL CONCLUSIONS

AZOBENZENE AND PHENYLAZOPYRIDINE

- The computational study developed for azobenzene allows to propose a mechanism for isomerization of this compound that explains the experimental observations regarding the absorption spectrum data, the measured quantum yields for photoisomerization when exciting to $^1(n\pi^*)$ and $^1(\pi\pi^*)$ states, and the variation of these quantum yields for systems with free and restricted rotation.
- The CASSCF/CASPT2 strategy used usually to study mechanisms of photochemical reactions is not accurate enough in this case. The CASSCF method does not describe properly the topography of the potential energy surfaces of some of the states involved in the mechanism, so the CASPT2 method is necessary, not only to compute energies but also to optimize geometries.
- In spite of the similarities between azobenzene and phenylazopyridine, small quantitative energy changes produce noticeable qualitative changes in the computed reaction mechanisms for these systems. Based on our

computational results, we predict that for systems with restricted rotation, the photoisomerization quantum yield will be larger when the phenylazopyridine is excited to the $^1(\pi\pi^*)$ state. CASPT2 optimizations are necessary also for this system to properly describe the potential energy surfaces of some of the excited states involved in the reactivity.

- It has been proved that the protocol used by our group to reproduce experimental spectra gives much more accurate results than single point calculations in flexible compounds. It means that comparison of vertical excitations computed from ground state equilibrium geometries with experimental data of band maxima, should be done cautiously in flexible systems, and be only taken into account in a qualitative way.

9-PHENYLPHENALENONE

- The computational study performed on 9-phenylphenalenone provide enough information to understand the photochemistry of this compound and explain satisfactorily why the oxygen sensitization efficiency of this compound is much smaller than the one of its parent system, phenalenone.
- The different photochemical properties are not derived from differences on the characteristics of the excited states of both systems, nor in energetic reasons, given that the landscape of the potential energy surfaces of 9-phenylphenalenone around the Frank Condon zone is very similar to the one obtained for phenalenone in previous works. The difference is given by an alternative reaction path, only possible in 9-phenylphenalenone, that is the cyclisation to naphthoxanthene. This reaction competes efficiently with population of the $^3(\pi\pi^*)$ state, responsible of the oxygen sensitization, critically decreasing the quantum yield of this latter process.
- To get the required accuracy in the computational description of this system, inclusion of dynamic electron correlation is essential not only for the energy calculations, but also for the description of some of the excited states involved in the photochemistry of interest. The size of the system and the complexity of the reactions studied, impose the application of

reductions and approximations relative to the active spaced used in the calculations, which have proved to yield reliable results.

DEHIDROSQUALENE

- The excited states and processes involved in the photophysics of dehidrosqualene, a carotenoid of short conjugation length, have been determined and described in detail by means of ab initio calculations.
- The suitability of the RASSCF/RASPT2 protocol to provide accurate results for this kind of problems has been tested by comparison with the more accurate and expensive CASSCF/CASPT2 protocol.
- The influence of the flexibility of the backbone of dehidrosqualene on the excitation energies and consequently on the photochemical processes studied has been analysed. The quantitative differences in the values of the relative energies due to the simplification of an imposed symmetry in the system, do not lead to qualitative differences in the description of the mechanism of the processes studied.

LIST OF CONTRIBUTIONS

PUBLICATIONS

RELATED TO THIS THESIS

1. **Excited states decay in the photoisomerization of azobenzene: a new balance between mechanisms.** Casellas, J., Bearpark, M., Reguero, M. (Submitted to ChemPhysChem)
2. **Elucidating the reversible light-induced mechanism for the photoisomerization of phenylazopyridine.** Casellas, J., Alcover, G., Reguero, M., de Graaf, C. (Manuscript in preparation)
3. **Photosensitization versus photocyclisation: competitive mechanisms in play for phenylphenalenone.** Casellas, J., Reguero, M. (Manuscript in preparation)
4. **Effect of structural flexibility in the theoretical description of photochemical processes in the carotenoid dehydrosqualene.** Casellas, J., Reguero, M. (Submitted to Journal of photochemistry and photobiology A: Chemistry)

NOT RELATED TO THIS THESIS

5. **Anti-Lippert-Mataga behaviour explained. Computational predictions on Stokes shifts corroborated by measurements in Ru(II) polypyridil complexes.** Alcover, G., Casellas, J., Ielasi, G., de Graaf, C., Orellana, G., Reguero, M. (Manuscript in preparation)

POSTERS AND ORAL PRESENTATIONS

Cis-trans isomerization of phenylazopyridine. Rotation or inversion? A never ending discussion.

XXXI XRQTC Annual Meeting

25/06/2015

Science Park of the University of Girona, Girona, Spain.

CASSCF/CASPT2 study of the mechanism of the cis-trans isomerization of phenylazopyridine.

Advances in computational spectroscopy 2014

23/10/2014 - 27/10/2014

Hotel Crowne Plaza, Bratislava, Slovakia.

Shedding light on the photochemical process of phenylphenalenone derivatives competitive with photosensitization.

50th Symposium on Theoretical Chemistry

14/09/2014 - 18/09/2014

University of Vienna, Vienna, Austria.

RESEARCH STAY

**Imperial College
London**

Project: To map out the excited-state reaction pathways of the azobenzene system with accurate ab initio methods.

Supervisor: Dr. Michael Bearpark

Period: September 2013 – December 2013

Nothing in life is to be feared, it is only to be understood.
Now is the time to understand more, so that we may fear less.

Marie Curie

UNIVERSITAT ROVIRA I VIRGILI

ELUCIDATING DEACTIVATION AND REACTION PATHS OF PHOTSENSITIVE ORGANIC SYSTEMS THROUGH COMPUTATIONAL METHODS.

Josep Casellas Soler

UNIVERSITAT ROVIRA I VIRGILI

ELUCIDATING DEACTIVATION AND REACTION PATHS OF PHOTSENSITIVE ORGANIC SYSTEMS THROUGH COMPUTATIONAL METHODS.

Josep Casellas Soler

UNIVERSITAT ROVIRA I VIRGILI

ELUCIDATING DEACTIVATION AND REACTION PATHS OF PHOTSENSITIVE ORGANIC SYSTEMS THROUGH COMPUTATIONAL METHODS.

Josep Casellas Soler